AD-A063 161 NORTH TEXAS STATE UNIV DENTON DEPT OF PHYSICS F/G 20/12
INVESTIGATION OF LASER OPTICAL BIASING ON THE QUANTUM TRANSPORT--ETC(U)
OCT 78 D G SEILER N00014-76-C-0319
UNCLASSIFIED NL

1 OF 2
AD A063161

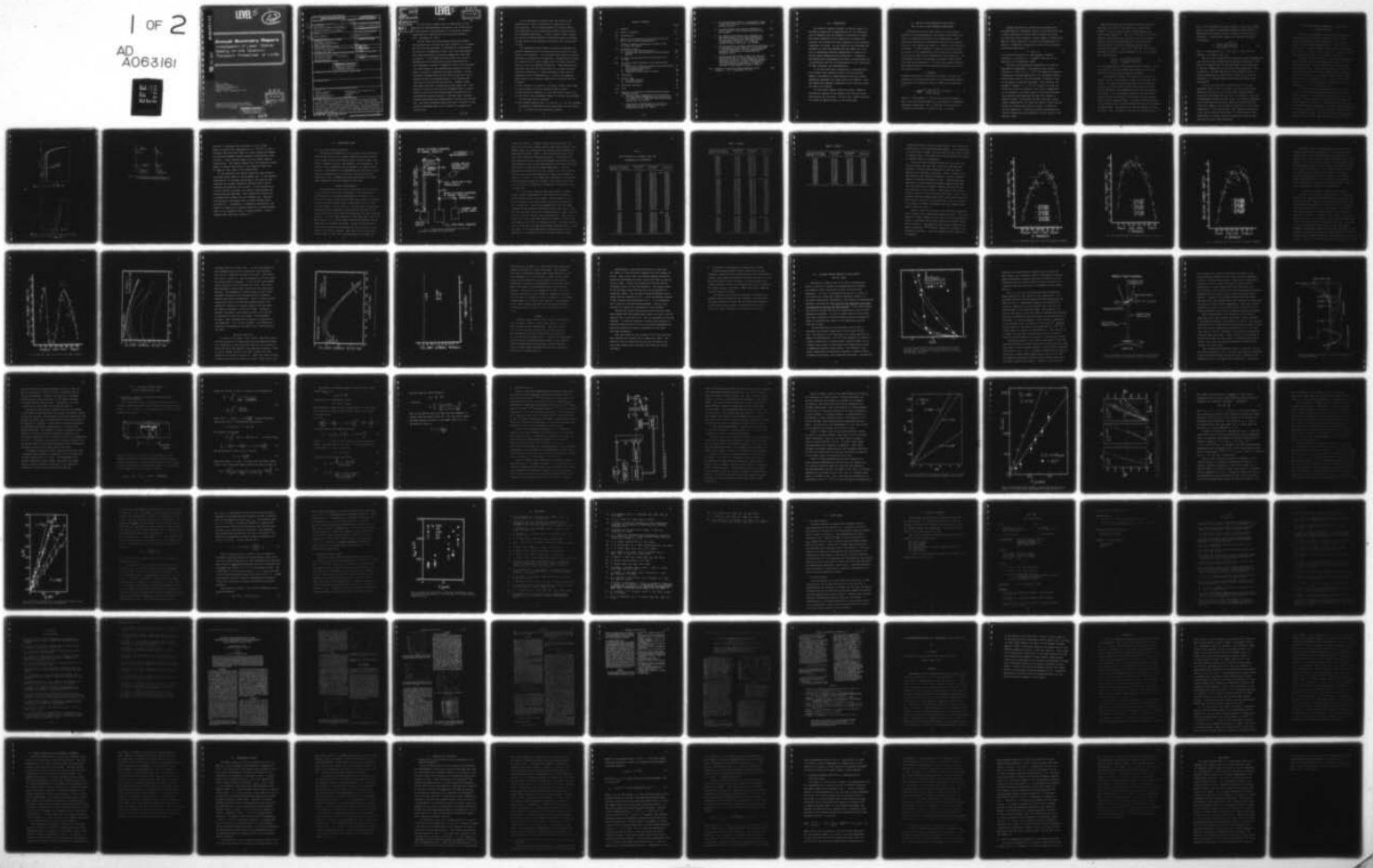

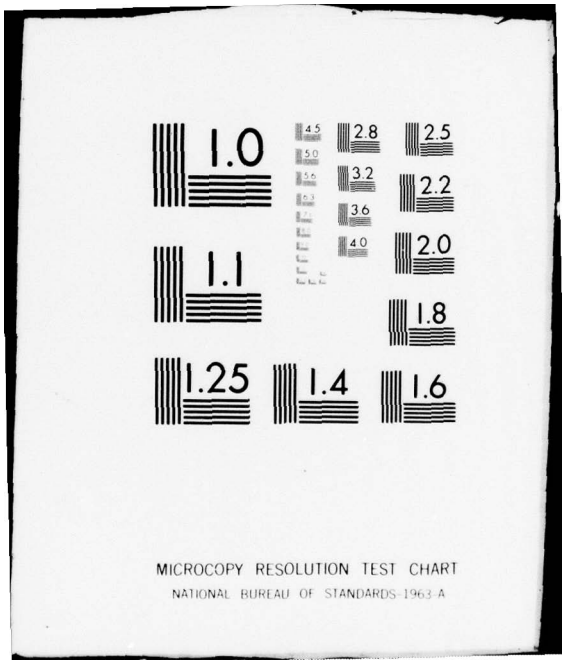
1.0
1.1
1.25
1.4
1.6
1.8
2.0
2.2
2.5
2.8
3.2
3.6
4.0
4.5
5.0
5.6
6.3
MICROCOPY RESOLUTION TEST CHART
NATIONAL BUREAU OF STANDARDS-1963-A

LEVEL II

12

B.S.

Annual Summary Report

Investigation of Laser Optical Biasing on the Quantum Transport Properties of n-InSb

by
David G. Seiler
Department of Physics
North Texas State University
Denton, Texas 76203
October 1, 1977 - September 30, 1978

Prepared for the Office of Naval Research
Electronic and Solid State Sciences Program
Under Contract NR 318-039

SECURITY CLASSIFICATION OF THIS PAGE (When Data Entered)

REPORT DOCUMENTATION PAGE

READ INSTRUCTIONS BEFORE COMPLETING FORM

1. REPORT NUMBER

2. GOVT ACCESSION NO.

3. RECIPIENT'S CATALOG NUMBER

4. TITLE (and Subtitle)
Investigation of
LASER OPTICAL BIASING ON THE QUANTUM TRANSPORT PROPERTIES OF n-InSb.

5. TYPE OF REPORT & PERIOD COVERED
Annual summary rept.
1 Oct. 1977 - 30 Sept. 1978

6. PERFORMING ORG. REPORT NUMBER

7. AUTHOR(s)
DAVID G. SEILER

8. CONTRACT OR GRANT NUMBER(s)
N00014-76-C-0319

9. PERFORMING ORGANIZATION NAME AND ADDRESS
DEPARTMENT OF PHYSICS
NORTH TEXAS STATE UNIVERSITY
DENTON, TEXAS 76203

10. PROGRAM ELEMENT, PROJECT, TASK AREA & WORK UNIT NUMBERS

11. CONTROLLING OFFICE NAME AND ADDRESS
ONR Electronic and Solid State Sciences Program
Office of Naval Research
Arlington, VA 22217

12. REPORT DATE
October, 1978

13. NUMBER OF PAGES
141 pages

14. MONITORING AGENCY NAME & ADDRESS (if different from Controlling Office)
ONR Resident Representative
528 Federal Building
300 East 8th Street
Austin, Texas 78701
147 p.

15. SECURITY CLASS. (of this report)
Unclassified

15a. DECLASSIFICATION/DOWNGRADING SCHEDULE

16. DISTRIBUTION STATEMENT (of this Report)

DISTRIBUTION STATEMENT A
Approved for public release;
Distribution Unlimited

17. DISTRIBUTION STATEMENT (of the abstract entered in Block 20, if different from Report)

18. SUPPLEMENTARY NOTES

19. KEY WORDS (Continue on reverse side if necessary and identify by block number)

InSb
Quantum Transport
Optical Biasing
Photoexcited carriers
Photoconductivity
Interaction of laser radiation with semiconductors
CO_2 Laser
CO Laser

20. ABSTRACT (Continue on reverse side if necessary and identify by block number)

The interaction of CO_2 and CO laser radiation with the semiconductor InSb has been studied at liquid helium temperatures with the Shubnikov-de Haas effect and the photoconductivity at zero magnetic field. The electron heating that results is characterized by a determination of the electron temperature for various CO_2 and CO laser frequencies and powers. The CO_2 laser-induced heating is shown to result from free carrier absorption processes, while the CO laser-induced heating is shown to result from impurity level and/or direct interband transitions.

DD FORM 1 JAN 73 1473 EDITION OF 1 NOV 65 IS OBSOLETE
S/N 0102-014-6601

SECURITY CLASSIFICATION OF THIS PAGE (When Data Entered)

409 923

LEVEL II

I. SUMMARY

In this annual summary report a description of the theoretical and experimental progress in the investigation of laser optical biasing effects on the quantum transport properties on n-InSb is given for the period October 1, 1977 - September 30, 1978.

We have shown that free-carrier absorption-induced photoconductivity of tuned CO_2 laser radiation is a valuable new tool for the extraction of information on photoheated hot carriers in degenerate n-InSb. The first measurements that allow extraction of electron temperatures have been carried out. A new hybrid technique which uses parallel photoheating and dc-electrical heating experiments has been developed to extract information on free carrier absorption coefficients in low concentration samples of n-InSb where no previous information has been available. We had originally proposed that carrier-carrier scattering transferred the optically absorbed power of the photoexcited electrons to the electron gas directly. However, these experiments and their interpretation have shown that a substantial fraction of the optically absorbed power is transferred to the lattice by optical-phonon cascading as the photoexcited electrons scatter to energies where electron-electron scattering then predominates in heating the electron gas. The major difference being that only a fraction of the optically absorbed power now is effective in heating the electron gas.

It was pointed out recently that the origin of the absorption tail below the band gap of InSb has not yet been resolved. The CO laser-induced hot electron effects in n-InSb which we are investigating involve impurity-level and interband transitions. In fact, these CO laser induced hot electron studies provide an alternative means of unraveling the nature of the absorption processes near the band gap of InSb.

The Shubnikov-de Haas effect was used to determine the electron temperature of the electron gas at various CO laser powers and wavelengths. For the wavelengths used free carrier absorption processes can be neglected. Photoexcited electrons are created with an excess energy above the Fermi energy by impurity level or interband transitions. These photoexcited electrons then heat the electron gas via electron-electron scattering resulting in a quasi-equilibrium state with an increased electron temperature T_e. In fact, the proposed model explains all pertinent heating data obtained with the CO laser:

(1) the increase of T_e with P_I, the peak incident laser power
(2) the increase of T_e with increased photon energy
(3) the saturation behavior of T_e at the higher values of P_I
(4) the lack of any measurable change in electron concentration for the lower photon energies
(5) the unusual behavior for $\lambda = 5.245$ μm, i.e. (a) the increase in electron concentration with laser power, but not before $T_e \simeq 3.3$ K and (b) the saturation behavior.

TABLE OF CONTENTS

III. INTRODUCTION

The effect of optical biasing, or optical control, of electronic properties of semiconductors is an interesting area of research into the dynamics of electrons in solids. The overall objective of our research is to measure and interpret the influence of laser radiation on the electronic properties of n-InSb. In this regard we have developed and pioneered in using the Shubnikov-de Haas Effect as a new tool in determining electron temperatures at specific CO and CO_2 laser frequencies and intensities. In addition, photoconductivity measurements have been also developed into a quantitative tool for the investigation of the interaction of laser radiation with semiconductors.

It is well-known that illumination of semiconductors with intense laser radiation leads to carrier heating. However, the physics or understanding of the hot carrier generation processes is in many cases quite obscure. Even the absorption processes themselves are not entirely known and need to be studied.

In this annual summary report we review a number of significant features of the research work that has taken place during the last year. We also list a number of exciting things we shall be doing in the coming year.

IV. REVIEW OF THE SHUBNIKOV-DE HAAS EFFECT AND ITS ROLE IN HOT ELECTRON MEASUREMENTS

The Shubnikov-de Haas (SdH) effect is an oscillatory variation of magnetoresistance with magnetic field which can occur in a degenerate material at low temperatures. The conditions necessary for the SdH oscillations to be observed are $\omega_c\tau >> 1$ and $k_B T_e < \hbar\omega_c < E_F$, where $\omega_c = eB/m^*c$ is the cyclotron frequency, τ is the lifetime of a state at the Fermi energy E_F, and T_e is the temperature of the electron gas, which may or may not be equal to the temperature of the lattice T_L. As the magnetic field B is increased, successive Landau levels rise past E_F and depopulate. As long as E_F remains constant, the magnetoresistance oscillations are periodic in B^{-1} with the period given by

$$P = \hbar e/E_F m^* c \quad . \tag{1}$$

Provided the magnetic field does not become too large, the amplitude of the SdH oscillations in the longitudinal magnetoresistance of the material such as n-InSb can be expressed as [1,2]

$$A = \left(\frac{P}{2B}\right)^{1/2} \frac{\beta\, T_e m' \cos(\pi\nu)}{\sinh(\beta\, T_e m'/B)}\, e^{-\beta\, T_D m'/B} \quad , \tag{2}$$

where $\beta = 2\pi^2 k_B\, cm/\hbar e$, $m' = m^*/m$ is the ratio of effective mass to be free electron mass, T_D is the Dingle or nonthermal broadening temperature, and ν is the spin splitting factor related to the effective g factor g* by $\nu = m^* g^*/2m$.

Although the SdH oscillations can be observed with straightforward dc techniques, magnetic field modulation and a lock-in amplifier are often used to improve the signal to noise ratio and to observe a larger number of oscillations. When the lock-in amplifier is tuned to the modulation frequency, it measures an oscillatory signal with an envelope-to-envelope amplitude of [3,4]

$$V = 4 A J_1 (\alpha) \tag{3}$$

at a particular value of B. The argument of Bessel function J_1 is given by $\alpha = 2\pi B_M/PB^2$, where B_M is the amplitude of the modulation field.

The first hot electron SdH experiment in n-InSb was performed by Komatsubara [5] who applied large electric fields (>0.1 V/cm) to a 1.5×10^{15} cm^{-3} sample and observed a decrease in the SdH amplitude for the transverse configuration and a shift of the SdH extrema to higher B values as the electric field was increased. Later Isaacson and Bridges [6] studied a 1.7×10^{15} cm^{-3} sample of n-InSb and found that either an increase in the lattice temperature or an increase in the large electric field would decrease the transverse SdH amplitude and shift the extrema to higher B values. By matching the SdH curves for various lattice temperatures at a fixed low electric field with the curves for various high electric fields at a fixed low lattice temperature, Isaacson and Bridges determined the electron temperatures corresponding to given values of the electric field.

Bauer and Kahlert have investigated the hot electron SdH effect in n-InSb [7,8] (as well as in n-InAs [9] and n-GaSb [10]) using a pulsed electric field technique to avoid lattice heating [11]. For 5.9×10^{15} and 1×10^{16} cm^{-3} samples, T_D varied with T_L, so the T_e values for various electric fields were determined from the longitudinal oscillations by the direct comparison method used by Isaacson and Bridges [6]. For a 6.9×10^{16} cm^{-3} (more highly degenerate) sample, T_D was independent of T_L, so T_e values were obtained using

$$\frac{A(T_{e,1})}{A(T_{e,0})} = \frac{T_{e,1}\sinh(\beta\, T_{e,0} m'/B)}{T_{e,0}\sinh(\beta\, T_{e,1} m'/B)} \tag{4}$$

from the amplitudes of longitudinal SdH oscillations. Little or no shift in the longitudinal SdH extremal positons was observed for these high concentration samples.

In the present studies the conduction electrons are heated, not by a large electric field, but by optical excitation. For photon energies much less than the band gap energy E_g, carrier heating should take place due to free carrier absorption and thermalization by electron-electron collisions. For larger photon energies, carriers should also be excited from impurity levels and from the valence band into the conduction band. A radiation induced increase in the steady state concentration should raise E_F and decrease the SdH period. This would shift the SdH extrema to higher B values. Also, according to the work of Kalushkin et al. [12],

even if the concentration remains constant, the B and T_e dependence of E_F caused by incomplete degeneracy should cause P to decrease and the extrema to move to higher B values as T_e is increased. To take period changes into account, we define the function

$$F \equiv \frac{V(T_{e,1}, P_1) P_0^{1/2} J_1(\alpha_0)}{V(T_{e,0}, P_0) P_1^{1/2} J_1(\alpha_1)} \quad , \tag{5}$$

where V is given by Eq. (3). If P, T_D, m', and ν are all constant, F is equal to Eq. (4).

The fact that ionized impurity scattering, which depends only upon carrier energy, dominates the momentum relaxation in InSb below 40 K insures that the SdH amplitudes will be functions of electron temperature T_e and not lattice temperature. Thus a decrease in the SdH amplitudes with increasing values of lattice temperature T_L reflects an increase in T_e since the electrons are in equilibrium with the lattice during these measurements.

Plots of the function F, defined in Eq. (5) or the amplitude ratios in Eq. (4) versus T_L and P_I can be used to determine the value of T_e for each laser, along with the parcticular wavelength and value of P_I by making a one-to-one correspondence between the two curves. An electron temperature can be extracted by the direct comparison method since the quantities compared are not explicit functions of the lattice temperature. [11] As noted earlier, this comparison method was first used by Isaacson and Bridges [6] in high electric field measurements to extract electron temperatures from SdH data and has since been used extensively.

V. REVIEW OF IMPURITY ABSORPTION IN InSb IN THE 5 μm BAND GAP REGION

In any real semiconductor both donors and acceptors are present to some degree. The normal case in one of partial compensation of the impurities. If N_D is the number of donor impurity atoms per unit volume and N_A is the number of acceptor impurity atoms then partial compensation occurs if $N_D \neq N_A$. If $N_d > N_A$ we talk about an n-type semiconductor and if $N_A > N_d$ a p-type semiconductor.

The highest mobility samples of n-InSb are usually doped with tellurium impurity atoms which have essentially zero activation energy, i.e. the donor levels are merged with the conduction band. Since there are always some acceptor level impurities present, these acceptor levels acquire an electron resulting in N_A electrons occupying these compensating states. Consequently, there is only an electron density $n = N_d - N_A$ occupying the conduction band at low temperatures. If $N_A << N_d$, then $n \simeq N_d$.

For review purposes we reproduce several published figures dealing with the absorption edge region of InSb. Figure 1 shows how the absorption coefficient α varies as a function of photon energy for a relatively pure sample.[15] At low temperatures there is a sharp transition which is due to direct interband transitions. At higher temperatures there is some contribution to α on the low energy side because of the presence of phonons. The way that impurities effect the absorption near the band edge can be seen in Figure 2.[16]

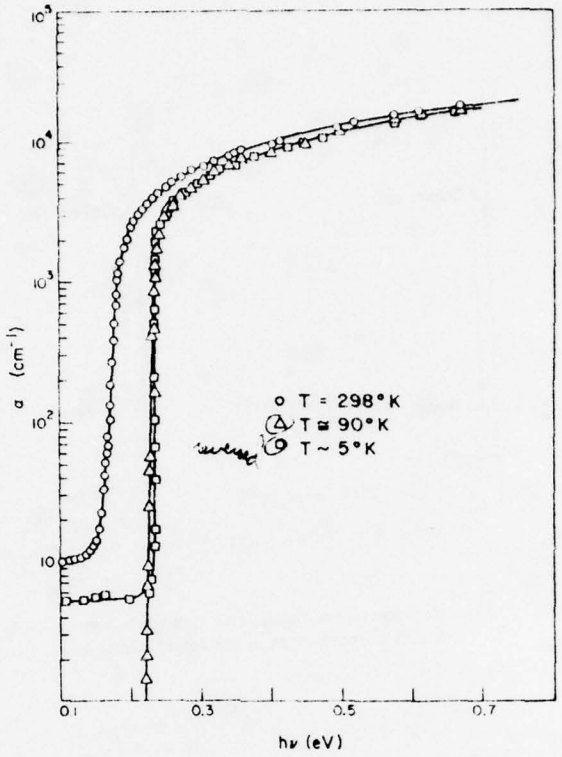

FIG. 1 Absorption edge of pure *InSb*. **(Ref. 15)**

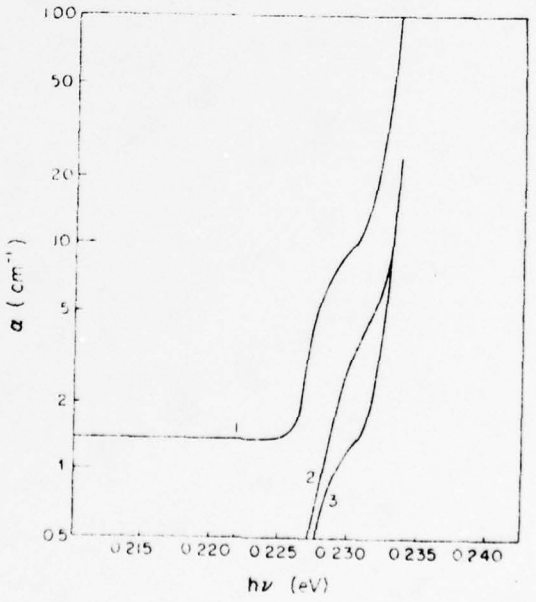

FIG. 2 The effect of impurity concentration on the absorption step for InSb at ~10°K (1) *p*-type $p = 3.37 \times 10^{15}$ cm^{-3}, $\mu = 5900$ cm^2/V sec at 80°K; (2) *n*-type $N_A = 1.79 \times 10^{15}$ cm^{-3}; (3) *n*-type $N_A \lesssim 0.6 \times 10^{15}$ cm^{-3}. **(Ref. 16)**

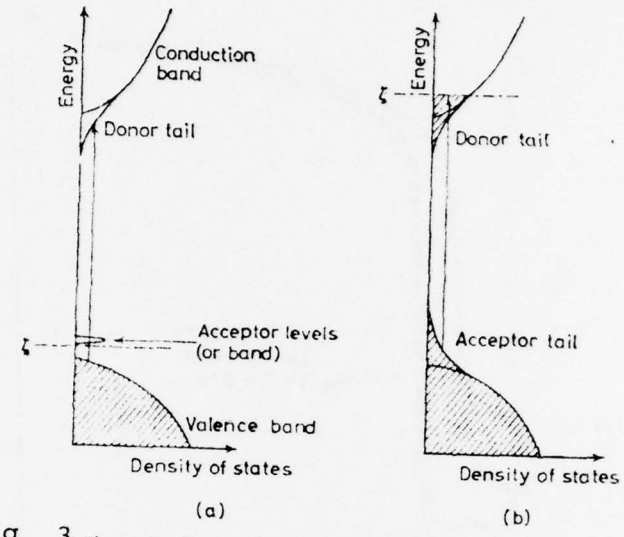

Fig. 3 *Absorption due to tail states: (a) Transitions to the conduction-band tail, (b) Transitions from the valence-band tail* (Ref. 17)

Curve No. 1 represents the variation of α of a p-type sample of InSb of hole concentration $\simeq 3 \times 10^{15}$ cm^{-3} at 80 K. The other two curves were taken on n-type, degenerate samples on InSb with different ionized acceptor concentrations, with curve No. 3 taken from the sample with the lowest acceptor concentration. The results suggest that the absorption corresponds to electron transitions to the conduction band from an impurity level close to the valence band.

At low densities, the shallow impurities form discrete localized energy levels in the forbidden gap. If the impurity concentration is increased sufficiently, the impurity wave functions can overlap, forming an impurity band in which electrons and holes are free to move. If the concentration is still further increased, the impurity bands broaden and overlap the main band edge. Thus a density-of-states tail is formed which extends into the forbidden gap. Realistic calculations of the doping level at which overlap occurs are difficult. Furthermore, in absorption experiments, the effect of a band tail is usually masked by the Burstein-Moss shift of the absorption edge to larger energies. Figure 3 schematically shows this situation. [17]

VI. EXPERIMENTAL WORK

A. cw CO_2 Laser Characterization

The operating parameters of a CO_2 laser must be characterized for the laser to be a useful laboratory research device. It is useful to know the working ranges of output power, wavelength, discharge current, gas pressure, and temperature. The effect on other parameters as one parameter is changed should be known. Repeatability of measurements and changing of output power and parameters as a function of time would be useful information also. Attempts were made when possible to study these parameters and their effects on the laser.

Spectral Measurements

The wavelength of the output is controlled by a rotating grating which is driven by a micrometer. The experimental arrangement for the spectral measurements is shown in Fig. 4. For a set current, mirror reflectivity, and pressure, the power of each line was recorded using a beam splitter and a Scientech Calorimeter as seen in Fig. 4. The micrometer reading was recorded and the wavelength of the line was ascertained from viewing the line using an Optical Engineering CO_2 Laser Spectrum Analyzer. For the laser operating in the TEM_{00} mode, the micrometer was set on a line by using the Spectrum Analyzer and the Calorimeter to maximize the power. Using the beam splitter, only relative powers were obtained but could be directly compared to full power readings. More than 90 lines with power greater than one watt were obtained between wavelengths of

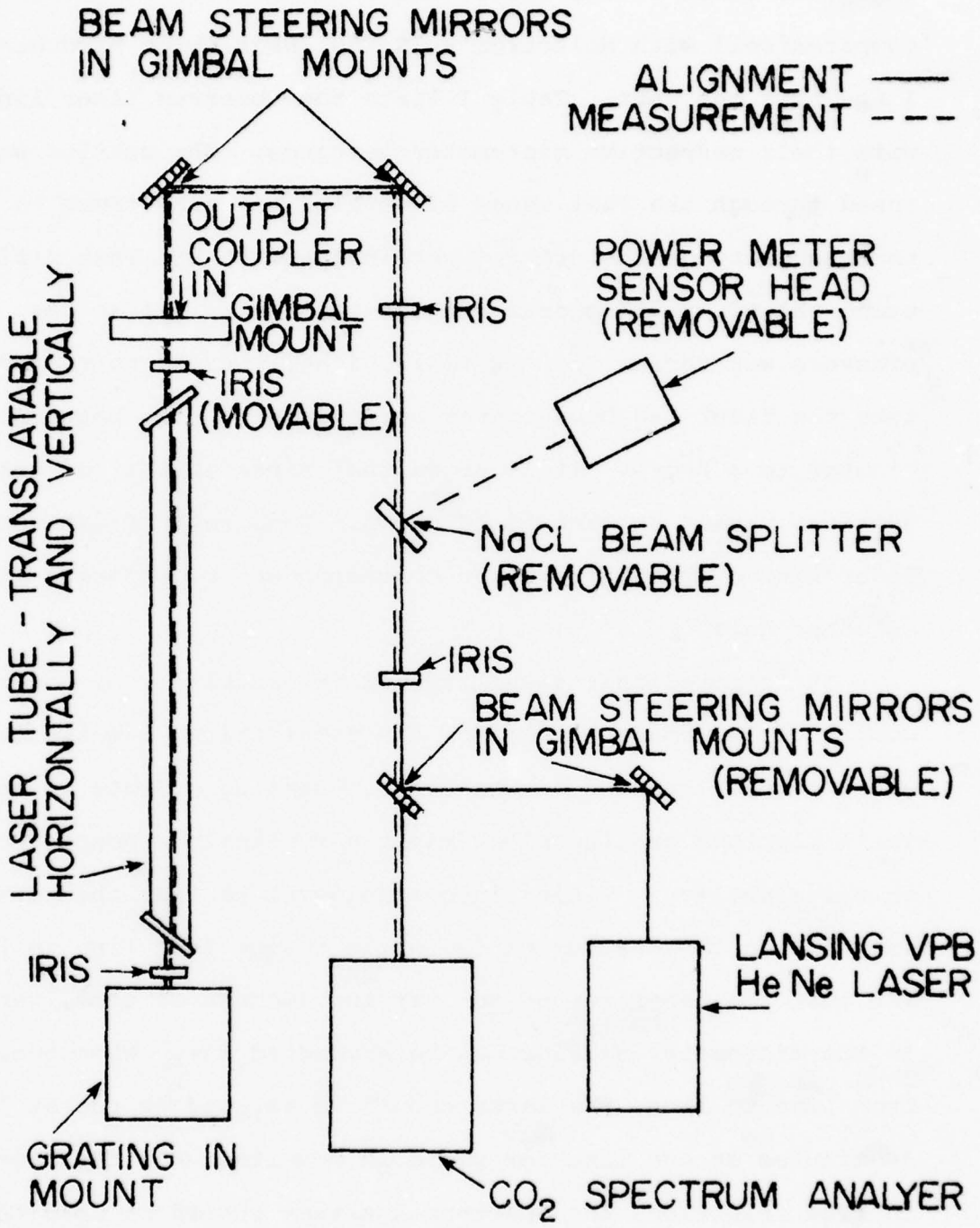

Fig. 4--Experimental Arrangement for Optical Alignment and Spectral Measurements.

9.192 and 10.885 μm. Seventy lines are available over two watts, 59 lines over 5 watts, and 25 lines over 10 watts. This compares well with Molectron's IR 250 laser which produces 90 lines over one watt. Table I lists the observed laser lines with their respective micrometer settings. The grating was tuned through the full range of wavelengths many times to check repeatability of the grating settings and to see what difference using the 62 or 70% output coupler would make. Also the pressure was varied from 12 to 18, finally to 23 torr, and the time the laser had been operating was varied from between 10 minutes to 3 hours. It is noted that repeatability of grating settings varied as much as ±0.04 mm. Some sets of data have lines listed at settings that corresponded to different lines in other data.

It is noted that stability and repeatability of power output varies considerable for the first thirty minutes to an hour after turning on the laser. Heating effects in the solid aluminum grating block might very easily account for this instability. Taking into consideration that the power incident on the grating varied while tuning from line to line, and that the laser was on for varying amounts of time, variance in the micrometer setting can be accounted for. When tuning from line to line, the laser should be allowed to run at least 30 minutes on one line for reliable results. For best accuracy in line selection, the Spectrum Analyzer should be used to view the line. It is also noted that at several places in the spectrum it is possible to lase on two and sometimes three

TABLE I

IDENTIFICATION OF SPECTRAL LINES AND

CALIBRATION OF MICROMETER

Grating Micrometer Reading in 0.001 mm	Wavelength in μm	Wavelength in cm^{-1}		Transition
8187	9.149	1092.93	020	R(46)
8218	9.157	1091.98		R(44)
8253	9.166	1091.01		R(42)
8291	9.174	1090.01		R(40)
8325	9.183	1088.98		R(38)
8362	9.192	1087.93		R(36)
8403	9.201	1086.86		R(34)
8434	9.210	1085.75		R(32)
8481	9.219	1084.62		R(30)
8516	9.229	1083.47		R(28)
8550	9.239	1082.29		R(26)
8600	9.250	1081.08		R(24)
8647	9.260	1079.85		R(22)
8690	9.271	1078.58		R(20)
8743	9.282	1077.30		R(18)
8791	9.293	1075.98		R(16)
8840	9.305	1074.64		R(14)
8890	9.317	1073.27		R(12)
8940	9.329	1071.88		R(10)
9001	9.342	1070.46		R(8)
9060	9.355	1069.01		R(6)
9104	9.367	1067.53		R(4)
9362	9.428	1060.57	020	P(4)
9415	9.442	1058.94		P(6)
9490	9.458	1057.30		P(8)
9553	9.473	1055.62		P(10)
9617	9.488	1053.92		P(12)
9686	9.504	1052.19		P(14)
9752	9.519	1050.44		P(16)
9819	9.536	1048.66		P(18)
9885	9.552	1046.85		P(20)
9971	9.569	1045.02		P(22)
10027	9.586	1043.16		P(24)
10105	9.603	1041.27		P(26)

TABLE I (CONTD.)

Grating Micrometer Reading in 0.001 mm	Wavelength in μm	Wavelength in cm^{-1}		Transition
10171	9.621	1039.36		P(28)
10258	9.639	1037.43		P(30)
10323	9.657	1035.46		P(32)
10417	9.676	1033.48		P(34)
10495	9.694	1031.46		P(36)
10573	9.714	1029.43		P(38)
10651	9.733	1027.36		P(40)
10745	9.753	1025.28		P(42)
10828	9.773	1023.16		P(44)
10917	9.794	1021.03		P(46)
11016	9.815	1018.87		P(48)
11101	9.836	1016.68		P(50)
12210	10.095	990.78	100	R(46)
12249	10.105	989.78		R(44)
12289	10.115	988.76		R(42)
12352	10.126	987.71		R(40)
12396	10.137	986.64		R(38)
12434	10.148	985.55		R(36)
12500	10.159	984.43		R(34)
12545	10.171	983.29		R(32)
12592	10.182	982.13		R(30)
12648	10.195	980.94		R(28)
12708	10.207	979.73		R(26)
12757	10.220	978.49		R(24)
12840	10.233	977.23		R(22)
12870	10.247	975.94		R(20)
12945	10.260	974.63		R(18)
13017	10.275	973.30		R(16)
13055	10.289	971.94		R(14)
13145	10.304	970.56		R(12)
13181	10.319	969.15		R(10)
13296	10.333	967.72		R(8)
13327	10.350	966.26		R(6)
13743	10.441	957.81	100	P(4)
13819	10.458	956.20		P(6)
13893	10.476	954.56		P(8)
13974	10.494	952.89		P(10)
14039	10.513	951.20		P(12)
14133	10.532	949.49		P(14)
14226	10.551	947.75		P(16)
14321	10.571	945.99		P(18)
14403	10.591	944.21		P(20)

TABLE I (CONTD.)

Grating Micrometer Reading in 0.001mm	Wavelength in μm	Wavelength in cm^{-1}	Transition
14500	10.611	942.40	P(22)
14575	10.632	940.56	P(24)
14680	10.653	938.71	P(26)
14728	10.675	936.83	P(28)
14862	10.696	934.92	P(30)
14964	10.719	933.00	P(32)
15059	10.741	931.05	P(34)
15153	10.765	929.07	P(36)
15263	10.788	927.08	P(38)
15368	10.812	925.06	P(40)
15449	10.836	923.02	P(42)
15575	10.860	920.95	P(44)
15690	10.885	918.86	P(46)
15801	10.911	916.76	P(48)
15910	10.936	914.63	P(50)

lines with powers as great as single lines. The only way to avoid this is to use the Spectrum Analyzer. It is found that once the laser is stable, the line will not move over a period of several hours. The laser can be left overnight and turned on without change in wavelength.

Along with the micrometer setting for each line, the relative powers for each line in the four branches were recorded. Figure 5 shows three sets of data for the R branch of the (001→020) transition. Shown is data for the 70% reflector and different pressures. The 62% reflector shows no noticable difference in data. Superimposed upon the data is a curve showing the general shape of the data. This curve follows the general behavior observed for the gain and power of this branch. Other people have noticed similar scatter in the data around the general curve. This scatter might be somewhat explained by the heating effect on the grating. When left on one particular line for a period of at least 30 minutes, the power level will stabilize and remain stable for hours.

Figure 6 shows the P branch of the (001→020) transition with a general curve shape drawn through the data. The curve shows the highest powers for the lines 22-18 as also shown in Figure 5, although overall power levels are slightly higher than in Figure 5. The peaks and the relative powers are as would be expected. [18,19] Figure 7 shows the R branch of the (001→020) transition. Again the powers and curve shape are as expected.

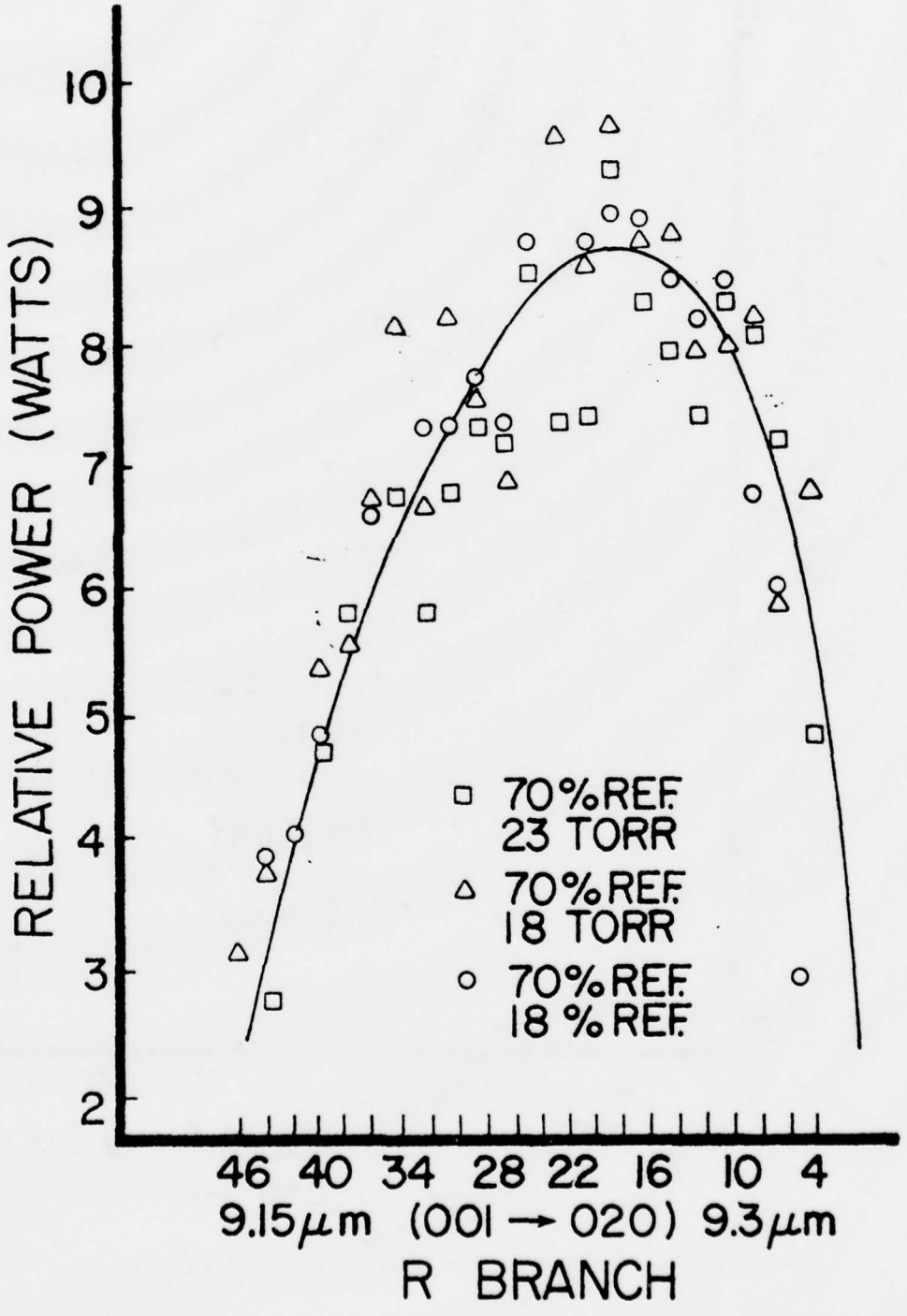

Fig. 5--Relative Power for Lines of CO_2(020) R Branch.

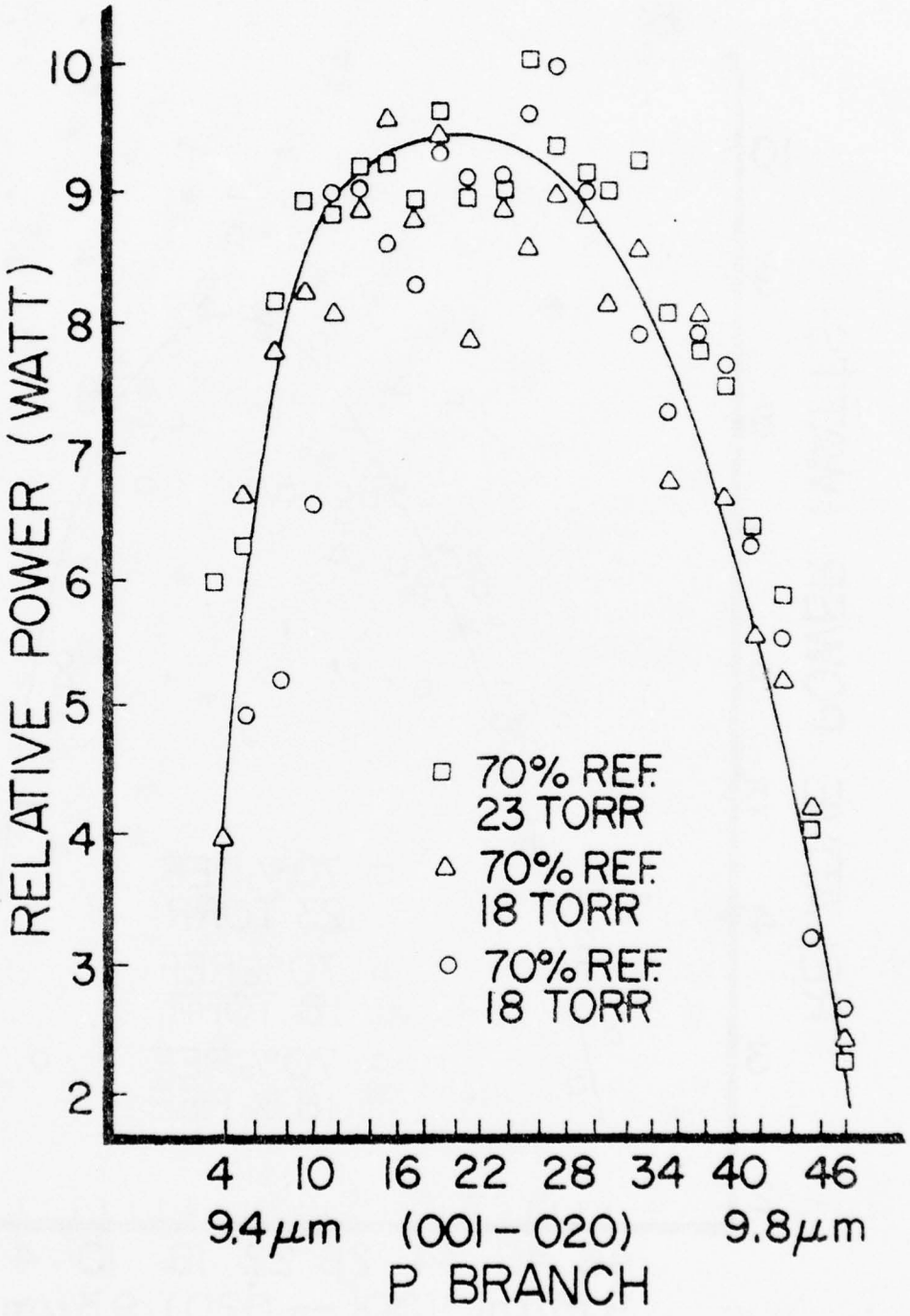

Fig. 6--Relative Power for Lines of CO_2(020) P Branch.

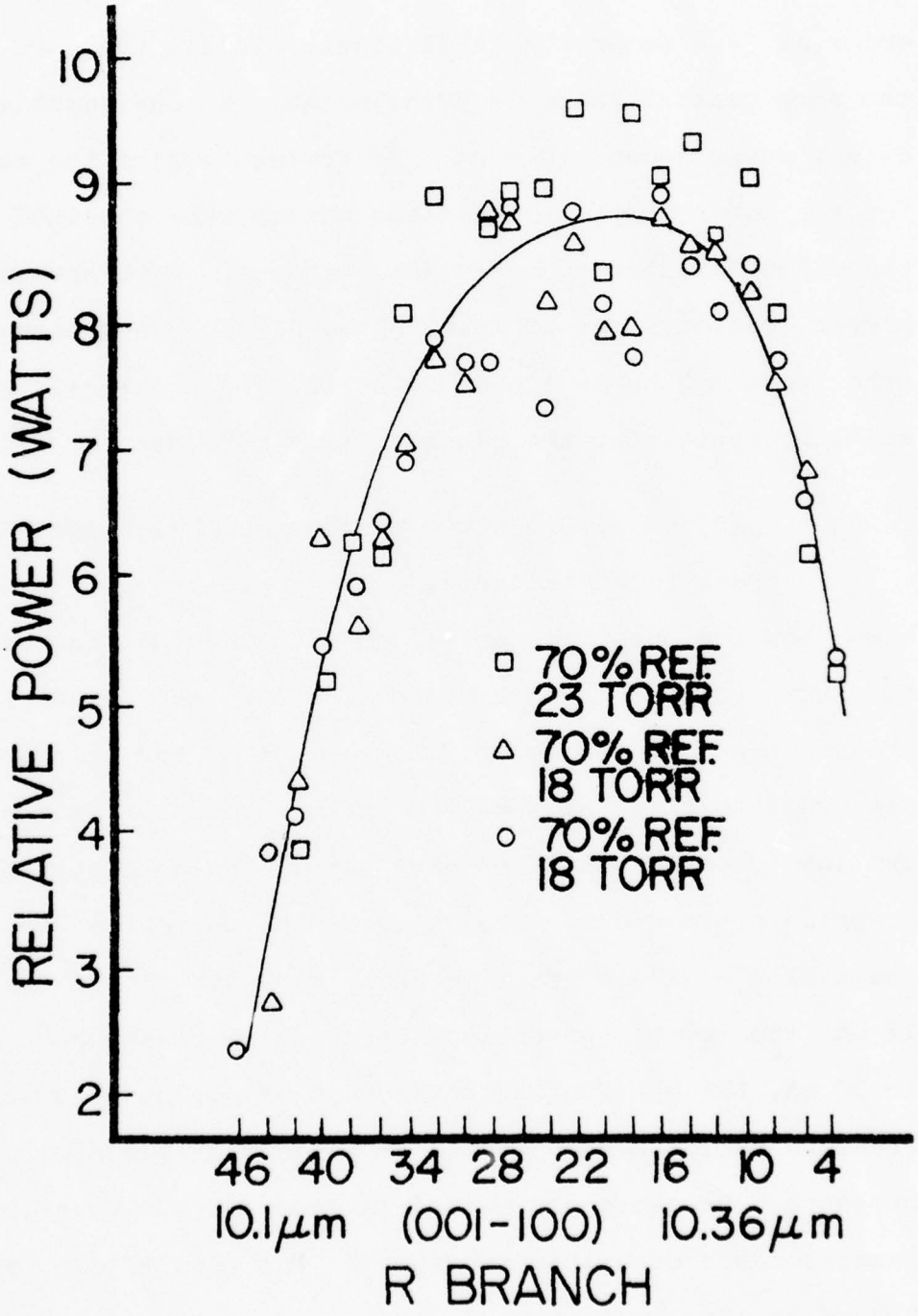

Fig. 7--Relative Power for Lines of CO_2(100) R Branch.

In Figure 8 quite unexpected behavior is seen in the P branch of the (001→020) transition. It would be expected that the data would follow the general curve shape as in the previous figures and that the largest power output would occur at 10.6 μm or the 18-22 lines. In all the data taken, the same general shape is seen, notably a considerable lack of any power around 10.6 μm. In trying to find the reason for the power drop, transmission curves were obtained on the output couplers and the NaCl windows. Both showed proper transmissions at 10.6 μm and did not vary enough at other wavelengths to appear to be causing problems. We are still investigating the cause of this behavior.

Effect of Discharge Current and Gas Pressure

In order to characterize a laser properly, it should be known how the output power varies with varying pressure and discharge current. The laser output was taken directly into the Scien-tech Calorimeter. The output of the calorimeter was fed into the Y-axis of the chart recorder. Provisions are incorporated into the power supply for automatically sweeping the current. The value of the current is fed into the X-axis of the chart recorder. The current was swept from 12 mA, the lowest current to sustain high pressure discharges, to 30 mA, the maximum current output of the power supply. Pressure could then be varied and a current sweep made at each pressure. Pressure was varied in steps of two torr to get the general range of usable pressures. The results can be seen in Figure 9. The curve for 22 torr is left off because it closely

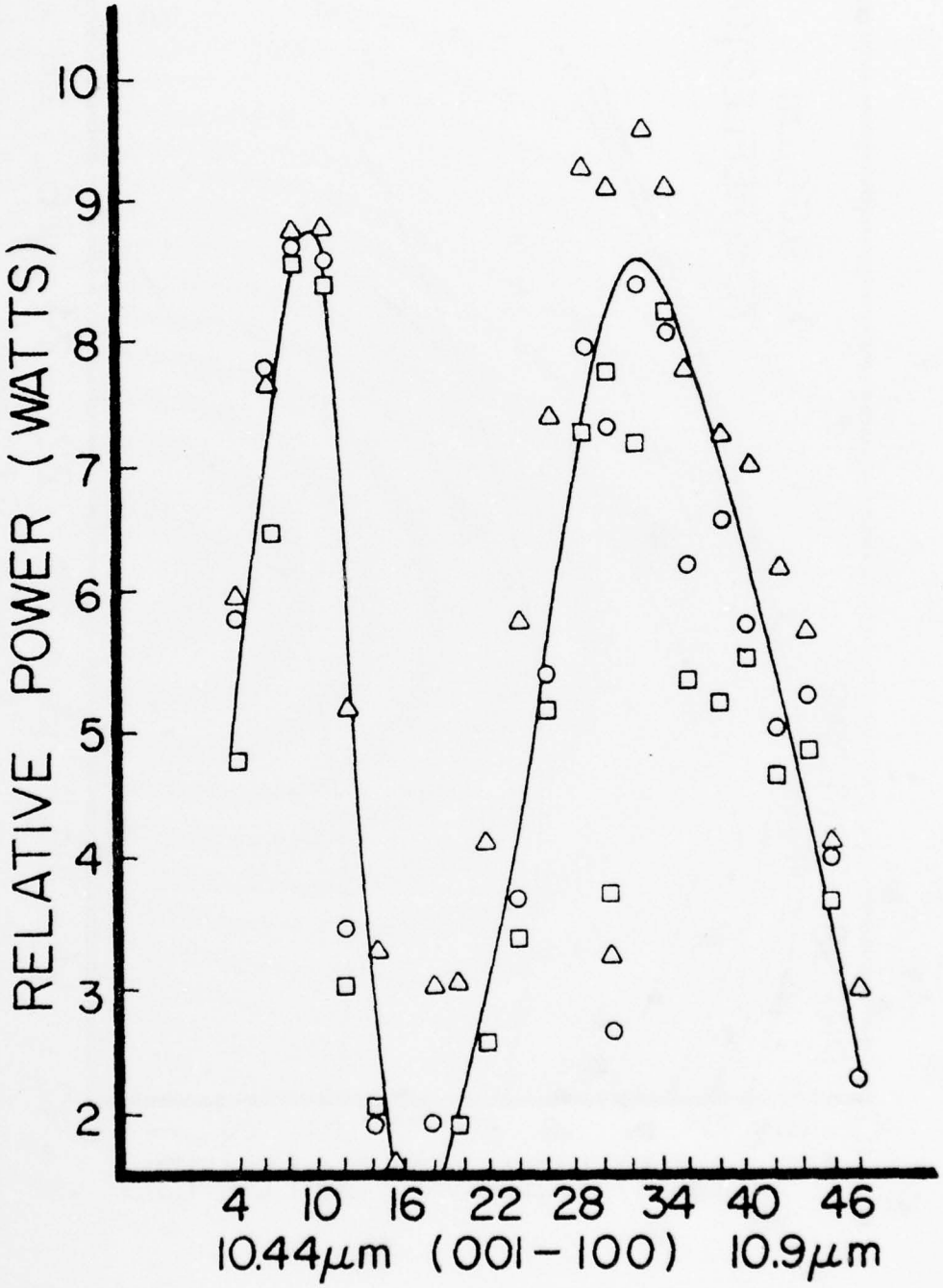

Fig. 8--Relative Power for Lines of CO_2(100) P Branch.

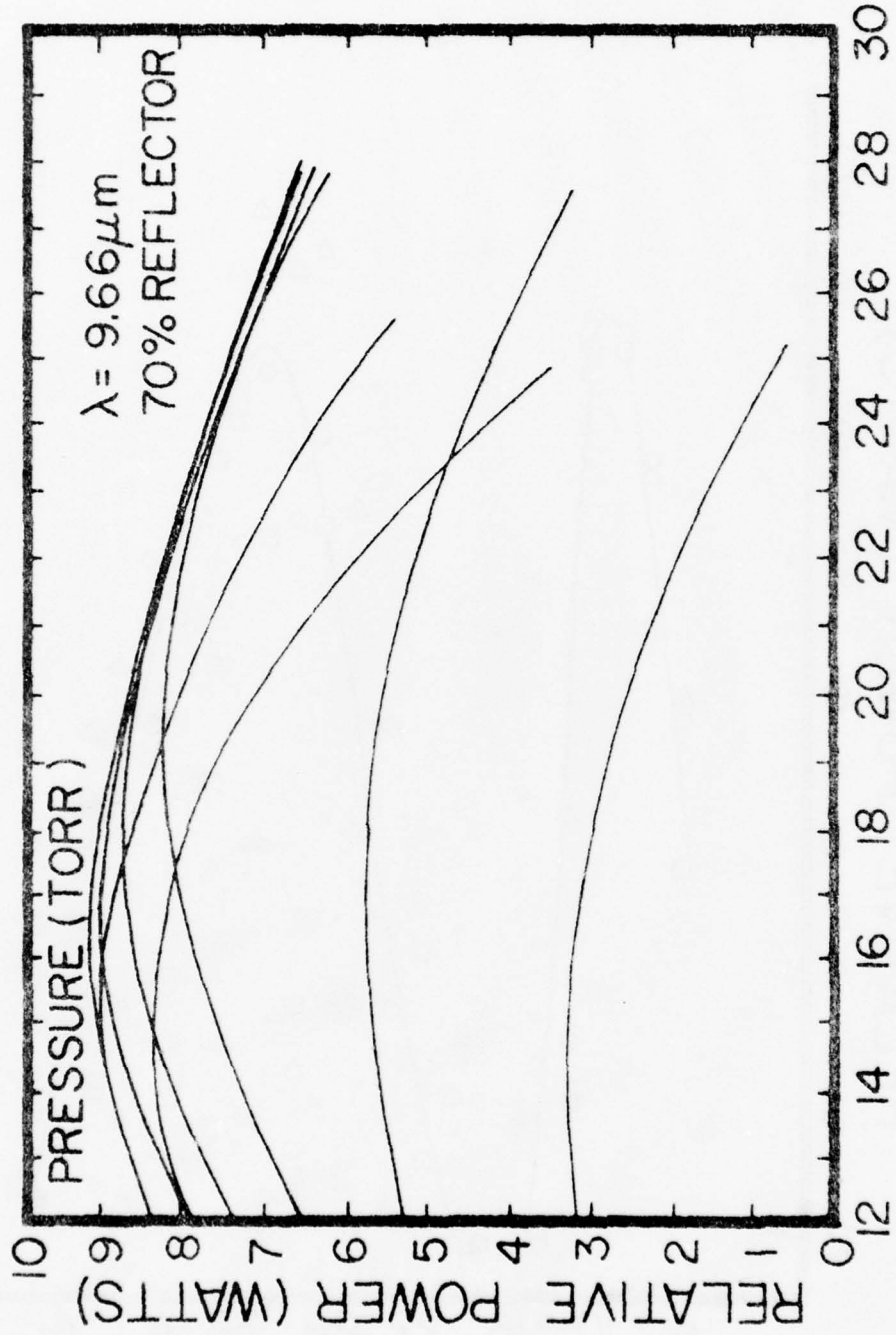

Fig. 9--Relative Power vs. Current for Several Pressures.

coincides with the 20 torr curve. To find the pressure at which maximum output occurs, curves were taken starting with 19 torr increasing in steps of one torr. The results are given in Figure 10. The last pressure is 22 torr since the output power is dropping. It can be seen that maximum output occurs at 21 torr pressure for 16 mA. All curves were repeated at least twice to make sure they were reproducible. The dependence on current shown is quite understandable considering that increased current increases pumping rates and gas temperature. Above a certain current, temperature effects overcome the enhanced pumping, and population inversion is lessened reducing gain and power. The effect of pressure is also well known. Increasing pressure increases gain and power as more active CO_2 and N_2 molecules are fed into the system. With increased pressure, comes increased field intensity, increasing the gas temperature. At a certain pressure, gas temperature dominates and depopulates the upper level, decreasing gain and power.

Amplitude Stability

In order for the laser to be a useful laboratory instrument the variation of output power with time should be known. It is important to know long term stability over periods of hours and short term stability over periods of seconds. After an initial warmup period of one hour, typical long term stability can be seen in Figure 11. Power fell from 9.9 watts to about 9.4 watts in a period of 3 hours. This gives a long

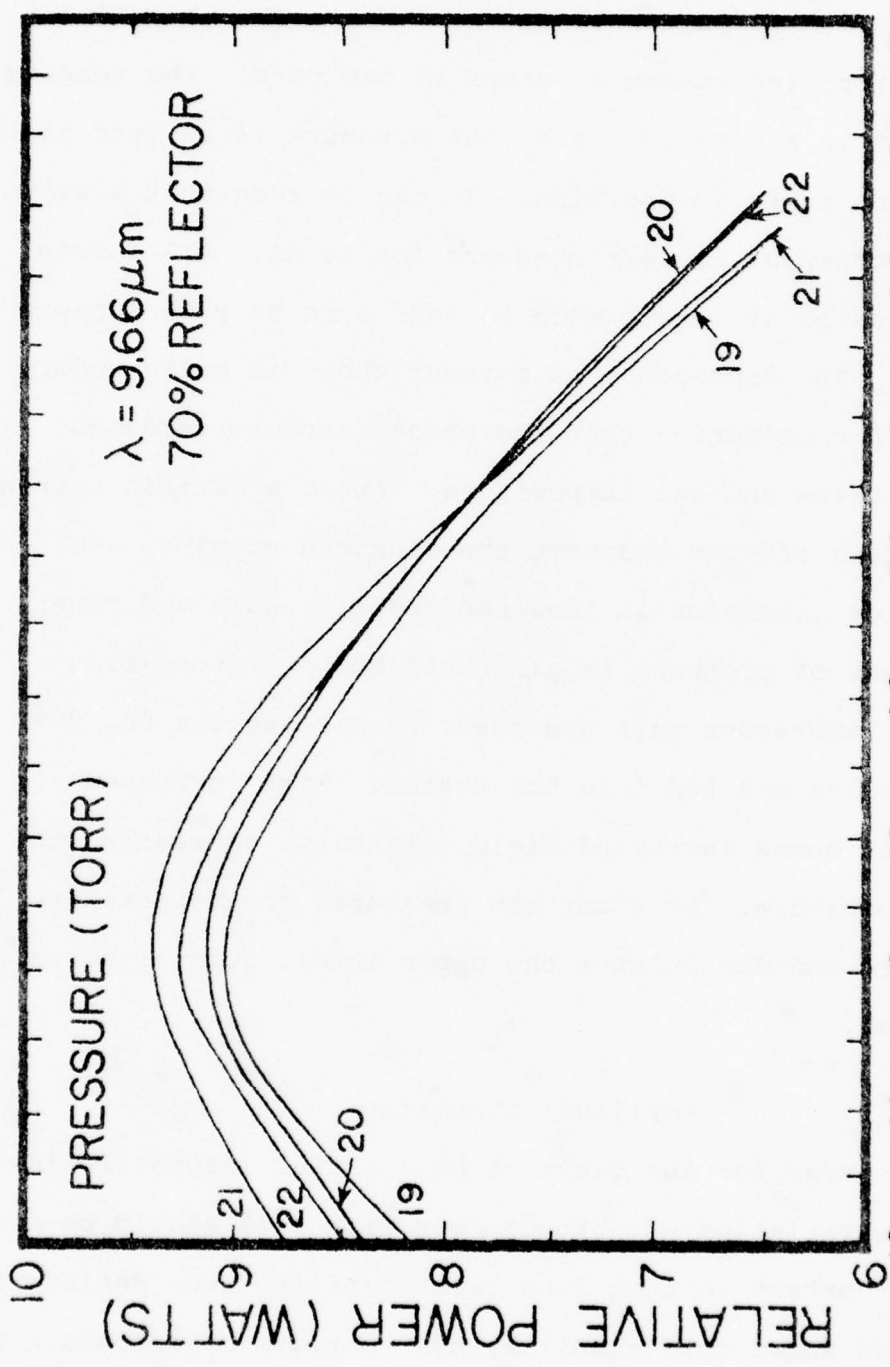

Fig. 10--Relative Power vs. Current for Several Pressures.

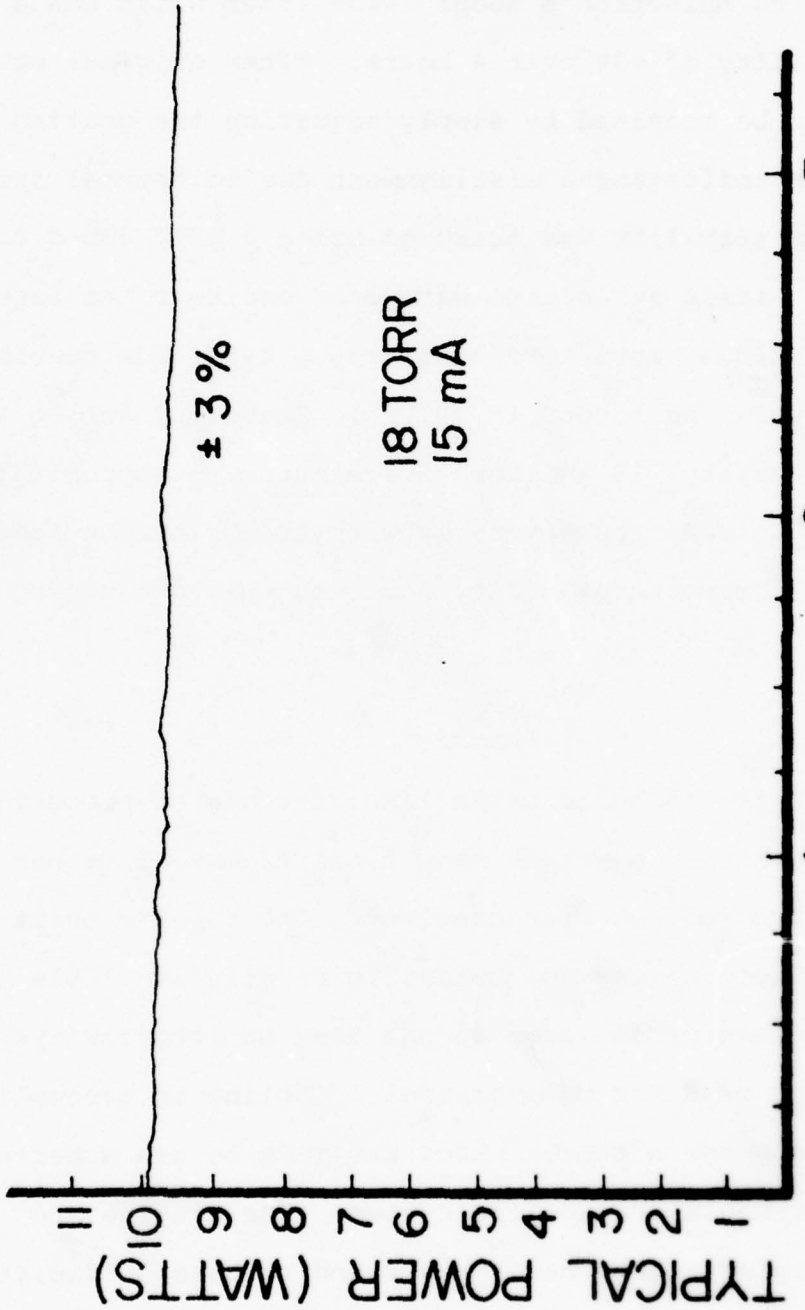

Fig. 11--Power vs. Time, Long-Term Stability.

term stability of about ±3%. This stability has been maintained for periods of 5 hours and longer. This compares very well to Molectron's Model IR250 laser which has a long term stability of ±3% over 4 hours. Often original power levels can be regained by simply adjusting the grating micrometer indicating a misalignment due to thermal drifts. Short term stability was measured using a gold doped Ge detector. After an initial warmup of one hour the laser reached maximum short term stability. Amplitude stability for less than one second is ±0.75%. Stability for 30 seconds is approximately ±1% and for five minutes is approximately ±1.5%. This compares favorably with the Molectron Model IR250 which reports stability for less than one second of ±0.5%.

Summary

A working carbon dioxide laser capable of producting over ten watts of power on many lines from 9-11 μm has been constructed and characterized. The tube is built with the best designs and materials readily available. The tube diameter is large enough that an intracavity iris can be used for mode control. Cooling is accomplished using tape water although plans are made to use a better, variable temperature cooling system. The grating and output coupler mounts have been found to have sufficient precision and reproducibility.

Measurements on wavelength selectibility show that the number of lines available compares well with commercial lasers. Left on one line, the grating assembly allows for excellent reproducibility after turning the laser on and off several times. Varying the pressure and current had not noticeable effect on line selectability. The overall power of the strongest lines was less than can be obtained in commercial lasers. All the power versus wavelength curves, except the one centered on 10.6 μ, gave the expected results. A lack of power was noted around 10.6 μ. It is suspected that it may be a grating related problem. Trying a new grating will supply more information on this problem.

Varying the current and pressure and noting the output power showed that the maximum power output for the 12.5 mm ID tube was for 21 torr and 16 mA. This is the behavior that was expected. It would be desirable to have output couplers of differing reflectivities to use in the power measurements so that the reflectivity could be optimized for the other optimized parameters.

Long term stability for periods of over five hours has been achieved that equals that of commercial lasers. The stability and line selectibility are the features of the laser that compare most favorable with commercial lasers available.

B. Installation and Operation of Electro-Optic Switch

Electro-Optic devices are very attractive for beam chopping. Currently we are installing one that will provide variable laser beam pulse widths from about 50 nsec to 5 μsec. With this device we shall be able to directly measure the energy relaxation time of the electron gas that is controlled by acoustic phonon processes. These time scales sometimes approach hundreds of nsec.

The difficulty in operation has been in removing the unwanted signals produced by the radiation emmitted during the fast rise and fall times of the voltage pulse applied to the electro-optic device. We think that this can be solved by proper shielding and termination techniques.

VII. CO-LASER INDUCED HEATING OF THE ELECTRON GAS IN n-InSb

Absorption in InSb in the 5 μm region is interesting, since it involves a variety of processes such as interband and impurity level transitions, as well as free carrier absorption. In fact, it was pointed out by Dr. A. Miller in an invited talk ("Nonlinear Effects Induced by Lasers") at the 14th International Conference on the Physics of Semiconductors. Edinburg, Scotland that the origin of the absorption tail below the band gap of InSb has not been resolved.[20] The laser-induced hot electron effects which we are investigating involve these absorption processes. In fact, we shall show in this section that laser induced hot electron studies provide an alternative means of unraveling the nature of the absorption near the band gap of InSb.

As described earlier, the SdH effect can be used to determine the electron temperature of the heated electron gas. The results of our first study on CO laser heating in a sample of concentration $\simeq 10^{15}$ cm^{-3} are presented in Figure 12. A model consisting of a valence band, conduction band, and an acceptor level lying 7-10 meV above the valence band is shown to adequately describe these results. The effects of free carrier absorption are negligible compared to those of direct interband and acceptor level absorption processes. Photoexcited

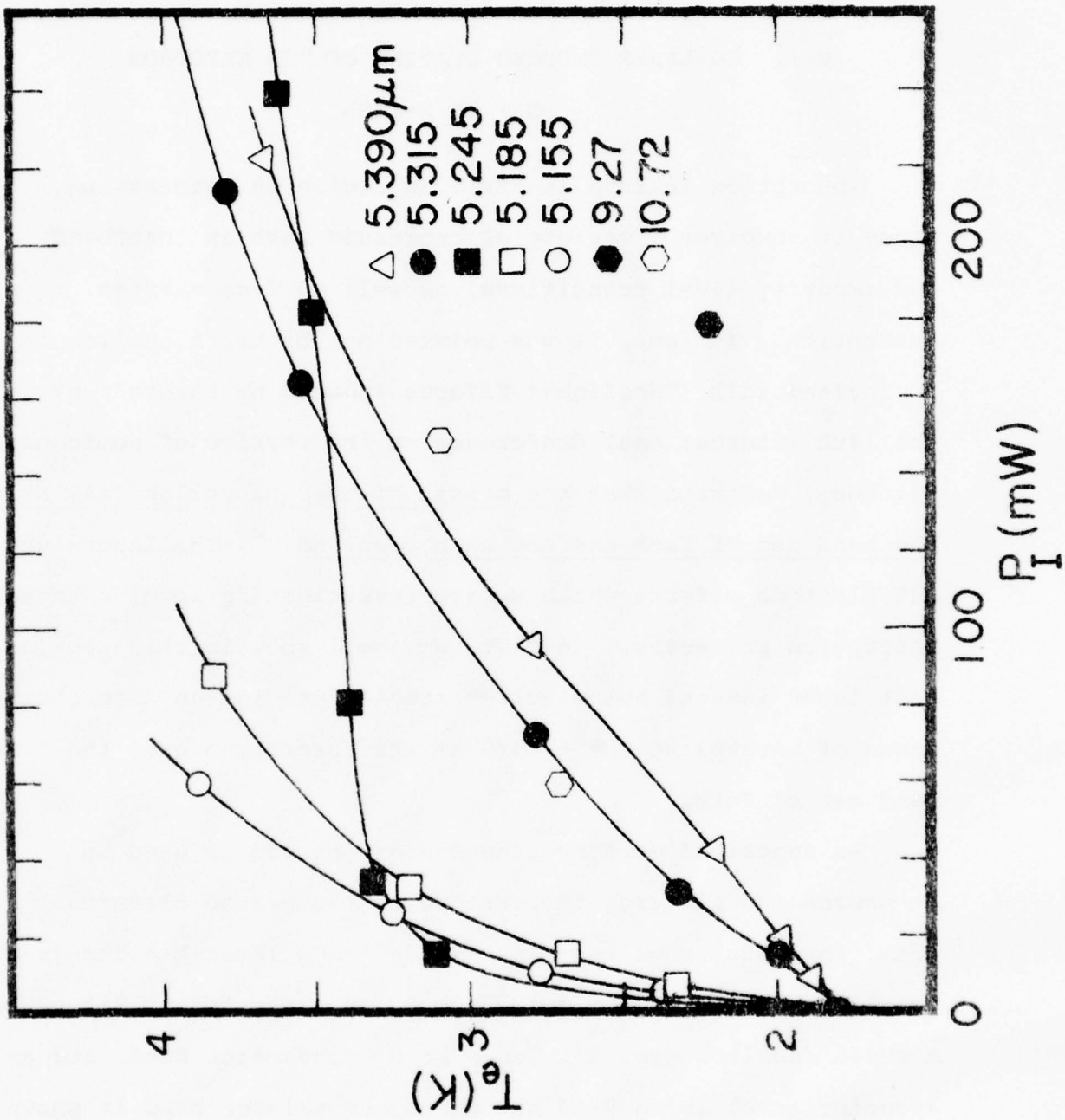

Fig. 12--Variation of electron temperature T_e with peak incident laser power P_I for several different CO laser wavelengths. Also shown are several data points obtained for CO_2 laser heating.

electrons are created with an excess energy ΔE above the Fermi energy, E_F, by impurity level or interband transitions. These photoexcited electrons then heat the carriers in the conduction band via carrier-carrier scattering resulting in a quasi-equilibrium state with an increased electron temperature T_e.

The 5.39 and 5.315 μm wavelengths used correspond to photon energies of 230.2 and 233.5 meV respectively. The pertinent features of these impurity-to-band transitions are shown in Fig. 13. These photon energies are sufficient to stimulate transition from the acceptor level (but not the valence band) to the conduction band. The value of T_e is seen to rise with P_I since the number of photoexcited electrons and hence the amount of electron heating is increased as P_I is increased. T_e finally appears to level off due to depletion of the acceptor level (as there are only about 10^{13} uncompensated acceptors), the change in concentration of a 10^{15} cm^{-3} n-type sample is limited to approximately 1%. The value of T_e is higher for the higher photon energy line for a fixed P_I since the excess energy ΔE is greater, so more heating occurs.

The photon energy of the 5.245 μm wavelength is 236.6 meV and is sufficient to excite acceptor level transitions but falls just short of being energetic enough to excite direct interband transitions at T_e = 1.8 K. Electrons excited from the impurity level have a larger excess energy than in the 5.315 μm case and therefore substantial heating of the electron gas occurs for small incident laser powers. However, as the electron

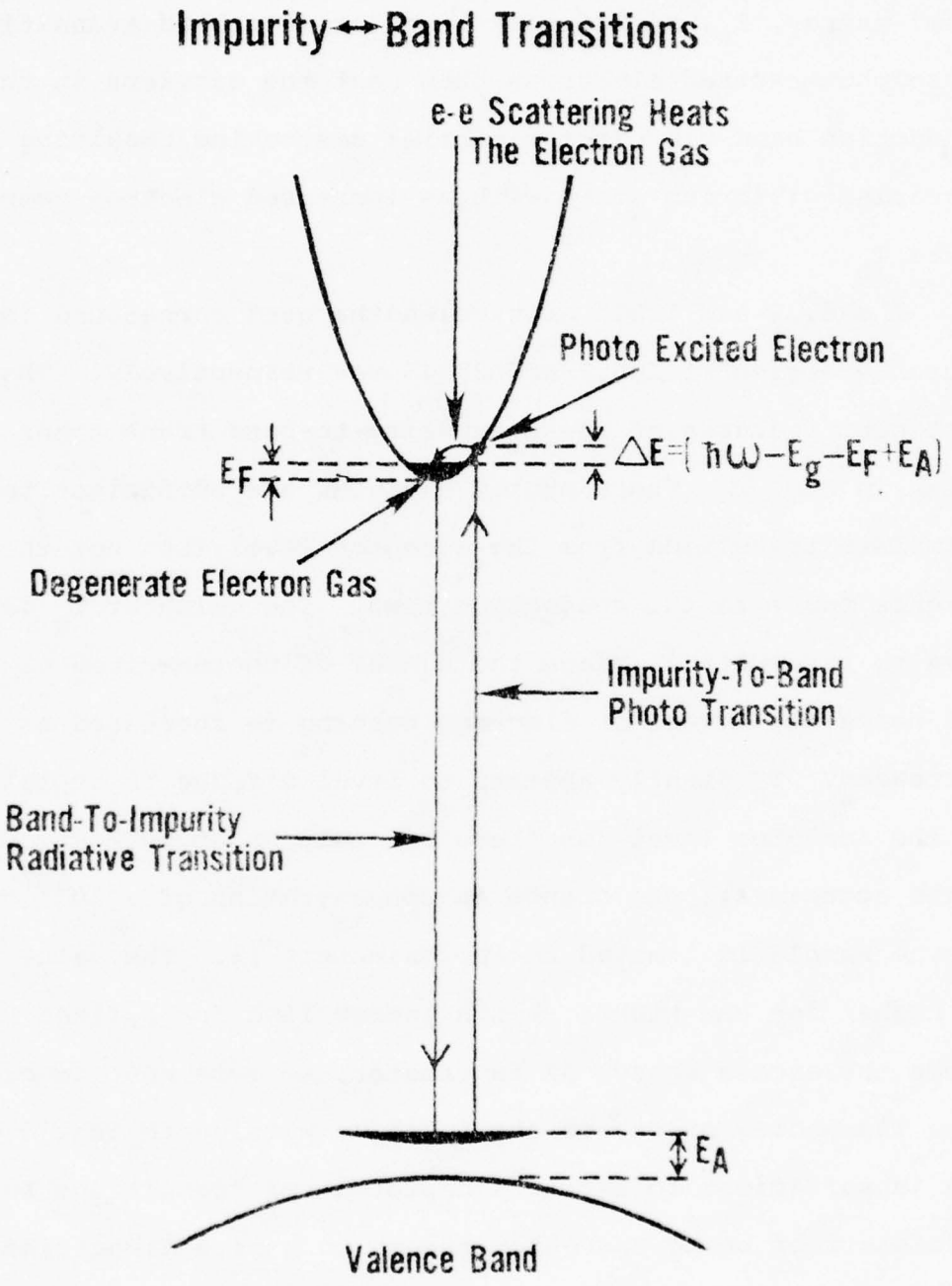

Fig. 13--Schematic depiction of impurity-to-band photo-transition and band-to-impurity radiative transition.

gas is heated, the electron distribution function or the occupied density changes so that states are made accessible for direct interband transitions. These case is shown schematically in Fig. 14. Hence, initially at lower electron temperatures no direct transitions could take place, but after heating of the electron gas by the photoexcited electrons produced from the acceptor level, these transitions become possible. However, the electrons excited from the valence band have very little excess energy and thus make no significant contribution to the electron temperature. Thus, the electron temperature is seen to rise quickly and then level off as the acceptor levels are depleted and interband transitions commence.

This interpretation of the variation of the electron temperature with peak incident laser power is also confirmed by the observed changes in SdH period at 5.245 μm. The electron concentration (as determined by the SdH period) remains constant until the electron temperature reaches about 3.3 K at a peak laser power of ≃40 mW. Thereafter, the electron concentration increases with laser power. There is about a 25% increase in concentration when the laser power is increased from 40 mW to 240 mW, even though the electron temperature remains fairly constant over this range.

The two shortest wavelengths studied (5.185 and 5.155 μm) have photon energies of 239.3 and 240.7 meV which are sufficient to excite direct interband transitions with a significant ΔE remaining as well as acceptor level transitions. The absorp-

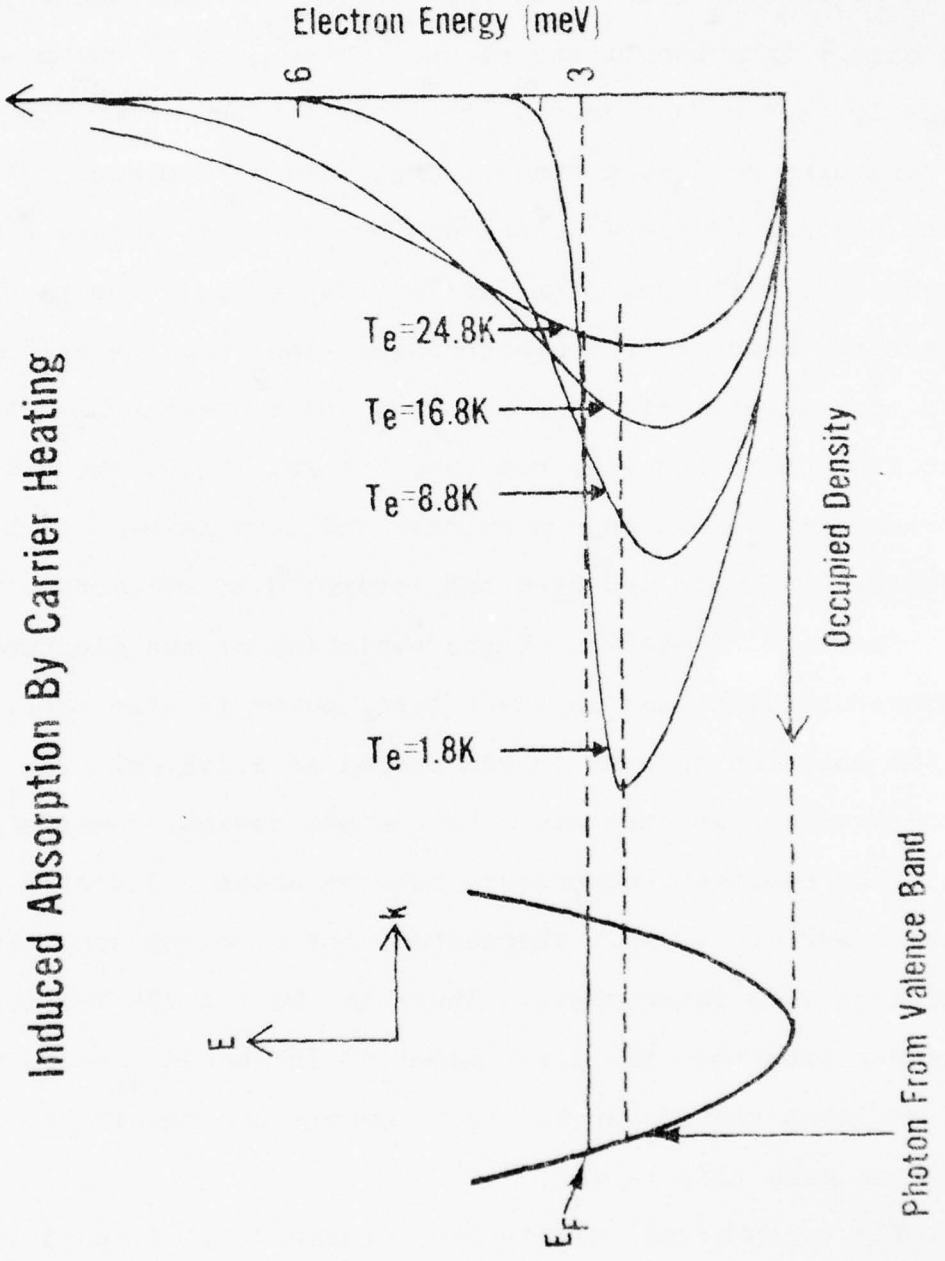

Fig. 14--Schematic presentation of induced absorption by carrier heating.

tion coefficient here becomes extremely large, so that the sample is probably no longer uniformly illuminated through its entire thickness. Instead, the radiation is absorbed almost entirely in the first part of the sample resulting in intense carrier heating there. Consequently, T_e shows a rapid rise to high values for relatively small P_I.

The optical heating data presented here can be compared to that which is obtained using only pulsed, dc electric fields to heat the carriers. The increase of electron temperature with applied electrical power is controlled by energy loss rates of the conduction electrons to the lattice from some combination of deformation-potential, piezoelectric, or polar-optical phonon scattering. We find that it takes an applied electric field of ≃70 mV/cm to heat the conduction electrons up to an electron temperature of 5 K with the lattice at a temperature of 1.8 K. In contrast, the increase of electron temperature in the optical case is controlled by absorption and recombination processes, as well as the above energy loss rates.

In summary, Shubnikov-de Haas experiments have been used to determine the increase in temperature of the electron gas in InSb irradiated by a CO laser. The dependence of the electron temperature upon incident laser power and photon energy is shown to provide information on the absorption processes in InSb in the vicinity of the band gap.

VIII. CO_2-LASER INDUCED HEATING OF THE ELECTRON GAS IN InSb

A. Extraction of Mobility Values from Photoconductive Voltage Measurements

The illuminated region of the model shown below has a different conductivity than that of the nonilluminated regions, namely $\sigma = \sigma_o + \Delta\sigma$ where σ_o is the conductivity of the nonilluminated regions and $\Delta\sigma = \sigma - \sigma_o$.

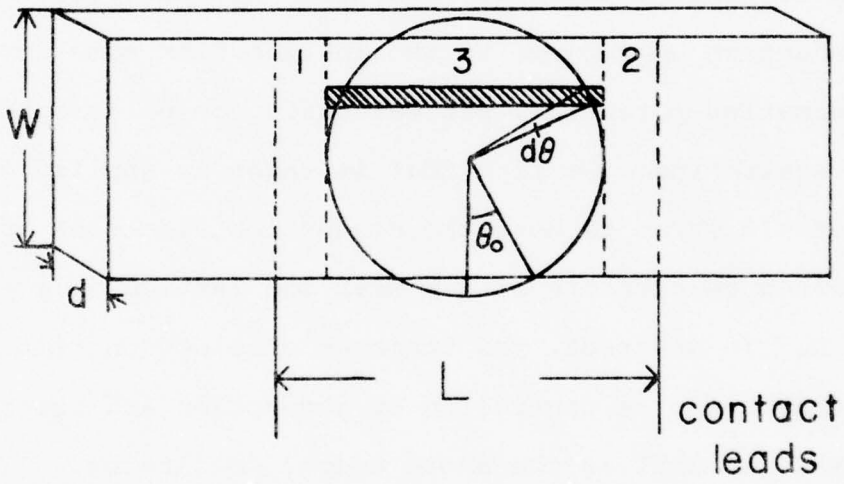

The voltage drop V_p read off of the oscilloscope is the difference between the voltage drop with illumination and without illumination. In terms of the geometry of the sample V_p can be calculated in the following manner. The resistance of the shaded area above is added in series:

$$R_{sliver} = R_{ill} + R_{dark} = \frac{2}{\sigma d\, d\theta} + \frac{2\ (1-\sin\theta)}{\sigma_o\, d\, \sin\theta\ d\theta} \qquad (1)$$

Adding the slivers of area 3 in parallel and integrating:

$$\frac{1}{R_3} = \int_{\theta_o}^{\pi-\theta_o} \frac{1}{\frac{2}{\sigma d\ d\theta} + \frac{2\ (1-\sin\theta)}{\sigma_o\ d\ \sin\theta\ d\theta}}$$

$$= \frac{\sigma_o d}{2} \int_{\theta_o}^{\pi\ \theta_o} \frac{\sin\theta\ d\theta}{1 - \frac{\Delta\sigma}{\sigma}\sin\theta} \qquad (2)$$

where $\frac{\Delta\sigma}{\sigma} = 1 - \frac{\sigma_o}{\sigma}$ and $\theta_o = \cos^{-1}\left(\frac{W}{2r}\right)$. Making the approximation that $\frac{\Delta\sigma}{\sigma} << 1$, approximates the quantity

$$(1- \frac{\Delta\sigma}{\sigma}\sin\theta)^{-1} \simeq 1 + \frac{\Delta\sigma}{\sigma}\sin\theta \quad .$$

The integral now becomes:

$$\simeq \frac{\sigma_o}{2} \int_{\theta_o}^{\pi-\theta_o} \sin\theta\ (1 + \frac{\Delta\sigma}{\sigma}\sin\theta)\ d\theta \quad , \text{ so that finally}$$

$$\frac{1}{R_3} \simeq \sigma_o d\left[\cos\theta_o + \frac{\Delta\sigma}{2\sigma}\left(\frac{1}{2}\pi - \theta_o + \sin\theta_o\cos\theta_o\right)\right] \quad . \qquad (3)$$

The resistances of areas 1 and 2 are both:

$$R_1 = R_2 = \frac{L - 2r}{2\sigma_o Wd} \quad . \qquad (4)$$

Adding the areas 1, 2, and 3 in series the final total resistance of the illuminated sample between the contact leads is:

$$R_{ill} = \frac{1}{\sigma_o d}\left[\frac{1}{\cos\theta_o + \frac{\Delta\sigma}{2\sigma}\left(\frac{\pi}{2} - \theta_o + \frac{1}{2}\sin 2\theta_o\right)} + \frac{L - 2r}{W}\right] \qquad (5)$$

The sample's resistance between contacts without illumination (R_{dark}) is

$$R_{dark} = \frac{1}{\sigma_o} \frac{L}{Wd}$$

The difference in resistance is thus

$$\Delta R = R_{ill} - R_{dark} \quad ,$$

which produces a change in the voltage drop across the leads. This change in voltage, defined as V_p, leads to the following relationship:

$$V_p = I\Delta R$$

$$\simeq \frac{I}{\sigma d}\left\{\left[\cos\theta_o + \frac{\Delta\sigma}{2\sigma}\left(\frac{\pi}{2} - \theta_o + \frac{1}{2}\sin 2\theta_o\right)\right]^{-1} + \frac{L-2r}{W} - \frac{L}{W}\right\} . \quad (6)$$

By simplification and expansion we have:

$$V_p \simeq - \frac{I}{2d\cos^2\theta_o} \frac{\Delta\sigma}{\sigma_o \sigma}\left[\frac{\pi}{2} - \theta_o + \frac{1}{2}\sin 2\theta_o\right] \quad , \quad (7)$$

where $\Delta\sigma = \sigma - \sigma_o$ and I is the constant current through the sample. Note that when $\Delta\sigma = 0$, $V_p = 0$. The photoconductive voltage when $\theta_o = 0$ or $(W = 2r)$ is:

$$V_p = - \frac{\pi}{4} \frac{I}{d} \frac{\Delta\sigma}{\sigma_o \sigma} \quad , \quad (8)$$

which agrees with Hattori et.al.[21] Now

$$\frac{\sigma}{\Delta\sigma} = \frac{\mu}{\Delta\mu} \simeq \frac{I\left[\frac{\pi}{2} - \theta_o + \frac{1}{2}\sin 2\theta_o\right]}{V_p 2\sigma d\cos^2\theta_o} \quad , \quad (9)$$

and

$$\frac{\Delta\sigma}{\sigma_o} = \frac{\Delta\mu}{\mu_o} \simeq \frac{1}{\frac{I\left[\frac{\pi}{2} - \theta_o + \frac{1}{2}\sin 2\theta_o\right]}{2\sigma_o V_p d\cos^2\theta_o} - 1} \quad . \quad (10)$$

Thus the mobility ratio defined as

$$\frac{\mu}{\mu_o} = \frac{\mu}{\Delta\mu} \cdot \frac{\Delta\mu}{\mu_o} \quad ,$$

is given by

$$\frac{\mu}{\mu_o} \simeq \left[1 - \frac{2V_p\sigma_o d \cos^2\theta_o}{I\left(\frac{\pi}{2} - \theta_o + \frac{1}{2}\sin 2\theta_o\right)}\right]^{-1} \tag{11}$$

This is the mobility ratio for when the beam diameter is greater than the sample height (W). For the case in which the beam diameter is equal to the sample width ($\theta_o = 0$), the mobility ratio is

$$\frac{\mu}{\mu_o} = \frac{1}{1 - \frac{4V_p\sigma_o d}{\pi I}} \quad . \tag{12}$$

B. Photoconductivity

InSb is a well-known photoconductive material often used for detecting electromagnetic radiation via several types of electronic transitions. [22-25] Alternatively, photoconductivity measurements have been utilized for obtaining information on properties of InSb such as two-photon absorption rates, [26] donor impurity levels, [27-30] LO phonon energies, [31-32] and energy band parameters. [33] To a small extent, hot carrier effects generated by dc electric fields have even been found in the photoconductivity. [34] However, we know of no attempt to use the free carrier absorption induced photoconductiviy to investigate photo-heated electrons at the 10 μm wavelengths of the CO_2 laser.

Free carrier absorption processes at 10 μm wavelengths result in very small absorption coefficients in low concentration samples of InSb. Consequently, quantitative information about the laser-induced heating process is not available because experiments have been difficult to carry out. In this section we describe the first measurements of the electron temperature from photoconductivity measurements that describe quantitatively how the CO_2 laser affects the degenerate electron gas in a sample of concentration $\simeq 1 \times 10^{15}$ cm^{-3}.

Figure 15 shows a block diagram of the equipment used in these experiments. The sample, immersed in liquid helium in a variable temperature optical dewar, was illuminated with a laser pulse produced by mechanically chopping a beam (TEM_{00} mode) from a grating-tuned cw CO_2 laser which provided single line outputs of several watts from ~9.2 μm to ~10.9 μm. Typical

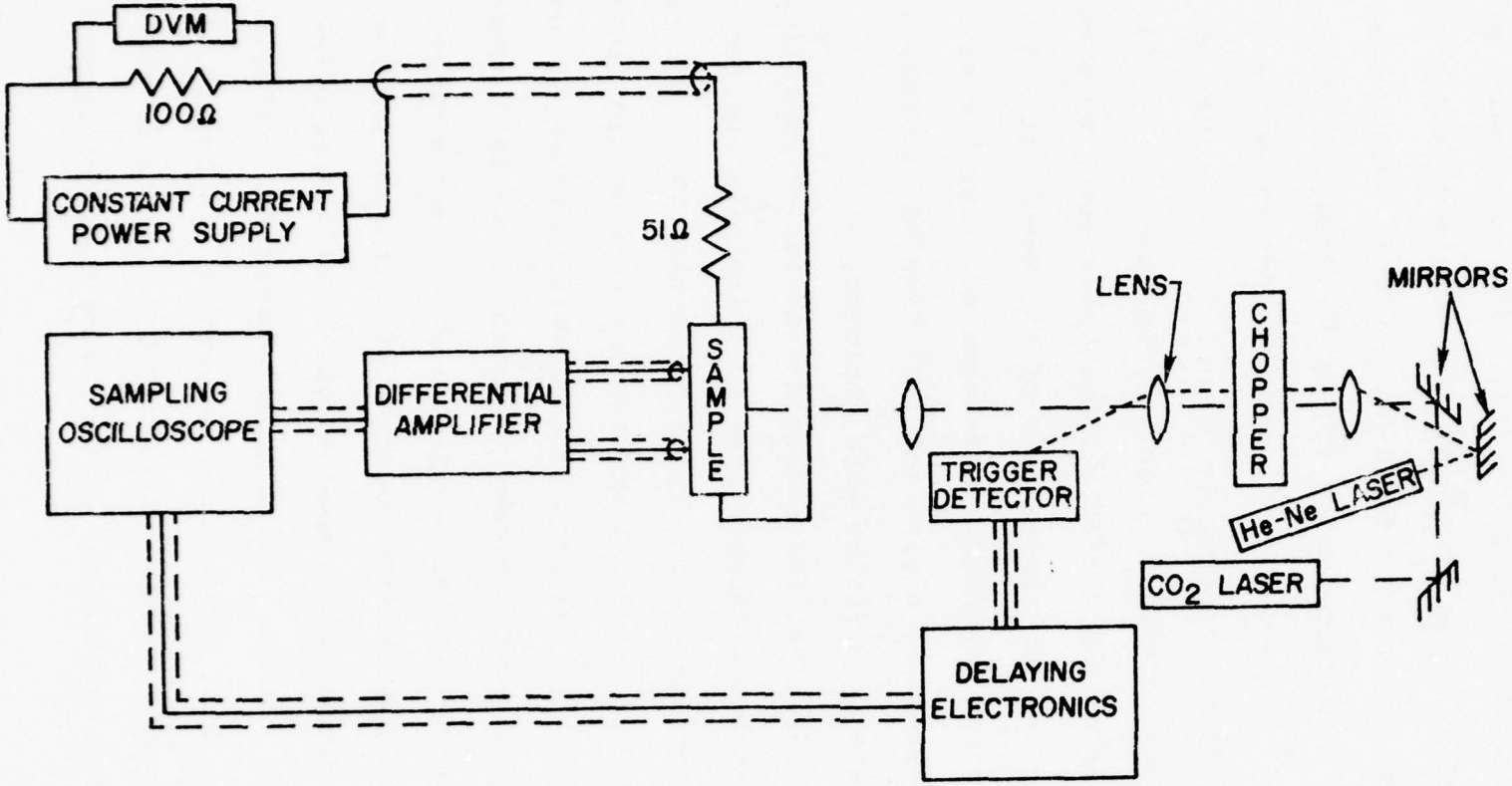

Fig. 15--Block diagram of experimental apparatus used in investigating the CO_2 laser-induced photoconductivity.

short term amplitude stability of this cw CO_2 laser as measured by a gold-doped germanium detector is ~±1%, with the longer term (4-8 hours) stability being ~±4%. The laser pulse width could be varied by using different slot widths on the chopper blade. The repetition rate could be varied by using blades with different numbers of slots and by changing the blade rotation speed. To avoid sample lattice heating by the laser the duty cycle of the chopper was kept below 3%. Even so, at the highest laser powers, a large pumping rate and liquid helium flow rate of the variable temperature dewar were needed to maintain the lattice temperature of the sample at 1.8 K.

In the present experiments, a laser pulse with a width of ~20 μsec (F.W.H.M.), a rise and fall time of ~2 μsec, and a repetition rate of ~1700 Hz were employed.

The laser pulse was focused to a diameter of approximately 1.8 mm at the sample and positioned to illuminate the region of the sample between the potential contacts. The laser spot size was determined using a 1 mm diameter hole mounted in the plane of the sample. The ratio of transmitted power through a 1 mm hole to the power transmitted without the hole gives a measure of the spot size, assuming a known beam profile. We ascertain the spatial beam profile with thermal imaging plates, and by scanning the beam across a small area detector using a rotating mirror. The optical components, including an intra-cavity iris, are aligned to produce a Gaussian beam profile. Calibrated filters of either CaF_2 sheets or sheets of Teflon or some conbination of both were used for beam attenuation.

Figure 16 shows a plot of the photoconductive voltage V_p as a function of dc bias current I through the sample for several different laser powers P_I incident on the sample. The negative sign means that the mobility increases with incident laser power. The linear behavior is understandable on the basis of a detailed analysis of the photoconductivity At high currents, a nonlinear behavior is observed which is attributed to either nonohmic electric field behavior or to lattice heating (since pulsed-current techniques were not used). We restrict all our measurements to a dc bias current of 2 mA which is way below this nonlinear region.

Figure 17 shows a plot of the photoconductive voltage V_p versus P_I the peak incident laser power for two different laser wavelengths. Again at low laser powers V_p seems to follow a linear behavior with P_I. At higher laser powers some deviations from linearity is observed. Using these voltages, the sample dimensions and lead placement positions, and the laser beam width one can then calculate the mobility of the sample region illuminated by the laser.

Figure 18 shows comprehensive results obtained from three separate experiments on how the mobility changes with (1) applied electrical power P_E (obtained from electrical heating experiments as $e\mu E^2$) as shown in Fig. 2(a); (2) lattice temperature T_L as shown in Fig. 2(b); and, (3) incident laser power P_I as shown in Fig. 2(c). The electron concentration is determined to be 1.4×10^{15} cm^{-3} from the period of Shubnikov-de

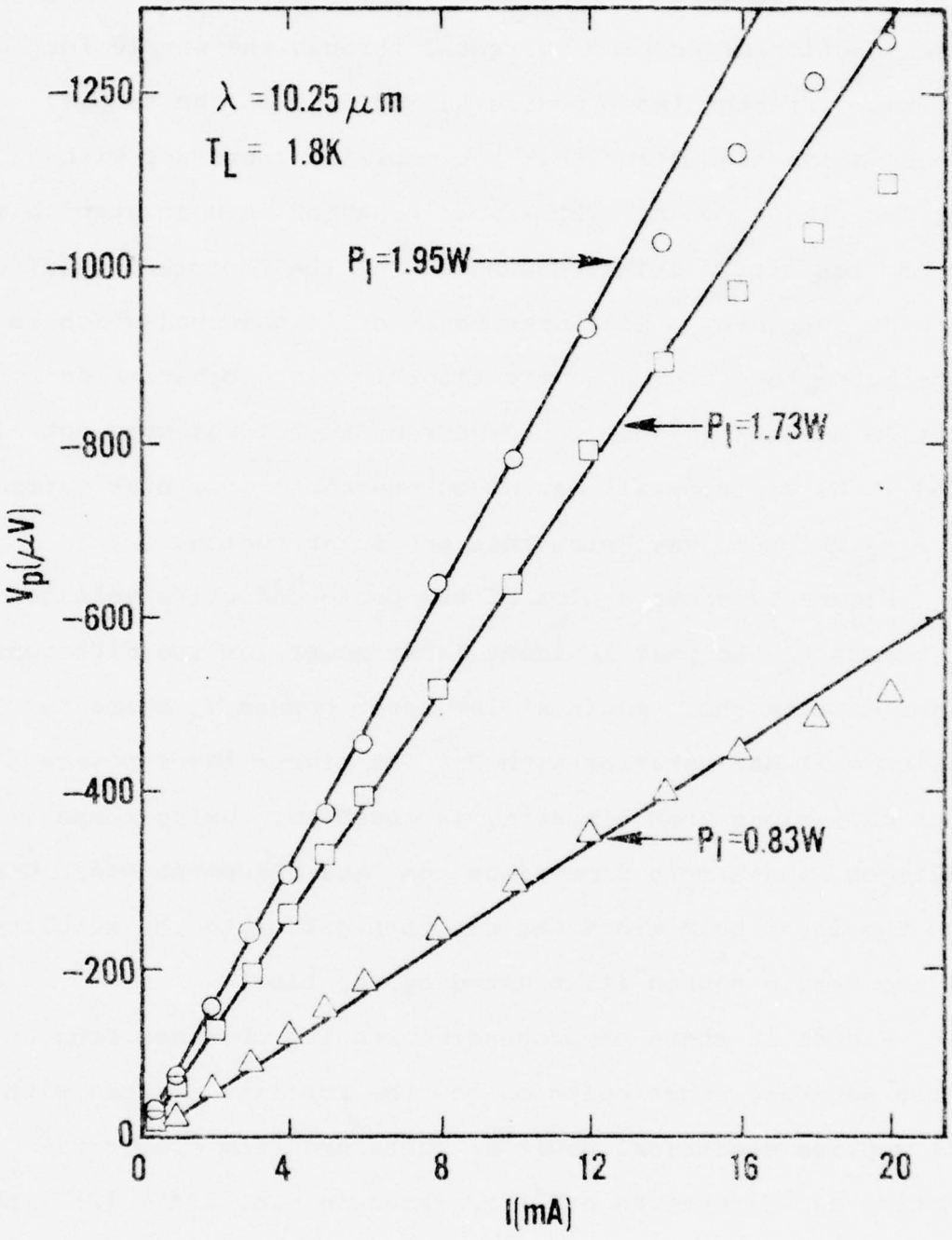

Fig. 16--Photoconductive voltage V_p versus dc bias current I through the sample for various peak incident laser powers.

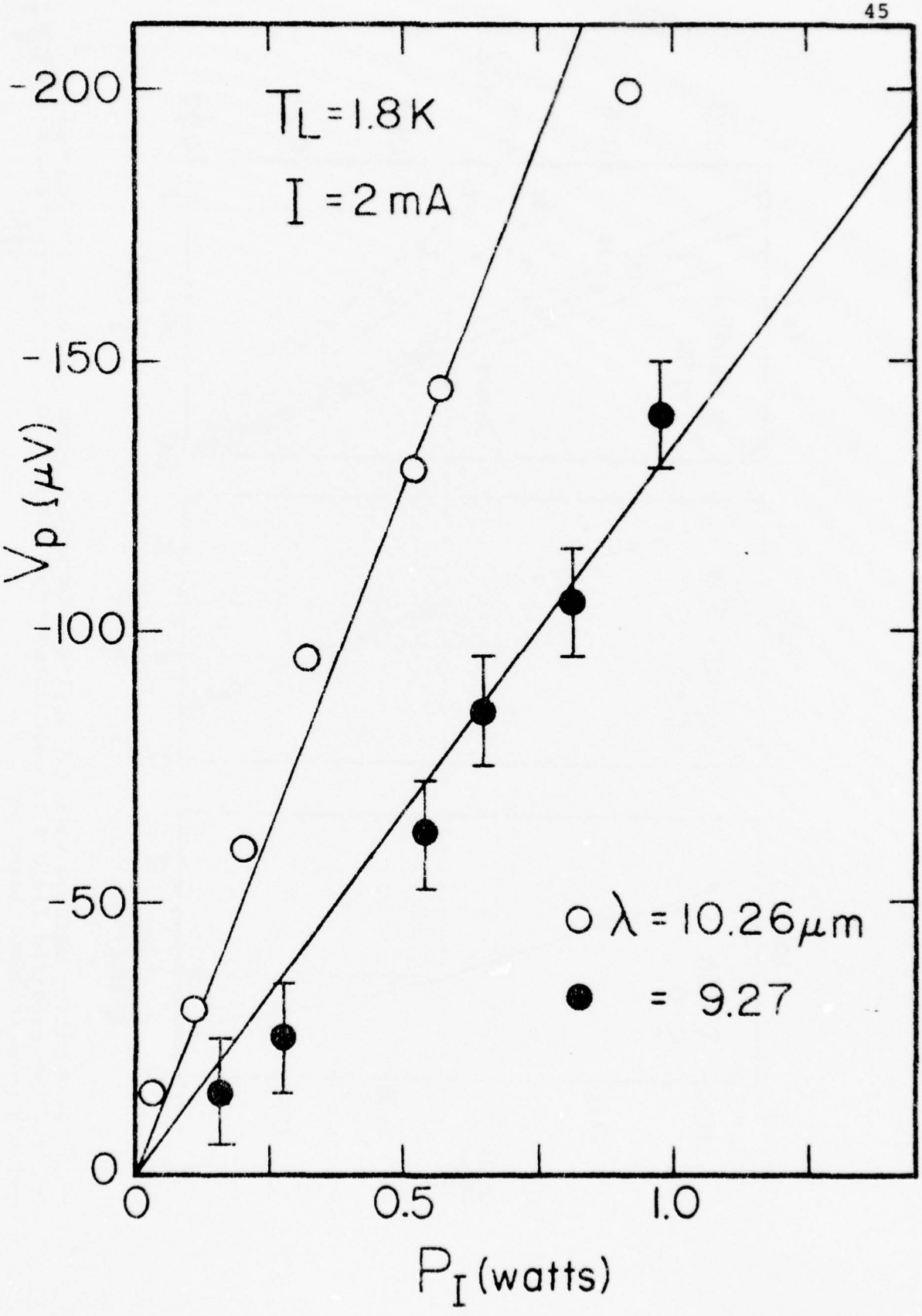

Fig. 17--Photoconductive Voltage V_p versus peak incident laser power P_I at the CO_2 laser wavelengths of 10.26 and 9.27 μm.

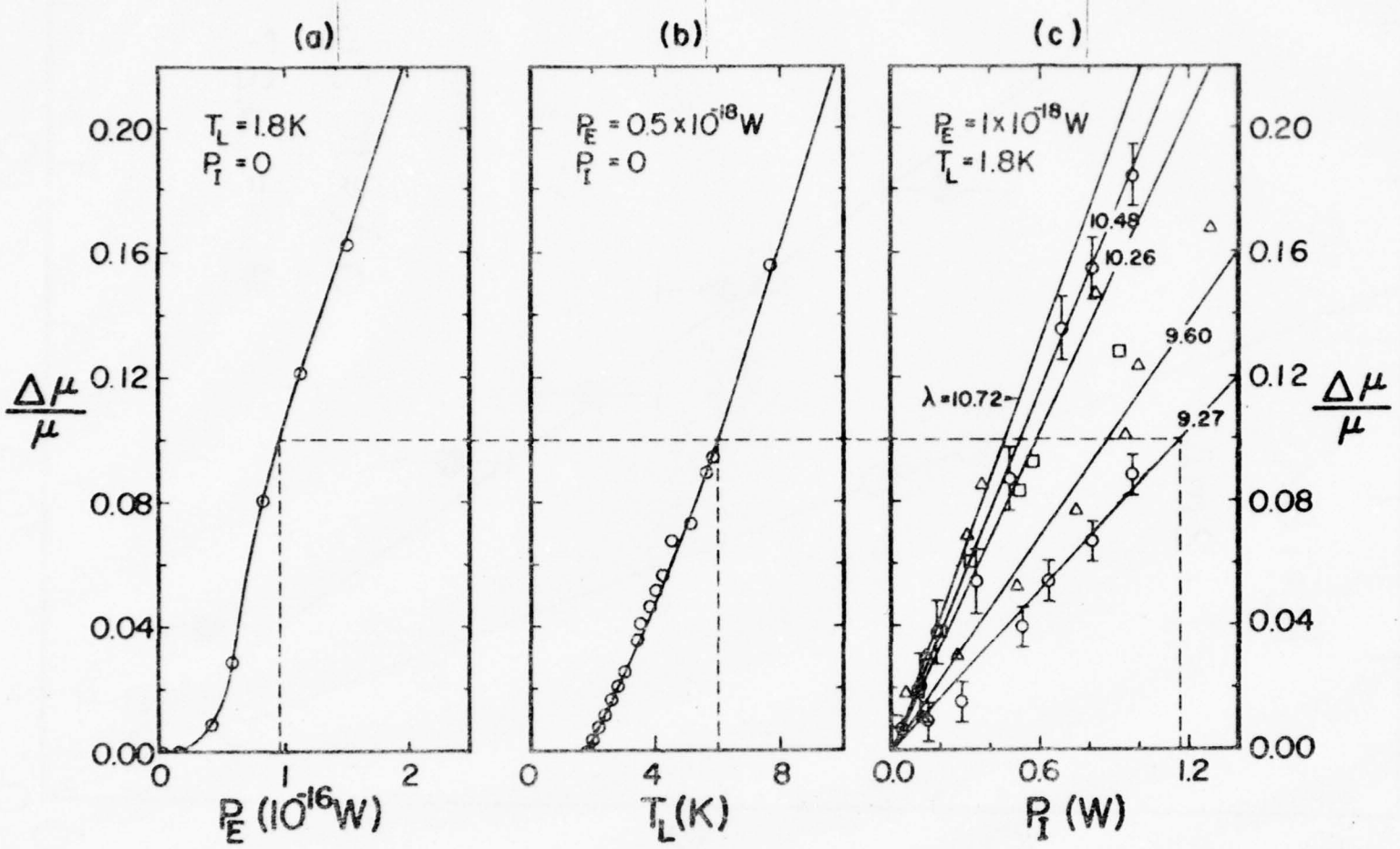

Fig. 18--Mobility changes with (a) applied electrical power per electron P_E (which for a given electric field E is calculated from $e\mu E^2$), (b) lattice temperature T_L, and (c) peak incident laser power P_I.

Haas (SdH) oscillations and is constant at these lattice temperatures and low laser powers where two photon absorption processes are completely negligible. Consequently,

$$\frac{\Delta\sigma}{\sigma} = \frac{\Delta\mu}{\mu} = \frac{\Delta V}{V_o} \quad , \tag{1}$$

where $\Delta\sigma = (\sigma - \sigma_o)$, $\Delta\mu = \mu - \mu_o$ and $\Delta V = V - V_o$ are the changes in the conductivity, mobility, and voltage drop across the sample leads, as either T_L, P_I or P_E are varied while the other two variables are held constant. The values of σ_o, μ_o, and V_o are determined at zero laser power ($P_I = 0$) under ohmic conditions at a lattice temperature of 1.8 K.

As shown in Figure 18(b), the mobility at $P_I = 0$ obtained using ohmic electric fields increases with lattice temperature which is consistent with completely dominant ionized impurity momentum relaxation.[11] We find $\sigma_o \sim 19.3$ (ohm - cm)$^{-1}$, $\mu_o \sim 8.6 \times 10^4$ cm^2/V sec, in agreement with other experimentally determined mobilities with similar electron concentrations and lattice temperatures.[35,36] At 77 K, σ_o and μ_o rise to 75 (ohm-cm)$^{-1}$ and 3.2×10^5 cm^2/V sec, respectively.

The CO_2 laser radiation is partially absorbed via free carrier absorption processes and subsequently leads to a mobility increase as observed in Figure 18(c) where $\Delta\mu/\mu$ is plotted versus P_I, the peak incident laser power at a constant lattice temperature of 1.8 K. An electron temperature T_e^o can be determined for each wavelength and value of P_I by making a one-to-one correspondence between the mobility changes in the

two cases shown in Figure 18(b) and 18(c). For example, Figure 18(c) shows that for a peak incident power of about 1.6 W, $\Delta\mu/\mu \hat{=} 0.10$, which corresponds to a temperature T_e ~6 K.

The lines shown in Figure 18 are the "best fit" lines through the data points. Consequently, a plot of T_e^o versus P_I can be made as shown in Figure 19. Provided the steady state is controlled by inter-carrier collisions, the carrier distribution will be heated Fermi-Dirac distribution with a true electron temperature T_e which may be identified with T_e^o if the carrier heating maintains the system within the regime dominated by ionized impurity limited mobilities. The steady state remnant excitation pulse at $\varepsilon \sim \hbar\omega + \varepsilon_F$ will have negligible effect on the mobility at our low excitation rates: the low energy carrier assembly is only minutely depleted by photoexcitation.

Electric field heating experiments were carried out at zero laser powers in order to calibrate the amount of optically absorbed power fed into the electron gas. A pulsed dc electric field of 20 μsec duration was used to avoid sample lattice heating so that only the electron gas was heated, while the lattice temperature remained at 1.8 K. Figure 18(a) shows the resultant mobility change versus applied electrical power P_E per electron for the same sample. The extracted effective electron temperatures $T_e^E(P_E)$ may be again identified with the true electron temperature T_e under appropriate conditions. In which case, we may invert the functional relations $T_e^o = T_e^o(P_I)$ and $T_e^E = T_e^E(P_E)$

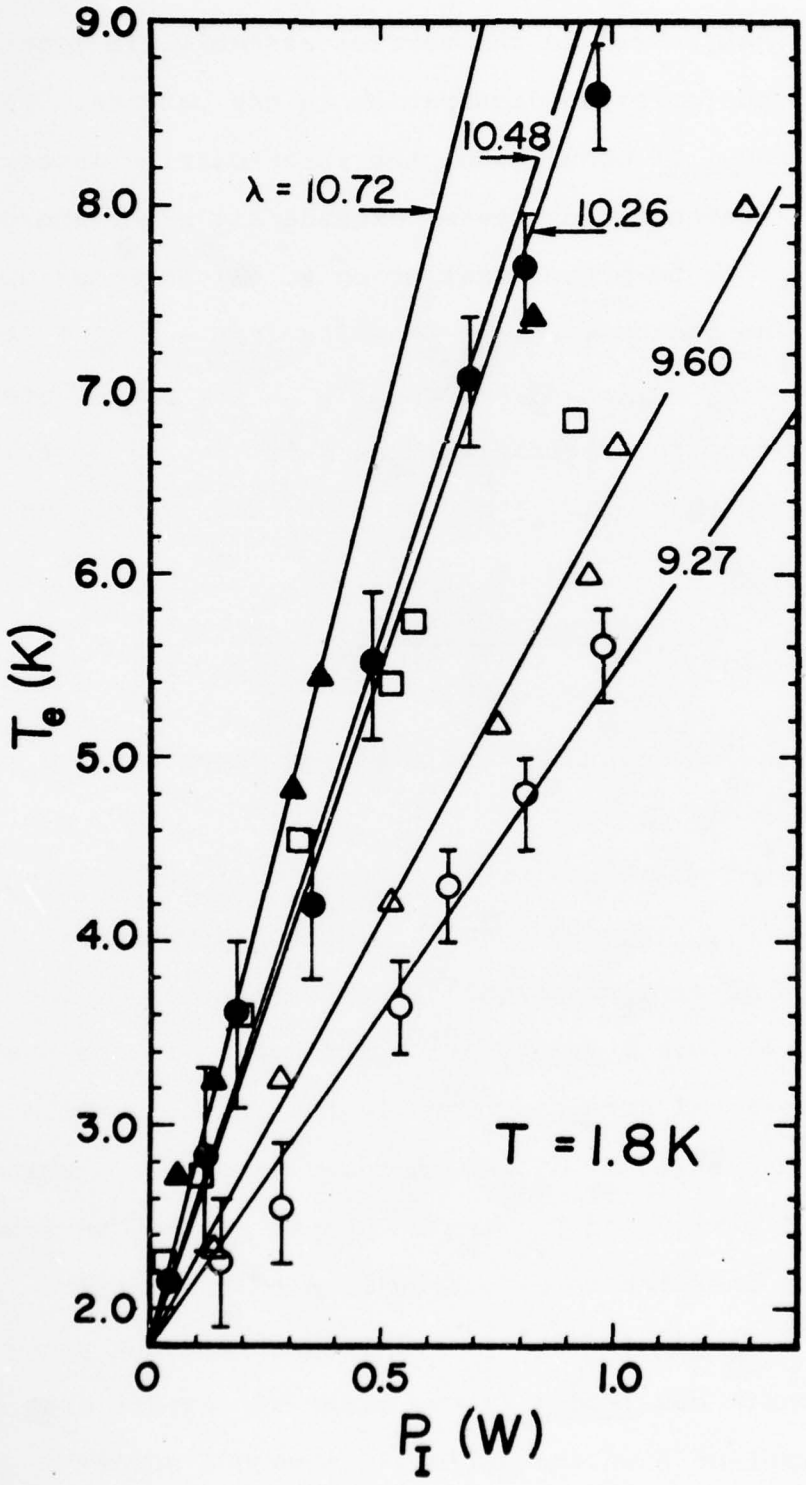

Fig. 19--Electron temperature T_e versus peak incident laser power P_I for various CO_2 laser wavelengths.

to deduce the thermodynamic relationship $P_E = P_a\ (P_I)$ under the constraint $T_e^O = T_e^E = T_e$, where P_a is the portion of absorbed optical power transferred to the carrier assembly via inter-carrier collisions prior to dissipation to the lattice. The extreme case (Model I) occurs when the inter-carrier energy loss rate Γ_{ee} (scattering out term) exceeds all other energy-loss rates Γ_{eph} due to phonon scattering at all energies up to and exceeding the photo-excitation energies ($\sim\varepsilon_F + 4\ k_B\ T_e + \hbar\omega$). In this instance $P_a = \alpha(\lambda)dP_I$, where $\alpha(\lambda)$ is the steady state free carrier absorption coefficient and d is the sample thickness. It follows that $\alpha(\lambda,T_e)$ may be extracted exactly as the ratio:

$$\alpha(\lambda,T_e) = \frac{P_E(T_e)}{P_I(T_e,\lambda)}\ \frac{1}{d} \qquad (2)$$

where we make the wavelength λ and electron temperature T_e dependences explicit.

Our estimates of the critical carrier concentration n_c for which $\Gamma_{ee} >> \Gamma_{eph}$ ensures a valid electron temperature model are based on similar calculations to Stratton [37] but for relaxation againse a degenerate distribution in the presence of Thomas-Fermi screening. While the present sample concentration satisfied $n>>n_c$ for energies $\varepsilon \lesssim \varepsilon_F + \hbar\omega_o$, where ε_F is the Fermi energy and $\hbar\omega_o$ the LO phonon energy, we find $n<n_c$ for higher energies where energy loss to the lattice is controlled by fast polar-mode optical phonon emission processes. In these circumstances (Model II) we might anticipate that a substantial fraction β of the optically absorbed power

$P_a^o = \alpha d P_I$ is transferred to the lattice by optical phonon cascading as the photo-excited electrons scatter to energies below the threshold for which $\Gamma_{eph} > \Gamma_{ee}$. The residual power, $P_a = [1 - \beta(\lambda)]P_a^o$, will then be effective in heating the carriers into a Fermi-Dirac distribution with electron temperature T_e via inter-carrier collisions. The subsequent quasi-thermalized distribution will then lose energy to the lattice via predominantly acoustic phonon processes at the rate $[1 - \beta(\lambda)]P_a^o$. In this case we find

$$[1 - \beta(\lambda)]\alpha(\lambda, T_e) = \frac{P_E(T_e)}{P_I(T_e, \lambda)} \frac{1}{d} \qquad (3)$$

Plots of $P_E(T_e)/P_I(T_e, \lambda)d$ versus λ^2 for the range of available wavelengths indicate an approximately linear variation with values extrapolated to zero wavelength being negative. These non-zero <u>negative</u> extrapolated values are consistent with a <u>non-zero</u> loss factor $\beta(\lambda) \sim 1/\lambda^2$ in the physical regime. The finite width of the excitation pulse $\Delta\varepsilon \sim \varepsilon_F + 4\, k_B T_e$ precludes a strong oscillatory photoconductivity effect ($\beta(\lambda) \sim 1$). Indeed, the presently available spread of photoexcitation energies $\Delta\varepsilon < \hbar\omega_o$ is not sufficient to expose any definite oscillatory structure.

The analysis of Models I and II may be summarized by the general expression

$$\alpha_{eff}(\lambda, T_e) = P_E(T_e)/P_I(T_e, \lambda)d \qquad (4)$$

which relates an effective free carrier absorption coefficient $\alpha_{eff} = \alpha[1 - \beta]$ to experimentally accessible quantities. Model I involves $\beta = 0$. Experimentally, as shown in Figure 20, we find values for α_{eff} in the range 0.005 cm^{-1} - 0.03 cm^{-1} for the electron temperature and wavelength ranges 3.5 - 6 K, and 9.271 - 10.719 μm, respectively. We note that at 10.6 μm typical values for α have been reported in the range 0.3 to 0.6 cm^{-1} for a higher concentration of ~10^{16} cm^{-3} at low temperature. [38] The ratios $\Delta[P_E(T_e)/P_I(T_e,\lambda)d] \equiv \Delta\alpha_{eff}(\lambda,T_e) \equiv \Delta\alpha(\lambda,T_e)$, evaluated at constant wavelength, indicate a weak variation of the true absorption coefficient $\alpha(\lambda,T_e)$ with electron temperature.

C. Shubnikov-de Haas Studies

Shubnikov-de Haas effect studies have been carried out in samples with electron concentrations of ~1 × 10^{15}, ~7 × 10^{15}, and ~2 × 10^{16} cm^{-3}. When a CO_2 laser pulse is incident upon the sample, carrier heating occurs and the amplitude of the SdH oscillations decreases. We have carried out a comprehensive investigation in which the carrier heating in these samples was investigated as a function of incident laser power for various laser frequencies. In addition, electrical heating experiments have also been carrier out in order to determine α_{eff}. Currently we are in the process of analyzing these experiments and thus will report on them next time.

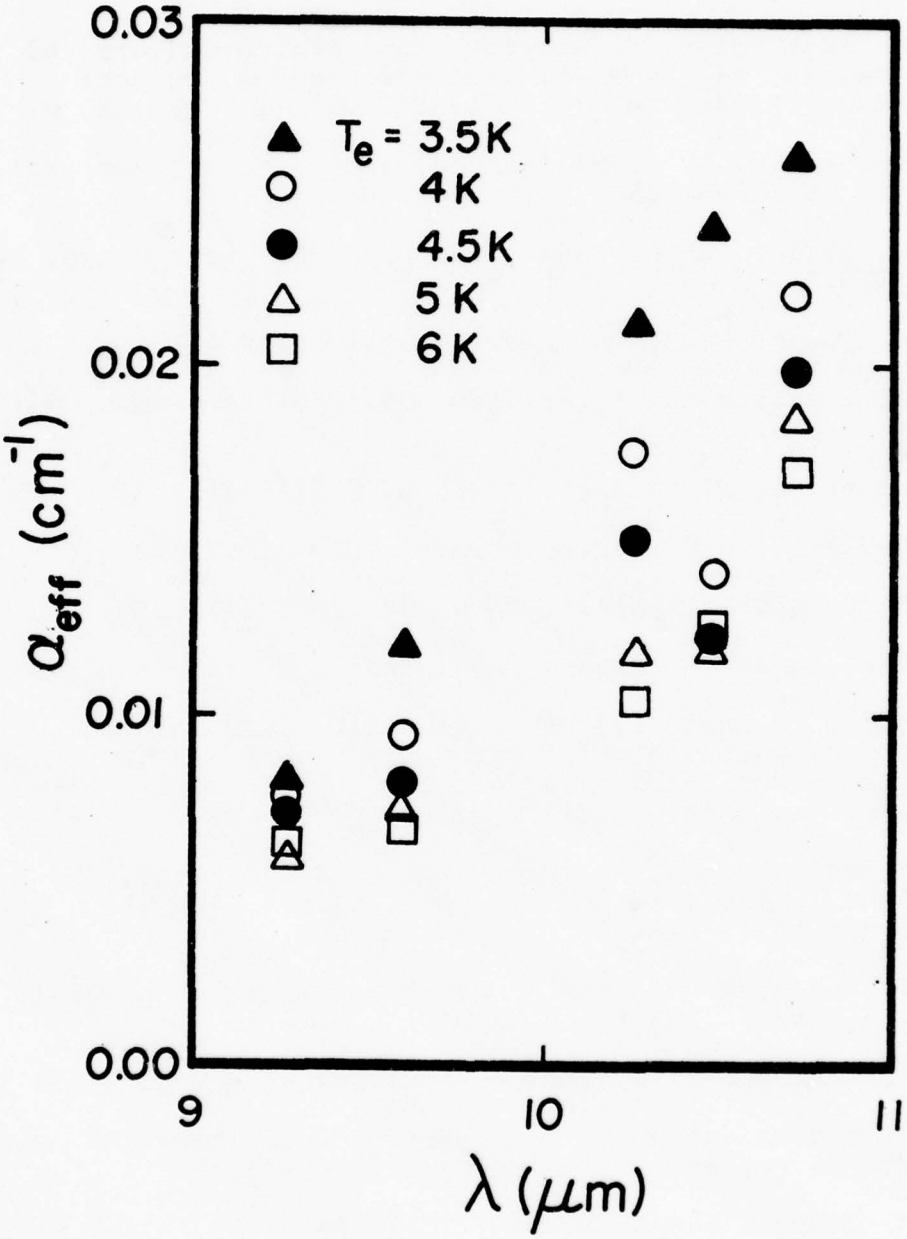

Fig. 20--Effective free carrier absorption coefficient, α_{eff}, versus several wavelengths of the CO_2 laser at various electron temperatures T_e.

IX. REFERENCES

1. A. E. Stephens, D. G. Seiler, J. R. Sybert, and H. J. Mackey, Phys. Rev. B 11(1975)4999.

2. L. M. Roth and P. N. Argyres, in: Semiconductors and Semimetals, ed. by R. K. Willardson and A. C. Beer (Academic Press, New York, 1966), Vol. I, Chap. 6, p. 159.

3. A. Goldstein, S. J. Williamson, and S. Foner, Rev. Sci. Instr. 36 (1965)1356.

4. D. G. Seiler B. D. Bajaj, and A. E. Stephens, Phys. Rev. B 16(1977)2822

5. K. F. Komatsubara, Phys. Rev. Lett. 16(1966)1044.

6. R. A. Isaacson and F. Bridges, Solid State Commun. 4(1966) 635.

7. G. Bauer and H. Kahlert, J. Phys. C 6(1973)1253.

8. H. Kahlert and G. Bauer, Phys. Rev. B 7(1973)2670.

9. G. Bauer and H. Kahlert, Phys. Rev. B 5(1972)566.

10. H. Kahlert and G. Bauer, Phys. Status Solidi 46(b) (1971) 535.

11. A review of these and other electric field induced hot electron experiments is given by G. Bauer in: Springer Tracts in Modern Physics, ed. by G. Höhler (Springer-Verlag, New York, 1974), Vol. 74, p. 1.

12. V. I. Kalushkin, E. A. Protasov, A. G. Rodionov, and N. A. Toloknov, Fiz. Tekh. Poluprovodn. 8(1974)1786 [Sov. Phys. Semicond. 8(1975)1154].

13. L. K. Hanes, M. S. Thesis, North Texas State University, Denton, Texas (1977).

14. H. Kahlert and D. G. Seiler, Rev. Sci. Instrum. 48(1977)1017.

15. G. W. Gobeli and H. Y. Fan, Semiconductor Research, Second Quarterly Report, Purdue University, 1956.

16. E. J. Johnson and H. Y. Fan, Phys. Rev. 139, A1991 (1965).

17. T. S. Moss, G. J. Burrell, and B. Ellis, Semiconductor Opto-Electronics (John Wiley and Sons, New York, 1973) p. 89.

18. N. N. Sobolev, and V. V. Sokovikow, Sov. Phys. Usp. 10 153 (1967).

19. C. K. N. Patel, Sci. Amer. 219, 23 (1965).

20. A. Miller, invited talk presented at 14th International Conference on the Physics of Semiconductors, Edinburg, Scotland, 1978.

21. H. Hattori, O. Fujitani and M. Umeno, J. Phys. Soc. Japan 36, 485 (1974).

22. P. W. Kruse, in Semiconductors and Semimetals, edited by R. W. Willardson and A. C. Beer (Academic Press, New York, 1970), Vol. 5, Chap. 2., p. 15.

23. E. H. Putley, Applied Optics 4, 649 (1965).

24. F. D. Morten and R. E. J. King, Applied Optics 4, 659 (1965).

25. E. H. Putley, Phys. Stat. Sol. 6, 571 (1964).

26. A. F. Gibson, M. J. Kent, and M. F. Kimmitt, Brit. J. Appl. Phys. (J. Phys. D) 1, 149 (1968).

27. R. Kaplan, J. Phys. Soc. Japan Suppl. 21, 249 (1966).

28. R. Kaplan, Applied Optics 6, 685 (1967).

29. R. Kaplan, Phys. Rev. 181, 1154 (1969).

30. F. Kucher, E. Fantner, and G. Bauer, J. Phys. C: Solid State Phys. 10, 3577 (1977).

31. E. Engeler, H. Levinstein, and C. Stannard, Jr., Phys. Rev. Letters 7, 62 (1961).

32. H. J. Stocker. H. Levinstein, and C. Stannard, Jr., Phys. Rev. 150, 613 (1966).

33. R. Grisar, H. Wachernnig, G. Bauer, S. Hayashi, E. Amzallag, J. Wlasak, and W. Zawadski, in Proceedings of the Thirteenth International Conference on the Physics of Semiconductors, Rome, 1976, (Tipografia Marves, Rome, 1976), p. 1265.

34. V. J. Mazurcz, G. U. Ilmenkov, and H. Y. Fan, Phys. Letters 21, 250 (1966).

35. H. P. R. Frederikse and W. R. Hosler, Phys. Rev. 108, 1136 (1957).

36. E. H. Putley, Proc, Phys. Soc. 73, 280 (1958).

37. R. Stratton, Proc. Phys. Soc. A246, 406 (1958).

38. R. B. Dennis, C. R. Pidgeon, S. D. Smith, B. S. Wherret, and R. A. Wood, Proc, R. Soc. Lond. A331, 203 (1972).

X. FUTURE PLANS

A. CO_2 Laser Heating

Continued studies on samples with different electron concentrations will be carried out. In addition, we are in the process of carrying out time-resolved hot electron measurements in order to measure τ_e, the phenomenological energy relaxation time. This will enable a direct calculation of α_{eff} without having to do a parallel electric heating experiment on the sample. Production of higher laser intensities by Q-switching will continue to be a high priority. This will enable us to extend our measurements into regions where the electron gas loses energy to the lattice via optical phonons. The application of the techniques for investigating laser-induced heating can also be applied to investigate other semiconductors of technological importance, such as GaAs. Continued emphasis will be placed on a quantitative theoretical understanding of the hot carrier generation process.

B. CO Laser Heating

The investigation of laser-induced hot electrons in InSb produced with the CO laser promises to be very fruitful in understanding the absorption processes near the band gap region. We shall continue to study the relationship between the absorption processes and the carrier heating. Samples with different electron concentrations and N_A values will be studied. An investigation of the photoconductivity in this complex region will be undertaken. There is also the possibility of observing laser-induced electron cooling effects.

XI. TECHNICAL PERSONNEL

The following persons worked as research associates for this project. Mr. Jim May did theoretical work and computer programing from October 1977 to January 15, 1978. Dr. Anthony Stephens did experimental work on the CO laser project during June and July of 1978.

The following graduate students have worked on various aspects of this research project:

Mr. Delbert Dowdy
Mr. Mike Goodwin
Mr. Larry Hanes
Mr. Jim May (became a student at NTSU, Spring 1978)
Mr. Brad Moore
Mr. Larry Tipton

In addition one undergraduate student, Kay Hansen, has worked during the past year.

XII. VITA

DAVID GEORGE SEILER

Office:

Department of Physics
North Texas State University
Denton, Texas 76203

Tel: 817-788-2626

Home:

2119 Emerson
Denton, Texas 76201

Tel: 817-387-7230

Present Position: Associate Professor of Physics
Department of Physics
North Texas State University
Denton, Texas 76203

Personal:

Date of Birth: December 17, 1940
Place of Birth Green Bay, Wisconsin
Marital Status: Married, two children
Citizenship: USA

Education:

B.S. in Physics, 1963, CASE Western Reserve

M.S. in Physics, 1965, Purdue University

Ph.D. in Physics, 1969, Purdue University
Thesis: "Investigation of the Band Structure of GaSb Using the Shubnikov-de Haas Effect"
Supervisor: Professor W. M. Becker

Scholarships: Tuition scholarship at CASE

Employment:

Teaching Assistant, Department of Physics, Purdue University, 1963-66, 1969

Research Assistant, Department of Physics, Purdue University, 1966-69

Assistant Professor of Physics, Department of Physics, North Texas State University, 1969-72

Curriculum vitae: David George Seiler

Employment (Cont'd)

Physicist, National Bureau of Standards, Boulder, 1972

Associate Professor of Physics, Department of Physics, North Texas State University, 1973-present

Membership in Professional Societies:

American Physical Society
Optical Society of America

Membership in Honorary Societies:

Pi Delta Epsilon
Sigma Pi Sigma
Sigma Xi

D. G. Seiler

Publication List

1. D. G. Seiler and W. M. Becker, "Observation of Beating Effects in Shubnikov-de Haas Oscillations in GaSb", Phys. Letters 26A, 96 (1967).

2. D. G. Seiler and W. M. Becker, "Warped Fermi Surface in GaSb from Shubnikov-de Haas Measurements", Phys. Rev. 183, 784 (1969).

3. D. G. Seiler and W. M. Becker, "Effect of Hydrostatic Pressure on the Band Structure of GaSb", Phys. Rev. 186, 784 (1969).

4. D. G. Seiler, W. M. Becker, and L. M. Roth, "Inversion Asymmetry Splitting of the Conduction Band in GaSb from Shubnikov-de Haas Measurements, Phys. Rev. 1B, 764 (1970).

5. D. G. Seiler, "Shubnikov-de Haas Frequency Anisotropy in GaSb", Phys. Rev. 1B, 2824 (1970).

6. D. G. Seiler, "Warped Fermi Surface of the Conduction Band in InSb", Phys. Letters 31A, 309 (1970).

7. R. R. Galazka, W. M. Becker, and D. G. Seiler, "Warping and Symmetry of Conduction Band in HgSe from Shubnikov-de Haas Measurements", J. Phys. and Chem. Solids Suppl. 32, 481 (1971).

8. R. J. Sladek, E. R. Gertner, and D. G. Seiler, "de Haas-van Alphen Effect in n-InSb", Phys. Rev. 3B, 2608 (1971).

9. D. G. Seiler, R. R. Galazka, and W. M. Becker, "Band Structure of HgSe: Band Parameter Determinations from Effective Mass Data, and Concentration Dependence and Anisotropy of Beating Effects in the Shubnikov-de Haas Oscillations", Phys. Rev. B3, 4274 (1971).

10. D. G. Seiler, "Concentration Dependence of the Warped Fermi Surface in n-InSb", Phys. Status Solidi (b), Vol. 49, K15 (1972).

11. D. G. Seiler, D. L. Alsup, and R. Muthukrishnan, "Effect of Uniaxial Stress on the Magnetophonon Effect in n-InSb", Solid State Comm., Vol. 10, 865 (1972).

12. D. G. Seiler and F. Addington, "A Uniaxial Stress Apparatus", Rev. Sci. Instr., Vol. 43, 749 (1972).

13. D. G. Seiler and K. Hathcox, "Shubnikov-de Haas Effect Under Stress: A New Tool for Determining Deformation Potentials and Band Structure Information", Phys. Rev. Letters, Vol. 29, 647 (1972).

14. D. G. Seiler and K. L. Hathcox, "Effect of Uniaxial Stress on the Shubnikov-de Haas Effect in HgSe", Proceedings of the 11th International Conference on the Physics of Semiconductors, Warsaw, Poland, 287 (1972).

15. R. Muthukrishnan and D. G. Seiler, "Deformation Potential Parameters of n-InSb", Physica Status Solidi (b) 54, K83 (1972).

16. D. G. Seiler, T. J. Joseph and R. D. Bright, "Effect of Uniaxial Stress on the Longitudinal Magnetophonon Oscillations in n-InSb", Phys. Rev. B, Vol. 9, No. 2, 716-722 (1972).

17. D. G. Seiler and K. Hathcox, "Effect of Uniaxial Stress on Shubnikov-de Haas Oscillations in HgSe", Phys. Rev. B, Vol. 9, No. 2, 648-657 (1974).

18. D. G. Seiler, "Effects of Uniaxial Strain on the Shubnikov-de Haas and Magnetophonon Effects in Semiconductors", International Conference on the Application of High Magnetic Fields in Semiconductor Physics, Wurzburg, Germany, 492-565 (1974).

19. H. J. Mackey, B. J. Vaughn, L. M. Rater, and D. G. Seiler, "Evidence for a Deep Acceptor Level in p-InSb from the Variation of Hole Density with Uniaxial Stress", Solid State Commun. 16, 997 (1975).

20. A. E. Stephens, D. G. Seiler, J. R. Sybert, and H. J. Mackey, "Determination of the g-factor from Unsplit Shubnikov-de Haas Oscillations in n-InSb", Phys. Rev. B 11, 4999 (1975).

21. Dwight Maxson, D. G. Seiler, and Larry Tipton, "Current Regulated High Voltage Power Supply for cw Gas Lasers", Rev. Sci. Instrum 46, 1110 (1975).

22. A. E. Stephens, J. R. Sybert, D. G. Seiler, and H. J. Mackey, "The Shubnikov-de Haas Relation and Determination of the g-factor for n-InSb", Proceedings of the Fourteenth International Conference on Low Temperature Physics, Helsinki, 1975 (American Elsevier, New York, 1975), Vol. 3, p. 79.

23. D. G. Seiler, B. D. Bajaj, and A. E. Stephens, "Inversion-Assymetry Splitting of the Conduction Band in InSb", Phys. Rev. B 16, 2822 (1977).

24. H. Kahlert and D. G. Seiler, "A Magnetic Field Modulation Technique for the Study of Hot Carrier Oscillatory Magnetoresistance Phenomena", Rev. Sci. Instrum. 48, 1017 (1977).

25. B. T. Moore, D. G. Seiler, and H. Kahlert, "CO_2 Laser-Induced Hot Electron Effects in n-InSb", Solid State Elec. 21, 247 (1978).

26. H. Kahlert, D. G. Seiler, and J. R. Barker, "Electric Field Dependence of the Positions and Amplitudes of Magnetophonon Oscillations in n-InSb at 77 K", Solid State Elec. 21, 229 (1978).

27. H. Kahlert and D. G. Seiler, "Observation of Magnetophonon Structure in Degenerate n-InSb", Solid State Commun. 25, 61 (1978).

28. D. G. Seiler, J. R. Barker, and B. T. Moore, New Hybrid Photoconductivity Technique for the Investigation of CO_2-Laser-Induced Hot-Carrier and Free-Carrier Absorption Effects in Degenerate n-InSb at 1.8 K," Phys. Rev. Letters 41, 319 (1978).

D. G. Seiler

Contributed Talks

1. D. G. Seiler and W. M. Becker, "Observation of Beating Effects in Shubnikov-de Haas Oscillations in GaSb", Bull. Am. Phys. Soc. 13, 94 (1968).

2. D. G. Seiler and W. M. Becker, "Warping of the k=0 Conduction Band in GaSb", Bull. Am. Phys. Soc. 14, 328 (1969).

3. D. G. Seiler and W. M. Becker, "Conduction Band Structure of GaSb", Bull. Am. Phys. Soc. 14, 328 (1969).

4. R. R. Galazka, W. M. Becker, and D. G. Seiler, "Symmetry of Conduction Band in HgSe", Conference on the Physics of Semimetals and Narrow Gap Semiconductors, March 1970.

5. D. G. Seiler, "Warped Fermi Surface on the Conduction Band in InSb", Bull. Am. Phys. Soc. 15, 312 (1970).

6. D. L. Alsup and D. G. Seiler, "Influence of Uniaxial Stress on the Magnetophonon Effect in n-type InSb", Bull. Am. Phys. Soc. 15, 1314 (1970).

7. K. L. Hathcox and D. G. Seiler, "The Influence of Uniaxial Stress on the Galvanomagnetic Properties of HgSe", Bull. Am. Phys. Soc. 16, 336 (1971).

8. R. Muthukrishnan and D. G. Seiler, "Effective Mass Tensor of n-InSb Under Uniaxial Stress", Bull. Amer. Phys. Soc. 17, 62 (1972).

9. D. G. Seiler and F. Addington, "Effect of Uniaxial Stress on the Magnetophonon Oscillations in the Longitudinal Magnetoresistance of n-InSb", Bull. Am. Phys. Soc. 17, 281 (1972).

10. D. G. Seiler and K. L. Hathcox, "Effect of Uniaxial Stress on the Shubnikov-de Haas Effect in HgSe", presented at the 11th International Conference on the Physics of Semiconductors, Warsaw, Poland, July, 1972.

11. D. G. Seiler and K. L. Hathcox, "The Influence of Uniaxial Stress on the Beating Patterns Observed in the Shubnikov-de Haas Oscillations in n-HgSe", Bull. Am. Phys. Soc. 19, 250 (1974).

12. B. Moore and D. G. Seiler, "Low Voltage TE-CO_2 Laser", J. Opt. Soc. Amer. 64, 1360 (1974).

13. D. G. Seiler, "Effects of Uniaxial Strain on the Shubnikov-de Haas and Magnetophonon Effects in Semiconductors", International Conference on the Application of High Magnetic Fields in Semiconductor Physics, Wurzburg, Germany, July 24-August 2, 1974.

14. A. E. Stephens, D. G. Seiler, H. J. Mackey, and J. R. Sybert, "The Shubnikov-de Haas Effect in n-InSb", Bull. Am. Phys. Soc. 20, 391 (1975).

15. B. D. Bajaj and D. G. Seiler, "Stress-Induced Beating Patterns in the Shubnikov-de Haas Effect in n-InSb", Bull. Am. Phys. Soc. 20, 391 (1975).

16. H. Kahlert, D. G. Seiler, and A. E. Stephens, "High Resolution Measurements of the Hot-Electron Magnetophonon Effect in n-InSb at 77 K", Bull. Am. Phys. Soc. 22, 460 (1977).

17. A. E. Stephens, R. E. Miller, J. R. Sybert, and D. G. Seiler, "Shubnikov-de Haas Effect in n-InAs and n-GaSb", Bull. Am. Phys. Soc. 22, 460 (1977).

18. B. T. Moore, D. G. Seiler, and H. Kahlert, "Laser-Induced Hot Electron Transport Effects in n-InSb at 2 K", Bull. Am. Phys. Soc. 22, 460 (1977).

19. D. G. Seiler and H. Kahlert, "A Magnetic Field Modulation Technique for the Study of Hot Carrier Oscillatory Magnetoresistance Phenomena", Bull. Am. Phys. Soc. 22, 460 (1977).

20. B. T. Moore and D. G. Seiler, "Wavelength Dependence of CO_2 Laser-Induced Hot Electron Effects in n-InSb", Bull. Am. Phys. Soc. 23, 329 (1978).

21. D. G. Seiler and B. T. Moore, "Determination of CO_2 Laser-Induced Hot Electron Temperatures from the Photoconductivity of n-InSb", Bull. Am. Phys. Soc. 23, 329 (1978).

22. D. G. Seiler, J. R. Barker, B. T. Moore, and K. E. Hansen, "Photoconductivity of Laser Excited Hot Electrons in Degenerate n-InSb", presented at the 14th International Conference on the Physics of Semiconductors, Edinburg, Scotland, September, 1978.

23. D. G. Seiler, L. K. Hanes, M. W. Goodwin, and A. E. Stephens, "Shubnikov-de Haas Effect Studies on Optically Heated Electrons in n-InSb", presented at the International Conference on Solids and Plasmas in High Magnetic Fields, Cambridge, Massachusetts, September, 1978.

Solid-State Electronics, 1978, Vol. 21, pp. 229–233. Pergamon Press. Printed in Great Britain

ELECTRIC FIELD DEPENDENCE OF THE POSITIONS AND AMPLITUDES OF MAGNETOPHONON OSCILLATIONS IN *n*-InSb AT 77 K†

H. KAHLERT‡ and D. G. SEILER
North Texas State University, Denton, TX 76203, U.S.A.

and

J. R. BARKER
University of Warwick, Coventry, England

Abstract—The influence of pulsed electric fields on the magnetophonon strcture in the transverse and longitudinal magnetoresistance of *n*-InSb at 77 K has been reexamined using a magnetic field modulation technique. For the transverse configuration, a shift to higher magnetic fields with increasing electric field is observed for the resistance maxima up to $N = 8$. The amplitudes decrease monotonously and disappear at about 60V/cm for $N = 3$. In the longitudinal case, the extrema shift to lower magnetic fields as the electric field is increased. In contrast to the transverse case, the amplitudes increase by a factor of 1.8 up to 15V/cm, and then either decrease or become saturated, depending on the harmonic number of the extremum under consideration. These experimental results are discussed within the context of calculations based on a quantum kinetic equation approach and predictions obtained from a simplified analytical theory.

1. INTRODUCTION

Several experimental investigations have been reported on the changes in the magnetophonon effect in *n*-InSb at 77 K under application of electric fields[1]. For the transverse configuration $B \perp J$, Curby and Ferry[2] found a shift of the resistance maxima to higher magnetic fields with increasing electric field. However, their experimental resolution only allowed the detection of the $N = 1$, 2 and 3 extrema and no quantitative information on the dependence of the amplitudes on the electric field was given. Restricting the applied electric field to values <1 V/cm, Hamaguchi *et al.*[3, 4] observed magnetophonon oscillations of the warm-electron coefficient β, but no shift of the extremal positions at these low fields was observed. For the longitudinal case $B \parallel J$, Ito *et al.*[5] reported the disappearance of the normal magnetophonon series by applying electric fields up to 70V/cm and the emerging of two new series of extrema which tentatively were explained by applying electric fields up to 70 V/cm and the emerging of two-LO-phonon scattering processes[6]. No shift of the positions of the ordinary series was reported. In contrast, Curby and Ferry[7] found a shift of these extrema in the longitudinal configuration to higher magnetic fields and gave an interpretation of this shift as being produced by the hot-electron induced population of higher Landau levels similar to the transverse case. No information on the electric field dependence of the amplitudes was determined for this case. In addition, it should be noted, that the duration of the electric field pulses was a few microseconds in both experiments[5, 7], so that the generation of acoustic flux via the acoustoelectric effect may have affected the results.

Some of the inconsistency of these findings might have been caused by the relatively poor resolution of the experimental techniques which were used to detect the hot-electron magnetophonon structure. The use of magnetic-field modulation techniques along with short electrical pulse sampling techniques has recently been demonstrated to increase the resolution dramatically[9] compared to conventional methods and to provide data, which are of the same quality as in the ohmic case. The purpose of this paper is to report high resolution measurements of the hot-electron magnetophonon structure in both the transverse and longitudinal configuration using these techniques with the electric field pulses short enough to prevent either generation of acoustoelectric effects or lattice heating. These experimental results are compared to predictions obtained from a simplified analytical theory and to calculations based on a quantum kinetic equation approach[10].

2. EXPERIMENTAL

Samples were cut from a single crystal of *n*-type InSb having a carrier concentration of $3 \times 10^{13}\,cm^{-3}$ and a mobility of $6.3 \times 10^5\,cm^2/Vsec$ at 77 K. They were needle-like with their long axis parallel to a ⟨211⟩ direction. They were polished to a thickness of about 60 μm and subsequently etched in a Br-methanol solution. Two current contacts were soldered to the ends using pure indium. The experimental set up and the measurement technique are described in detail in Ref.[9]. The resistance of the samples at 77 K was in all cases greater than 500Ω, so that the voltage across them was mainly determined by the current through a 50Ω parallel resistor. Consequently, the voltage remained approximately constant even in the transverse configuration, where the sample resistance increases strongly with magnetic field. Since in the actual measurement of the magnetophonon oscillations no potential probes were used to determine

†Work supported in part by the Office of Naval Research.
‡On leave from Ludwig Boltzmann Institute für Festkörperphysik and Institut für Angewandte Physik, Universität Wien, A-1090 Vienna, Austria.

the potential drop, the electric-field values might have been erroneous because of potential drops across the contacts. Therefore, after finishing the modulation measurements, potential probes were attached to the samples and it was verified that the contact resistance was negligible compared to the sample resistance in the range of electric and magnetic fields used in the experiment. The electric field pulses had a duration of 75 nsec and a repetition rate of 3 kHz. To prove the absence of any lattice heating effects, traces of the sample current versus magnetic field at the highest electric field were taken at 3 kHz, 300 Hz and 30 Hz; no change of the magnetoresistance as a function of the pulse repetition frequency could be detected.

3. RESULTS

The second derivative of the sample current with respect to the magnetic field strength B is plotted in Fig. 1 as a function of $B \perp J$. The ohmic trace was obtained with a constant d.c. current of 1 mA at an electric field of 0.5 V/cm. The other traces were recorded by setting the manual sweep control of the sampling oscilloscope to a time position of about 40 nsec after the application of the electric field pulse. The applied electric field strength is the parameter of the different traces and had values of 11, 21, 32 and 42 V/cm respectively. At electric fields exceeding 20 V/cm, anomalous structure appeared besides the magnetophonon structure. For clarity, these parts of the traces were replaced by dashed curves. The origin of this structure is not completely clear at present, but seems to be related to contact properties, since different samples from the same material exhibited this structure at different values of electric and magnetic field strength. The dashed line in Fig. 1 marks a field of 8 kG and helps to demonstrate the shift of the $N = 4$ and $N = 5$ extrema to higher magnetic fields with increasing electric field.

The normalized position of the transverse magnetoresistance extrema defined as $B(E)/B(0)$ is plotted as a function of E^2 in Fig. 2. For all extrema the magnetic field is shifted initially proportional to the square of the electric field and then tends to saturate. The slope of the increase is biggest for the high harmonic number extrema. However, their shift saturates at the lowest electric fields. The normalized amplitude defined as the quotient

$$\frac{\Delta I(E)}{I(E)} \Big/ \frac{\Delta I(3\ \mathrm{V/cm})}{I(3\ \mathrm{V/cm})},$$

$E = 3$ V/cm being the lowest electric field where pulsed measurements could be performed, is plotted in Fig. 3 versus the electric field for the extrema with $N = 3$, 4 and 5.

The second derivative of the sample current with respect to the magnetic field is plotted in Fig. 4 as a function of B for the longitudinal configuration $B \parallel J$. The lowest trace was obtained under ohmic conditions, whereas the other curves were measured at various applied electric fields. Two important features can be observed in these traces: (i) In accordance with results of Shirakawa *et al.*[5], additional structure appears at the right and left wing of the ordinary extrema. However, in contrast to their findings, (ii) the ordinary extrema do not disappear but are shifted to lower magnetic fields with increasing E. This shift is shown as a function of E in Fig. 5. After an initial decrease of about 4% the normalized extrema position $B(E)/B(0)$ finally saturate at about 40 V/cm fairly independent of the harmonic number of the extremum under consideration.

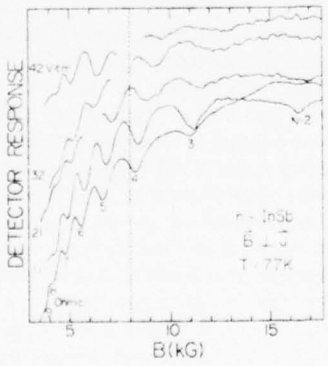

Fig. 1. Second derivative of the resistance with respect to the magnetic field B versus $B \perp J$. The lowest trace is obtained under Ohmic conditions; parameter of the other traces is the applied electric field.

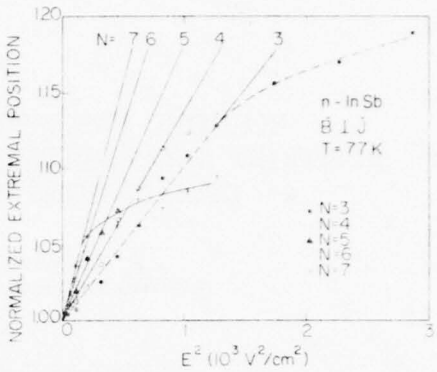

Fig. 2. Normalized extremal position $B(E)/B(0)$ versus square of the applied electric field for different harmonic number extrema and $B \perp J$.

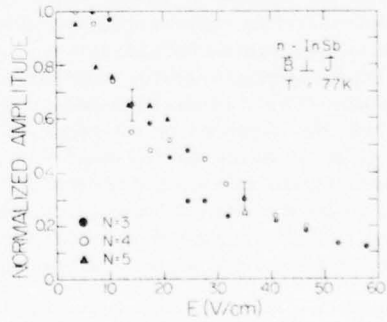

Fig. 3. Normalized amplitude as a function of the applied electric field for $B \perp J$.

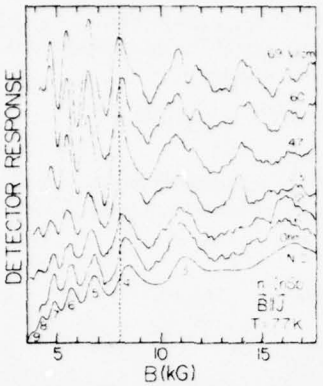

Fig. 4. Second derivative of the resistance with respect to B vs $B \parallel J$. The lowest trace is obtained under Ohmic conditions; parameter of the other traces is the applied electric field E.

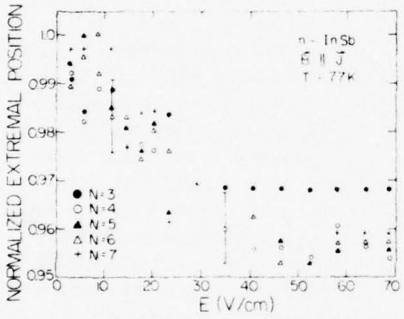

Fig. 5. Normalized extremal position $B(E)/B(0)$ versus the applied electric field for different harmonic number extrema and $B \parallel J$.

The normalized amplitude, defined similarly as in the transverse case, is plotted versus the electric field in Fig. 6 for the extrema with harmonic number $N = 3$, 4 and 5. The curves are guides for the eye only and show, that after an initial increase of the amplitude by a factor of 1.8, the amplitude decreases again, eventually exhibiting a second extremum at about 40 V/cm for $N = 3$ and 4, but saturates for the $N = 5$ extremum.

In order to investigate a possible influence of acoustoelectric amplification on the peak shift in the longitudinal configuration, which was considered by Peterson[1] to be important under the experimental conditions used by Ferry and Curby[8], measurements were performed on a [110] oriented sample in the longitudinal configuration as a function of time after the rise of the electric field pulse at an electric field of 46 V/cm. The sampling time was varied between 20 nsec and 2μsec. The result is shown in Fig. 7. For all times the extrema are shifted by the same amount to lower magnetic fields with respect to the positions under ohmic conditions (dashed lines). This experimental finding apparently rules out the acoustoelectric effect as a possible source for time dependent peak shifts in the longitudinal magnetophonon effect in the samples and the range of fields under consideration.

4. DISCUSSION

4.1 *Transverse configuration* $B \perp J$

The theoretical possibility of peak shifted magnetophonon structure was first emphasized by Barker and Magnusson[10] in numerical calculations based on solving the quantum kinetic equations for the electron density matrix in the crossed field representation[11]. The calculations have been recently extended[12] to include effects of non-parabolicity and inelastic acoustic phonon scattering. Since the numerical calculations are restricted to five Landau sub-band occupancy and single LO phonon processes in the vicinity of the first two magnetophonon extrema, only a qualitative comparison with the present data is possible. Nevertheless, the general experimental features appear to be interpretable via quantum transport theory. There are essentially four physical processes which could lead to electric field induced peak shifts and we discuss these separately.

(a) *Repopulation effects.* The first possibility is that carrier heating varies the effective electron temperature to successively populate higher Landau levels in the non-parabolic conduction band. Resonant magnetophonon transitions of the type $L + N \rightarrow L (N =$ harmonic number; $L = 0, 1, 2 \ldots)$ will then become increasingly contributory to the resistivity, and since the

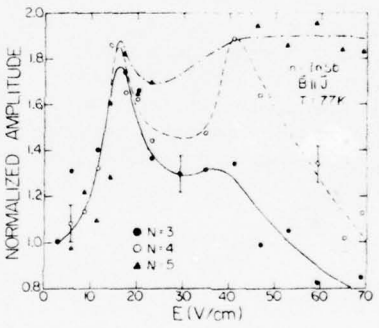

Fig. 6. Normalized amplitude as a function of the applied electric field for $B \parallel J$.

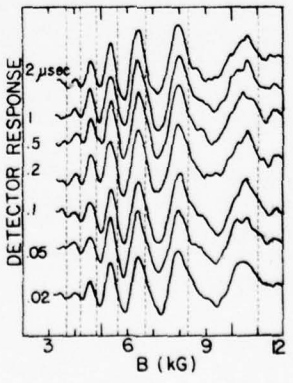

Fig. 7. Second derivative of the resistance with respect to B vs $B \parallel J$ for an electric field of 46 V/cm applied to a (110) oriented sample. Parameter of the traces is the time after application of the electric field pulse.

higher level sub-bands involve a decreasing cyclotron frequency, the resonance condition:

$$N\hbar\omega_c = \hbar\omega_0$$

predicts an extremum shift to higher magnetic fields. Within an electron temperature model[10] the effective temperature T_e is approximately quadratic in the total field E, which is not inconsistent with the data of Fig. 2.

Now the conductivity mobility μ_c is controlled by the dominant montonic part of the response and is found experimentally to decrease with increasing magnetic field. It follows that carrier heating will be more significant at lower magnetic fields, i.e. high harmonic number N, since the energy input rate is proportional to $\mu_c E^2$. The stronger peak shifts at high harmonic numbers are therefore not unexpected.

On the other hand it is by no means certain that an electron temperature argument is strictly operable since the numerically determined distribution functions [10, 12, 13] are markedly non-Maxwellian.

(b) *Electrically distorted band structure.* So far we have not included the electrical distortion of the non-parabolic spectrum[12, 14] which becomes significant for high total electric fields E (the resultant of the applied field and the much larger Hall field). Within a second order perturbation theory of the Kane two-band model it is known that significant sub-band mixing for small gap media results in a Stark shifted Landau structure, which lowers the higher Landau levels faster than the lower ones: the result is an additional decrease in the effective cyclotron frequency and a consequent extremum shift to higher fields. Thus for the two lowest sub-bands the electrically distorted energy levels are obtained as[12]:

$$\epsilon_0(E) = \epsilon_0(0) - \tfrac{1}{2}(eEl)^2/(\epsilon_1 - \epsilon_0)$$

$$\epsilon_1(E) = \epsilon_1(0) - \tfrac{1}{2}(eEl)^2\left[\frac{2}{\epsilon_2 - \epsilon_1} - \frac{1}{\epsilon_1 - \epsilon_0}\right],$$

where $\epsilon_N(0)$ is the Landau-Kane band structure, and $l \equiv (\hbar/m\omega_c)^{1/2}$ is the cyclotron length for the band-edge. In these expressions we have suppressed a linear shift term $eEk_y l^2$, which is the same for all levels. As befroe, the resultant peak shifts will be strongest for the higher harmonic numbers. Evidently , for large gap media, for which $\epsilon_N(0) - \epsilon_{N'}(0) = \hbar\omega_c(N - N')$, the Stark shift becomes independent of N and the peak shift contribution will vanish.

(c) *Intra-collisional field effects.* The third possibility is essentially a feature of the field assisted hopping-like diffusive conduction, which occurs in the transverse configuration. Here the current J parallel to the total electric field has the structure[10, 12]:

$$J = \tfrac{1}{2}e\sum_{\lambda,\lambda'}(X - X')[f(\lambda)R(\lambda,\lambda') - f(\lambda')R(\lambda',\lambda)]$$

where for a parabolic band

$$X \equiv -(\hbar k_y/eB + m^*E/eB^2),$$

$R(\lambda,\lambda')$ is the electric field dependent scattering rate between crossed-field states $\lambda(\equiv N, X, p_z)$ and λ', whilst $f(\lambda)$ is the *diagonal* part of the electron-density matrix and satisfies the rate equation:

$$\sum_{\lambda'}[f(\lambda')R(\lambda',\lambda) - f(\lambda)R(\lambda,\lambda')] = 0.$$

Now, within a collision-broadening second Born approximation the rates $R(\lambda,\lambda')$ involve an energy conservation factor:

$$\frac{1}{\pi}\Gamma(\lambda,\lambda')/\{[\epsilon_\lambda - \epsilon_{\lambda'} + \Delta(\lambda,\lambda') \pm \hbar\omega_q + eE(X - X')]^2 + \Gamma^2(\lambda,\lambda')\}$$

for a parabolic structure, where $\Gamma(\lambda,\lambda'), \Delta(\lambda,\lambda')$ are the joint level damping and level shifts associated with multiple scattering. For weak fields: $eE\Delta X \ll \Gamma$, it suffices to compute J from a linear expansion of $R(\lambda,\lambda')$ in powers of the total field E. The entire field dependence is then manifest in the distribution function $f(\lambda)$. In the opposite extreme, which occurs for $E_{\text{applied}} \geq 5\ \text{Vcm}^{-1}$ in our samples, such an expansion is not permissible and the electrically-induced inelasticity $eE(X - X')$ *by itself* leads to a removal of the Gurevich–Firsov singularity, progressively *damping* the magnetophonon amplitudes, and again entails a peak shift in the second derivative extremum positions to higher magnetic fields. It is useful to recall from earlier studies [15–17] that for strong collision damping the magnetophonon amplitudes for *ohmic conditions are modulated by an exponential factor* $\exp(-\gamma N)$, where N is the harmonic number and γ is the damping parameter. Second-derivative extrema are therefore displaced slightly to higher magnetic fields. If we heuristically argue that γ is controlled by the zero magnetic field mobility $\gamma \propto 1/\mu_c(0)$, and note that μ_c decreases with increasing applied electric field, it follows that collision damping will shift the second derivative extrema further for higher electric fields than for low fields. However, making use of the tabulated peak shifts as a function of γ given by Blakemore and Kennewell[18], we deduce from a change of $\gamma(E)/\gamma(0) = 1.25$ for $E_{\text{applied}} = 42$ V/cm an extremum shift of 0.4% compared with the observed 15% shift of the $N = 3$ extremum. On the other hand, for $E_{\text{applied}} > 5$ V/cm, the cattering contribution to γ is overwhelmed by the intra-collisional field effect[10], and much bigger shifts may be expected. To illustrate, we refer to a recent heuristic calculation due to Barker[12], which argues for an electrically induced modulation factor: $\exp[-2\pi|eE|l_0 N/(2^{1/2}\hbar\omega_c)]$, where $l_0 = (\hbar/m^*\omega_0)^{1/2}$, which replaces the factor $\exp[-\gamma N]$. The effective damping, $\gamma' \equiv 2\pi|eE|l_0/(2^{1/2}\hbar\omega_c)$, is evidently strongest for low magnetic fields so that the high harmonic number second-derivative extrema are shifted most.

(d) *Distortion of the distribution function.* All theoretical calculations to date[10, 12, 13] predict severe distortion of the carrier distribution $f(\lambda)$ at high electric fields. The main feature at high fields appears to be a pronounced hot carrier pile-up close to the LO-phonon emission threshold followed by a cold high energy

regime. Such a situation could lead to extremum inversion, which superficially resembles a peak shift effect. The continuous evolution of extrema reported here, however, would dictate against this possibility.

4.2 *Longitudinal configuration $B \| J$*

The conduction process is *relaxive* for this configuration and the much weaker peak shifts must be understood on a physically different basis from the diffusive picture outlined in Section 4.1. Here our data is reminiscent of recent calculations due to Barker[19] for n-GaAs at 120 K, which report a slight extremum shift to *lower* magnetic fields, which levels out at about 50 V/cm and is ascribed to a *barrier effect* whereby the relative population of sub-bands below to above the optical-phonon threshold is enhanced at high electric fields. Consequently, resonant contributions from higher Landau sub-bands, which are enhanced in the warm-electron regime $E \sim 0 \rightarrow 2$ V/cm, are suppressed in the hot electron regime. Thus, for the hot-electron regime the lower cyclotron effective masses are expected to be more efficacious in non-parabolic InSb, and a slight saturating extremum shift to lower fields is not unexpected.

REFERENCES

1. For recent reviews, see: R. L. Peterson, in *Semiconductors and Semimetals* (Edited by R. K. Willardson and A. C. Beer) Vol. 10, p. 221. Academic, New York (1975); P. G. Harper, J. W. Hodby and R. A. Stradling, *Rept. Progr. Phys.* **36**, 1(1973).
2. R. C. Curby and D. K. Ferry, *Proc. Int. Conf. Phys. Semiconductors Warsaw*, 1972, p. 312. Pol. Scientific Publ. Warsaw, (1972).
3. C. Hamaguchi, T. Shirakawa, T. Yamashita and J. Nakai, *Phys. Rev. Lett.* **28**, 1129 (1972).
4. T. Shirakawa, C. Hamaguchi and J. Nakai, *J. Phys. Soc. Japan* **35**, 1098 (1973).
5. M. Ito, T. Shirakawa, C. Hamaguchi and T. Nakai, *Solid State Commun.* **17**, 717 (1975).
6. T. Shirakawa, M. Ito, K. Kasai and C. Hamaguchi, *Phys. Lett.* **58A**, 123 (1976).
7. R. C. Curby and D. K. Ferry, *Bull. Am. Phys. Soc.* **18**, 354 (1973).
8. D. K. Ferry and R. C. Curby, *Phys. Lett.* **59A**, 471 (1977).
9. H. Kahlert and D. G. Seiler, *Rev. Sci. Instrum.* **48**, 1017 (1977).
10. J. R. Barker and B. Magnusson, *Proc. Int. Conf. Phys. Semicond. Stuttgart*, 1974 (Edited by H. Pilkuhn), p. 811. Teubner (1974).
11. H. F. Budd, *Phys. Rev.* **175**, 271 (1968).
12. J. R. Barker, *Solid-St. Electron.* **21**, 197 (1978).
13. E. Yamada and T. Kurosawa, *J. Phys. Soc. Japan* **34**, 603 (1973).
14. W. Zawadzki and B. Lax, *Phys. Rev. Lett.* **16**, 1001 (1966).
15. R. A. Stradling and R. A. Wood, *J. Phys. C: Proc. Phys. Soc., London* **1**, 1711 (1968).
16. L. Eaves, R. A. Hoult, R. A. Stradling, R. J. Tidey, J. C. Portal and S. Askenazy, *J. Phys. C* **8**, 1034 (1975).
17. J. R. Barker, *J. Phys. C* **5**, 1657 (1972).
18. J. S. Blakemore and T. A. Kennewell, *J. Phys. C: Solid State Phys.* **8**, 647 (1975).
19. J. R. Barker, unpublished.

Solid State Communications, Vol. 25, pp. 61-62, 1978. Pergamon Press. Printed in Great Britain

OBSERVATION OF MAGNETOPHONON STRUCTURE IN DEGENERATE n-InSb*

H.Kahlert** and D.G.Seiler

Department of Physics, North Texas State University, Denton, Texas 76203

(Received 4 August 1977 by R.C.C.Leite)

We report the observation of magnetophonon structure in the transverse magnetoresistance of degenerate n-InSb at 77 K in a sample of concentration 7.5 x 10^{15} cm^{-3}. The positions of the resistance maxima appear at higher magnetic fields than those found in pure ($\lesssim 10^{14}$ cm^{-3}) samples.

THE MAGNETOPHONON (MP) effect is a powerful tool for studying the band structure and transport properties of many semiconductors [1,2]. However, most of the experiments have been carried out at relatively high temperatures on non-degenerate samples with low carrier concentrations. Magnetophonon structure has been reported for several degenerate semiconductor samples: n-HgTe[3-5], n-GaSb[5], n-PbTe[6] and p-PbTe[7]. In this paper we report the observation of magnetophonon structure in the magnetoresistance of the highest concentration sample of n-InSb yet studied. To our knowledge this is the first time where the concentration has been high enough for the sample of n-InSb to also be degenerate at 77 K.

Studies of the magnetic field positions of the MP extrema in n-InSb have allowed a determination of the band-edge effective mass and its dependence on temperature, pressure and electric field[1]. However, up to the present time, no concentration dependence of the MP extremal positions in n-InSb has been reported. In contrast to previous studies, our measurement technique and high quality samples have permitted observation of an unambiguous concentration dependent shift to higher magnetic fields for the extremal positions in the transverse MP effect.

The single crystal n-InSb samples studied had concentrations of 9 x 10^{13} cm^{-3} and 7.5 x 10^{15} cm^{-3}, with mobilities of 6.1 x 10^5 cm^2/Vsec and 1.6 x 10^5 cm^2/Vsec, respectively. A constant current was passed through the InSb samples which were kept at 77 K in a glass Dewar system. Conventional ac magnetic field-modulation and phase-sensitive-detection techniques[8] were utilized where the resistance voltage from two potential probes on the sample was detected at the second harmonic of the modulation frequency. The electric field applied to the samples was kept in the ohmic range to avoid electric-field-induced shifts of the extrema[9].

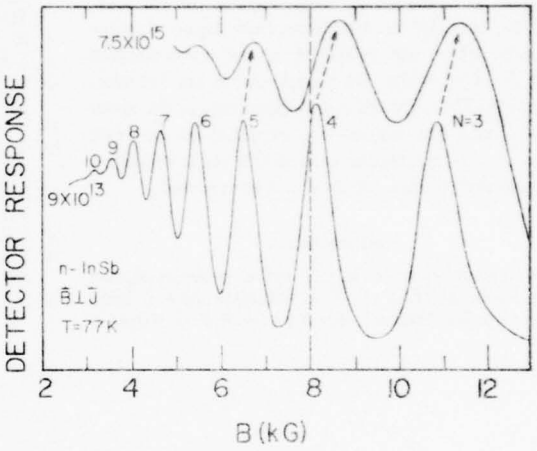

Fig. 1 - Reproduction of x-y recorder traces of oscillatory magnetoresistance data taken on two different concentration samples of n-InSb at 77 K using field-modulation and phase-sensitive detection techniques. The detector response was obtained while detecting at the second harmonic of the modulation frequency and thus corresponds to a second-derivative like behavior.

Figure 1 shows the recorded MP structure for the transverse configuration in pure InSb (9 x 10^{13} cm^{-3}) and in a much higher concentration (7.5 x 10^{15} cm^{-3}) sample of InSb. The observed positions of the MP maxima in the pure sample agree quite well with those reported by Stradling and Wood[10]. The MP structure for the N = 3, 4 and 5 maxima are clearly shown in Fig. 1 for the high concentration sample. This sample is weakly degenerate at 77 K according to the calculation presented in Fig. 1 of a paper by Kahlert and Bauer[11] where the Fermi energy of n-InSb is plotted as a function of temperature with the electron concentration as a parameter. The reduced Fermi energy ε_F/k_BT of this sample is +0.5 at 77 K, which means that the Fermi energy is above the bottom of the conduction band.

Not only does Fig. 1 show the first observed shift in the MP extremal position

* Work supported in part by the Office of Naval Research

** On leave from Ludwig Boltzmann Institute für Festkörperphysik and Institut für Angewandte Physik, Universität Wien, A-1090 Vienna Aust.

of n-InSb with electron concentration, but it also shows for the first time that MP structure can be observed in degenerate samples of n-InSb.

In principle, two different effects may contribute to the shift of the extrema in the transverse magnetoresistance to higher magnetic fields with increasing doping of the samples: (i) changes of the mobility and the related damping factor γ because of an increasing importance of ionized impurity scattering, (ii) changes of the Fermi energy and a related change of the population of higher Landau levels. The importance of the damping for the actual extremal positions observed in a magnetophonon experiment was already pointed out by Stradling and Wood[10].

Theoretical work describing the magnetic field dependence of the magnetophonon structure has not been carried out in detail for InSb, but often an empirical relation of the following form has been used to describe the structure in the resistivity [10]

$$\Delta \rho_{osc} \propto \exp(-\gamma B_o/B) \cos(2\pi B_o/B) \quad (1)$$

where γ is a constant depending upon the sample mobility and temperature and B_o is a parameter characterizing the semiconductor and is defined by

$$B_o = m^* \omega_o/e \quad (2)$$

In Eq. (2), m^* is the carrier effective mass, ω_o is the longitudinal optical phonon frequency and e is the magnitude of the electronic charge.

The presence of the exponential damping factor shifts the extrema obtained by second derivative techniques to higher magnetic fields compared to the extrema of just the simple cosine term, which occur at the magnetic fields where the resonance condition for transitions ending at the L-th Landau level $\varepsilon_{L+N} - \varepsilon_L = \hbar\omega_o$ is satisfied for $N = 1, 2, 3, \ldots$ For the pure sample a value $\gamma = 0.72$ could be deduced from the undifferentiated traces. From the difference of the mobility of the samples under consideration, it is reasonable to expect a value of γ of about 2.5 for the high concentration sample, assuming that it is inversely proportional to the Hall mobility of the sample. For the $N = 4$ extremum we estimate a damping-induced shift of 3.6% to higher magnetic fields by using tabulated values of the damping-induced shift given by Blakemore and Kennewell[12]. This shift has to be compared to the actual observed shift of 6% for the $N = 4$ extremum.

The second reason for the shift of the extrema to higher magnetic fields is a consequence of the nonparabolicity of the InSb-conduction band, where the energy of the Landau levels does not increase linearly with magnetic field. Consequently, transitions are expected to occur at higher magnetic fields, which involve a lower Landau level with quantum number L>0. An increasing contribution of these transitions and therefore a shift of the extrema to higher magnetic fields is expected for an increasing population of these levels when the sample is highly doped. More detailed theoretical work is needed in this area before a firm understanding of the doping-induced shift can be obtained.

REFERENCES

1. PETERSON,R.L. in "Semiconductors and semimetals" (R.K.Willardson and A.C.Beer, eds.) Vol. 10 p. 221, Academic Press, New York, 1975
2. HARPER,P.G., HODBY,J.W. and STRADLING,R.A., Rep. Prog. Phys. 36, 1 (1973)
3. TSIDIL'KOVSKII,I.M. and PONOMAREV,A.I., Int.Conf. II-VI Semicond. Compounds,Providence (D.G.Thomas, ed.) (Benjamin, New York, 1967), p.1103
4. PONOMAREV,A.I. and TSIDIL'KOVSKII,I.M., Sov.Phys. Semicond. 1, 1375 (1968)
5. POMORTSEV,R.V., PONOMAREV,A.I., KHARUS,G.I. and TSIDIL'KOVSKII,I.M., Proc. IX Int.Conf. Phys. Semicond., Moscow, (Nauka, Moscow, 1969), p. 720
6. TSUI,D.C., KAMINSKY,G. and SCHMIDT,P.H., Solid State Commun. 12, 599 (1973)
7. SREEDHAR,A.K., CHAUDHURI,N., WAKHALOO,P. and WADKEVA,R.S., Phys. Letters 29A, 398 (1969)
8. See for example the experimental set up given in SEILER,D.G. and BECKER,W.M., Phys. Rev. 183, 784 (1969)
9. KAHLERT,H. SEILER,D.G. and BARKER,J.R., to be published in Solid State Electronics
10. STRADLING,R.A. and WOOD,R.A., J. Phys. C 1, 1711 (1968)
11. KAHLERT,H. and BAUER,G., Phys. Rev. B 7, 2670 (1973)
12. BLAKEMORE,J.S. and KENNEWELL,T.A., J. Phys. C. Solid State Phys. 8, 647 (1975).

Magnetophonon-Oszillationen wurden im transversalen Magnetowiderstand von entartet dotiertem n-InSb bei 77 K in einer Probe mit 7.5×10^{13} Elektronen/cm^{-3} beobachtet. Die Magnetfelder, bei denen Widerstands-maxima auftreten, sind hoeher als jene, die fuer reine Proben ($n \leq 10^{14}$ cm^{-3}) gefunden werden.

THE MAGNETOPHONON EFFECT IN A NONPARABOLIC BAND: n-TYPE InSb*

By

H. Kahlert†

Department of Physics, North Texas State University

Denton, Texas 76203

ABSTRACT

Measurements of the transverse Ohmic magnetophonon effect have been performed at 77 K in a set of samples of n - InSb having carrier concentrations in the range from $n = 5 \times 10^{13}$ cm^{-3} to $n = 7 \times 10^{16}$ cm^{-3}. With increasing doping, the minima in the second derivative of the resistance with respect to the magnetic field are shifted to higher magnetic fields. Even in the purest samples the values of the resonant magnetic fields for harmonic numbers up to N = 12 can only be explained if the contributions of spin-conserving transitions involving both L = 0 spin levels and spin-split Landau levels with L > 0 are taken into account. These transitions occur at magnetic fields which are higher than the fields for the L = 0 lower spin level transition because of the nonparabolicity of the InSb-conduction band. A superposition of Lorentzian lines with an empirically determined halfwidth $\Delta(N)$ proportional to the harmonic number N and weighted with the value of the Fermi distribution function

at the energy of the lower level is shown to give a good fit to the data yielding a band-edge effective mass of $m_o^* = 0.0138\, m_o$. In higher doped samples, the shift of the extrema to higher magnetic fields is partially caused by the larger value of the damping parameter γ because of the lower mobility. After applying an appropriate correction to the extremal positions of the high concentration samples, a shift remains, which qualitatively can be explained by the increasing contribution of higher order transitions because of the higher population of these levels. Finally, the shifts in extremal position as a consequence of an increased electron temperature, e.g., induced by application of electric fields or photoexcitation, are discussed within the framework of this model.

I. INTRODUCTION

Since its theoretical prediction by Gurevich and Firsov,[1] the magnetophonon (MP) effect[2] has frequently been investigated in n-InSb in the transverse and longitudinal configuration.[3-7] Whereas in this early work the nonparabolicity of the conduction band of n-InSb has been neglected, it was clearly pointed out by Stradling and Wood[8,9] in the discussion of their extensive measurements of the MP effect in various III-V semiconductors using improved experimental techniques, that particularly in the interpretation of the extremal positions of magnetophonon oscillations in n-InSb the nonparabolicity of the conduction band plays an important role. However, in their evaluation of the band-edge effective mass[8] only extrema with harmonic number up to N = 6 were included. The application of the magnetic-field modulation and phase sensitive-detection technique has significantly improved the resolution of the oscillatory structure in the magnetoresistance and has allowed the detection of extrema up to N = 12 in the MP effect in n - InSb.[10-13]

The MP effect is generally accepted to be distinguishable from the Shubnikov-de Haas effect by the fact that it does not depend on the carrier concentration and no such dependence has been reported so far.[2] This can be understood by examining the resonance condition $N\omega_c = \omega_o$ with $\omega_c = eB/m^*$, where m^* is the effective mass and ω_o is an optical phonon frequency, since no quantity depends on the carrier concentration. However,

this relation is only correct for a parabolic band, where the Landau level energy increases linearly with magnetic field. In a nonparabolic band, the energies of the spin-split Landau levels do not increase linearly with magnetic field. As a result, the optical phonon energy fits between a pair of Landau levels characterized by quantum numbers L and L + N at higher magnetic fields for higher values of L.[8] The observed resistance maxima in the transverse configuration are therefore superpositions of all the lines produced by these transitions, which have to be weighted by the occupation factor of the lower level. If the population of higher levels is enhanced with increasing carrier concentration or mean carrier energy, we expect an increasing contribution of transitions between higher levels and consequently a shift of the extrema to higher magnetic fields. Such shifts have in fact been observed by Curby and Ferry[14] in the transverse MP effect in n-InSb at 77 K as a result of the application of pulsed electric fields up to 50 V/cm and the associated carrier heating. A quantitative study using an improved experimental setup[15] was recently reported by Kahlert et al.[16]

It is the purpose of this paper to describe a systematic study of the resistance extrema in the transverse MP effect measured in a set of eight different samples of n-InSb having carrier concentrations in the range between $5 \times 10^{13} cm^{-3}$ to $7 \times 10^{16} cm^{-3}$ at 77 K. In Sec. II the experimental technique is outlined and the sample properties are listed. The results of the measurements, namely an increasing shift of the resistance extrema to higher magnetic fields with increasing doping

of the samples, are described in Sec. III. For a few samples, values of the damping parameter γ are derived from the undifferentiated magnetoresistance versus magnetic field. In Sec.IV the shifts of the experimentally observed extremal positions away from the actual resonant magnetic fields are corrected, which arise from damping-dependent exponential prefactor to the oscillatory term in the magnetoresistance. Calculated extremal positions are found by superimposing resonance lines centered at the resonant magnetic fields, which depend not only on the harmonic number N, but also on the quantum number L of the lower level. These lines are weighted with the Fermi occupation factor of the lower level and added to form a composite line, the extremum of which is computed numerically. A superposition of cosine functions cannot explain all extremal fields in the range from N = 2 to N = 12 for the pure samples. Using Lorentzian lines with an empirically determined half-width proportional to the harmonic number N, a good fit is obtained yielding a value of the band-edge effective mass $m_o^* = (0.0138 \pm 0.00005) m_o$. The shift of the corrected experimental positions of the higher doped samples to higher magnetic fields is compared to calculations for various Fermi energies. Fair agreement between the observed and the calculated shifts is obtained. Finally, shifts are calculated as consequence of an increasing electron temperature. The conclusions concerning the interpretation of MP effect measurement in semiconductors having a nonparabolic band are drawn in Sec. V.

II. SAMPLE PROPERTIES AND EXPERIMENTAL TECHNIQUE

Unoriented samples were cut from eight different single crystals of n-InSb using a spark-cutting machine. They were polished with 0.3μm Al_2O_3 polishing powder and subsequently etched in CP4A twice for three seconds. Two end contacts, two potential probes, and two Hall contacts were provided by soldering 25μm gold wires with pure Indium solder. The samples were mounted in a holder equipped with six coaxial cables and suspended in a glass dewar between the pole faces of a 21kG electromagnet with the sample axis perpendicular to the magnetic field. Care was taken not to surround the sample with any conductive material to avoid the shielding of the magnetic modulation field by eddy currents. Prior to the MP effect measurements, the transverse magnetoresistance and the Hall effect were recorded by impressing a constant current and measuring the potential probe voltage and the Hall voltage in magnetic fields up to 20 kG for both directions of the current and both directions of the magnetic field. The carrier concentration $n = 1/(eR_H)$, where R_H is the Hall coefficient, the Hall mobility μ_H, and the value of the damping coefficient γ to be discussed in Sec. IV are listed in Table I.

The experimental equipment to produce an ac modulated magnetic field and to extract the second derivative of the magnetoresistance with respect to the magnetic field is described in detail in References 15 and 17. In order to increase the signal-to-noise ratio, particularly for the high concentration samples where the MP oscillation amplitudes are

very small, a modulation field of 400 G peak-to-peak was used. However, with the high mobility samples like S1 and S2, where the oscillations were observable with as small modulation fields as 50 G peak-to-peak, the extremal positions did not depend on the amplitudes of the modulation field. The dc magnetic field was swept at a rate of 500 G/min. A trivial shift of the recorded traces was caused by the fact that the time constant of the lock-in amplifier had to be set to 10 sec for a sufficient noise suppression. This shift was carefully eliminated by sweeping the magnetic field up and down and taking the average value of the magnetic fields, where extrema occurred in the upsweep and in the downsweep, as the true position of each extremum. The validity of this procedure was checked by taking traces on a high mobility sample with a 100 msec integration time, where at a magnetic-field sweep rate of 250 G/min no differences between the up-sweep and downsweep positions were observable. The so determined positions coincided with the positions obtained from an averaging of the traces taken with a 10 sec integration time. The magnetic field was calibrated using NMR techniques.

III. EXPERIMENTAL RESULTS

The output signal of the lock-in amplifier set at $2f_o$, where f_o is the ac magnetic field modulation frequency of 43 Hz, is plotted versus the magnetic field strength in Fig. 1. This signal corresponds to the second derivative of the resistance R with respect to the magnetic field. It shows minima at the resonant positions, since the transverse MP effect exhibits maxima of R whenever $\varepsilon_{L+N}-\varepsilon_L = \hbar\omega_o$, where ε_L is the energy of the Landau level characterized by the quantum number L, N is the harmonic number, and $\hbar\omega_o$ is the LO-phonon energy. By a proper setting of the phase of the lock-in amplifier the background magnetoresistance could be completely eliminated in most cases. Therefore, the actual extremal positions could be determined with high precision. The estimated error in the determination of the extremal magnetic fields is about ± 10 G for the purest samples S1 and S2, increasing to about ± 30 G for the highly doped sample S6. In sample S7 only weak structure corresponding to the N = 3 and N = 4 peaks was observed. No attempt was made to determine the position because of the comparably strong background magnetoresistance. No structure resembling MP oscillations could be found in the second derivative of the magnetoresistance of sample S8 within the given experimental resolution.

The dashed line in Fig. 1 marks a magnetic field of 8 kG. The higher the doping of the sample under consideration, the

more shift of the N = 4 extremum away from this line to higher magnetic fields is observed. Similar shifts were found for all other extrema. In addition, the traces show a more sinusoidal type of oscillation only for the impure samples. The peaks for the samples S1, S2, and S3, particularly those with $N \leq 6$, exhibit an appreciable amount of sharpening.

In considerations concerning possible explanations for the observed shift of the extrema to higher magnetic fields, the damping parameter γ plays an important role. This parameter shows up in an empirical formula for the amplitudes of the MP oscillations as a function of the magnetic field, which in many cases can be described by a term of the form $\exp(-\gamma B_o/B)$ times an oscillatory term, where B_o is obtained from the relation $eB_o / m^* = \omega_o$.[8] Unfortunately, it is not possible to determine γ from the second derivative traces in Fig. 1. They are distorted because of the peculiarities of the magnetic field modulation technique, because of changes of the phase for optimum detection during the field sweep, while the phase setting of the lock-in amplifier is kept constant, etc. However, for three samples, S2, S3, and S4, the oscillations in the undifferentiated raw magnetoresistance data with N = 2, N = 3, and N = 4 were sufficiently prominent to allow a determination of γ. These experimental values of γ are plotted versus the Hall mobility of the respective samples in Fig. 2.

IV. ANALYSIS AND DISCUSSION

A. Corrections of the Extremal Positions Depending on the Damping Parameter γ

It was already pointed out by Stradling and Wood[8] that the experimentally observed MP extrema are shifted away from the fields where the resonance condition is satisfied, since the oscillations are modulated by an exponential term of the form $\exp(-\gamma B_o/B)$. Later theoretical work by Barker[18] has related the damping factor to various scattering processes and has shown how the amplitude and lineshape may be expected to vary as a function of temperature and impurity content. In an extensive numerical study, Blakemore and Kennewell[10] have calculated the shifts introduced by such an exponential prefactor, with both the harmonic number N and the value of γ as parameters. Particularly, they have found a linear dependence of the shift of the minima in the second derivative of the transverse magnetoresistance as a function of γ for a fixed value of N, thus allowing easy interpolation between their tabulated correction factors.

As discussed in Sec. III, a determination of γ was possible only for the samples S2, S3, and S4. In order to enable a correction of the positions in those samples, for which γ could not be determined directly, a curve was fitted through the data points in Fig. 2. An optimal least squares fit was obtained with a relation of the form $\gamma = a + b/\mu$, which is a reasonable result, since one expects the damping to decrease with increasing mobility. Inserting the coefficients $a = 0.117$ and $b = 3.48 \times 10^5$ Vsec cm^{-2} the curve in Fig. 2 was obtained

and used to determine γ- values for the samples S5 and S6, for which the undifferentiated traces were unsatisfactory. Obviously, there is an appreciable amount of uncertainty connected with this procedure. However, a convincing check for the validity of this correction was obtained from the following observation: By inspecting Fig. 1, one finds that the shift of the extremal positions is substantially different for the samples S4 and S5, although they have almost the same carrier concentration of 1.5×10^{15} and $2 \times 10^{15} cm^{-3}$, respectively. Consequently, they have almost equal values of the Fermi energy and therefore almost equal contributions of higher order transitions to the resistance maximum. However, sample S5 has a substantially lower mobility, probably due to a higher impurity scattering contribution because of a higher degree of compensation. Deriving the appropriate γ-value corresponding to its mobility from the curve in Fig. 2 and applying the correction to the extrema according to Ref. 19 one arrives at corrected positions for the extrema of these two samples, which are very close to each other (see the B/B_p values of these two samples with $\varepsilon_F = -9$ meV and -7.5 meV, respectively, in Fig. 7 and Fig. 8). All experimental data, which in the subsequent paragraphs will be compared to calculated extremal positions, have been corrected according to this procedure using the correction factors tabulated in Ref. 19.

B. Calculated Extremal Positions as a Superposition of Cosine Functions

The corrected experimental magnetic field positions of MP extrema for sample S2, multiplied by their respective harmonic

number N, are plotted versus N in Fig. 3. The lines connect calculated NB products, where B is obtained from the general resonance condition

$$\varepsilon_{L+N,s} - \varepsilon_{L,s} = \hbar\omega_o \ . \qquad (1)$$

The energy $\varepsilon_{L,s}$ of a Landau level with quantum numbers L and s is given by[8]

$$\varepsilon_{L,s} = (\varepsilon_g/2)\{[1 + 4(L+\tfrac{1}{2}+sg_o m_o^*/2m_o)\hbar\omega_c/\varepsilon_g]^{\frac{1}{2}} - 1\} \qquad (2)$$

where ε_g is the energy gap, g_o is the electron g factor at the bottom of the band, and m_o^* is the band edge effective mass. The full curves are for the lower spin levels with $s = \frac{1}{2}$, and the dashed curves are for the upper spin levels with $s = -\frac{1}{2}$. Only spin-conserving transitions were considered. The numerical constants were $g_o = -51.3$,[20] $\varepsilon_g = 0.225$ eV at 77 K, $\hbar\omega_o$ 24.0 meV[20] and $m_o^* = 0.0138\ m_o$. Evidently, the observed NB-values cannot be explained by transitions involving only one particular pair of Landau levels, for example, by transitions starting (phonon absorption) or ending (phonon emission) on the $L = 0$, $s = \frac{1}{2}$ level. The fit cannot be improved by a better choice for m_o^* or $\hbar\omega_o$, since the curves are merely shifted to higher or lower NB products without the curvature being significantly altered. If one neglects the NB-value for $N = 2$, one even finds that the NB-values for $N \geq 3$ are all equal within the experimental accuracy. Consequently, a plot

of 1/B versus N gives a straight line through the origin, which leads to the wrong conclusion that the effective mass can be evaluated from the parabolic formula $N\omega_c = \omega_o$. The value of the effective mass $m^* = 0.0157\ m_o$ so deduced is appreciably different from the band-edge effective mass obtained by other techniques and leaves the position of the N = 2 and N = 1 extrema unexplained.

A method to determine the band edge effective mass by taking into account higher order transitions was proposed by Stradling and Wood.[8] They tried to explain the corrected experimental positions by a superposition of cosine functions centered at the appropriate resonant magnetic field for each of the contributing transitions, which were weighted by a Boltzmann factor to account for the population of each level. We repeated this procedure by adding contributions from eight levels (L = 0,...3, s = ½,-½) to obtain a resulting line of the form

$$A_N(B) = \sum_{L=0}^{3} \sum_{s=\frac{1}{2}}^{-\frac{1}{2}} \cos\left(\frac{2\pi N B_{L,s,N}}{B}\right) f[\varepsilon_{L,s}(B)] , \qquad (3)$$

where $B_{L,s,N}$ is a solution of Eq. (1) for the appropriate value of L, s, and N, and f is the Fermi distribution function giving the population of the energy level $\varepsilon_{L,s}$. The values of B for which $A_N(B)$ has a maximum were multiplied by N and plotted versus N in Fig. 4 for different values of the band-edge effective mass. With $m_o^* = 0.0138\ m_o$ a reasonable fit to the experimental data for $N \geq 8$ can be obtained (full curve), whereas

great discrepancies occur for $N < 6$. Reducing m_o^* to a value of $0.0136\ m_o$ yields a reasonable fit (dashed line) to the data for $N \leq 6$ similar to that obtained by Stradling and Wood,[8] but fails to explain the higher harmonic number extrema.

C. Calculated Extremal Positions as a Superposition of Lorentzian Lines

The reason for the failure to explain the observed positions by a superposition of cosine functions is found by inspecting the actual shape of the extrema in Fig. 1. Not all extrema exhibit a cosine-dependence on 1/B, but some are more sharpened, particular for the pure samples and for extrema with $N \leq 6$. This effect is clearly demonstrated, if one plots the second derivative of the resistance with respect to B versus 1/B.[21] In order to account better for the observed line shape, the extrema were described by a superposition of Lorentzian lines centered at the resonant positions and weighted with the Fermi occupation factor f in the form

$$\bar{A}_N(B) = \sum_{L=0}^{3} \sum_{s=\frac{1}{2}}^{-\frac{1}{2}} \{ 1 + (\frac{1}{B} - \frac{1}{B_{L,s,N}})^2 (\frac{\Delta(N)}{2})^{-2} \}^{-1} f[\varepsilon_{L,s}(B)], \quad (4)$$

where $\Delta(N)$ is the full width of the line at half amplitude. For each harmonic number N the value of $\Delta(N)$ was determined in such a way that the line calculated according to Eq. (4) had the same linewidth as the experimentally observed line

for sample S2. It was assumed that $\Delta(N)$ depends on N only and is independent of the value of L and s for a given N. The halfwidth so determinded is plotted in Fig. 5 versus N. Obviously $\Delta(N)$ increases linearly with N and can be written as $\Delta(N) = kN$ with $k = 1.93 \times 10^{-6} G^{-1}$. The values of B for which $\bar{A}_N(B)$ has a maximum were multiplied by N and plotted versus N in Fig. 6 for different values of the band-edge effective mass, together with the corrected experimental data for sample S2. The best fit was obtained using a value of $m_o^* = (0.0138 \pm 0.00005)m_o$, which is very close to the mass determined from intraband magnetooptical effects at lower temperatures by Johnson and Dickey.[20] Extending the summation in Eq. (4) up to L = 7, which means the inclusion of contributions of eight more possible transitions, did not significantly change the calculated curves. A comparison of the calculated and experimental line-shape is difficult, since the experimental lines are distorted both by the measuring technique and by the fact that they are multiplied by a magnetic-field dependent exponential, as discussed in the first paragraph of this section.

D. Concentration Dependence of the Extremal Positions

In order to determine the concentration dependence predicted by the two models discussed above, the magnetic field B for which the functions A_N and $\bar{A}_N$ have a maximum, is calculated as a function of the Fermi energy ε_F for several values of N. The extremal magnetic field obtained for a particular

Fermi energy divided by the field calculated for a large negative Fermi energy of -30 meV is plotted versus the Fermi energy ε_F in Fig. 7 for the N = 3 extremum and in Fig. 8 for the N = 6 extremum. The full lines are calculated from Eq. (3) and the dashed lines are obtained from Eq. (4). The data points were found by dividing the corrected extremal magnetic fields for a particular sample by the corresponding corrected field B_p for the pure sample S2. Use was made of the relation between the carrier concentration and the Fermi energy for the conduction band of InSb given by Kahlert and Bauer.[22] Good agreement between the experimental and the calculated shifts was obtained for the N = 3 extremum as evidenced in Fig. 7. For the N = 6 extremum the agreement was less satisfactory. This might be caused by the fact that no attempt was made to make the halfwidth dependent on the amount of doping. This assumption of a doping-independent halfwidth is not too well justified, since the halfwidth of the lines at a given N apparently does increase with increasing doping (see Fig. 1). Part of this linewidth increase is certainly caused by the stronger contribution of higher order transitions. A quantitative description, however, calls for a more refined model than that used for the description of the extrema in the pure sample S2.

E. Electron Temperature Dependence of the Extremal Positions

An obvious consequence of an increase of the electron temperature, which is a parameter of the Fermi occupation factors in

Eqs. (3) and (4), is again an increase of the contribution of higher order transitions and a resulting shift of the extrema to higher magnetic fields. The calculated shift of the extrema in a pure sample (ε_F = -30 meV) as a function of the electron temperature for the harmonic numbers N = 3 and 6 is shown in Fig. 9. Such shifts of transverse MP effect extrema in n-InSb at 77 K have in fact been observed as a consequence of the application of pulsed electric fields.[14,16] An increase of the mean carrier energy is also expected to result from an illumination of an n-InSb sample with CO_2 laser radiation.[23] However, because of the predominance of polar optical scattering at 77 K in n-InSb, an electron temperature model is certainly inappropriate. It has to be replaced by a calculation of the distribution function which takes into account the Landau-level structure of the conduction band. Therefore, the result of Fig. 9 cannot immediately be compared to observations in an actual electron-heating experiment, but merely demonstrates one of the basic physical processes which are to be expected.[16]

V. CONCLUSIONS

The transverse MP effect in a nonparabolic band is considerably more complex than in the simple parabolic case. The observed resonant magnetic fields can only be understood by a superposition of lines, which are centered at different magnetic fields because of the nonlinear dependence of the Landau-level energy on B, and which are weighted with the Fermi occupation factor. As a consequence, shifts of the extremal positions occur, whenever parameters of the distribution function, like the Fermi energy or the electron temperature, are changed. As a further consequence, the interpretation of the shift of the extrema as a function of lattice temperature becomes exceedingly complicated. Not only have the changes of the energy gap and the related changes of the band-edge effective mass to be considered as well as changes of the LO-phonon energy, but also an increase of the contributions of higher order transitions to the position and shape of the lines with increasing temperature. These implications do not only concern the MP effect in n-InSb, but in all small-gap semiconductors having nonparabolic bands. In particular, shifts of the extremal positions of the longitudinal and transverse MP effect in $Hg_{0.8}Cd_{0.2}Te$ with lattice temperature have been interpreted as resulting from the change of the band gap and the band-edge effective mass only, without giving proper consideration to the above described effects.[24,25] The temperature coefficient of the band gap derived to explain

the data was found to be a factor of two higher than obtained from independent determinations.[26] A calculation of the temperature dependent shifts including the higher order transitions, which were neglected in this interpretation,[24] might well remove this discrepancy.

AD-A063 161 NORTH TEXAS STATE UNIV DENTON DEPT OF PHYSICS F/G 20/12
INVESTIGATION OF LASER OPTICAL BIASING ON THE QUANTUM TRANSPORT--ETC(U)
OCT 78 D G SEILER N00014-76-C-0319
NL

UNCLASSIFIED

2 OF 2
AD A063161

END
DATE FILMED
3-79
DDC

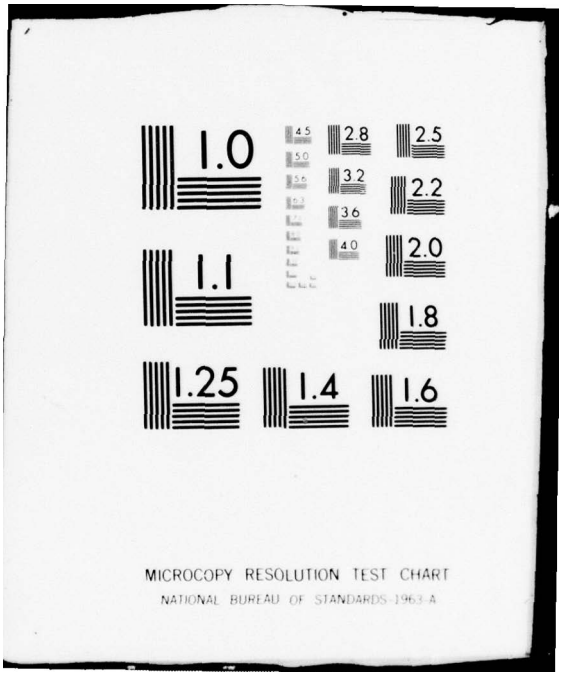
1.0
1.1
1.25
1.4
1.6
1.8
2.0
2.2
2.5
2.8
3.2
3.6
4.0
4.5
5.0
5.6
MICROCOPY RESOLUTION TEST CHART
NATIONAL BUREAU OF STANDARDS-1963-A

ACKNOWLEDGEMENT

I am indebted to Dr. D. G. Seiler for pointing my attention to the problem of the concentration dependence of the MP effect, to Dr. A. E. Stephens for allowing me to use a part of his experimental setup, to Dr. D. H. Kobe and Dr. J. R. Barker for critically reading the manuscript, and to all members of the Physics Department of NTSU for their hospitality and assistance during my visit.

REFERENCES

* Work supported in part by the Office of Naval Research

† On leave from Ludwig Boltzmann Institut füer Festkoerperphysik and Institut füer Angewandte Physik der Universitaet Wien, Vienna, Austria; present address: Kopernikusgasse 15 A 1060 Vienna, Austria

1. V. L. Gurevich and Yu. A. Firsov, Zh. Eksp. Teor. Fiz. 40, 198 (1961) [Sov. Phys. JETP 13, 137 (1961)] .
2. For recent review articles, see: R. L. Peterson, in "Semiconductors and Semimetals" (R. K. Willardson and A. C. Beer eds.) Vol. 10, p. 221, Academic Press, New York 1975; P. G. Harper, J. W. Hodby, and R. A. Stradling, Rep. Prog. Phys. 36, 137 (1973)
3. S. M. Puri and T. H. Geballe, Bull. Amer. Phys. Soc. 8, 309 (1963).
4. S. S. Shalyt, R. V. Parfen'ev, and V. M. Muzhdaba, Fiz. Tverd. Tela 6, 647 (1964) [Sov. Phys. Sol. State 6, 508 (1964)].
5. R. V. Parfen'ev, S. S. Shalyt, and V. M. Muzhdaba, Zh. Eksp. Teor. Fiz. 47, 444 (1964) [Sov. Phys. JEPT 20, 1131 (1964)] .
6. Yu. A. Firsov,V.L.Gurevich, R. V. Parfen'ev, and S. S. Shalyt,Phys. Rev. Lett. 12, 660 (1964).
7. V. L. Gurevich, Yu. A. Firsov, R. V. Parfen'ev, and S. S. S. Shalyt,Proc. 7th Int. Conf. Phys. Semicond., Paris p. 653, Academic Press, New York (1964).

8. R. A. Stradling and R. A. Wood, J. Phys. C: Solid State Phys. 1, 1711 (1968).

9. R. A. Stradling and R. A. Wood, J. Phys. C: Solid State Phys. 3, L94 (1970).

10. D. G. Seiler and F. Addington, Rev. Sci. Instrum. 43, 749 (1972) Bull. Am. Phys. Soc. 17, 281 (1972).

11. D. G. Seiler, D. L. Alsup, and R. Muthukrishnan, Solid State Commun. 10, 865 (1972); R. Muthukrishnan and D. G. Seiler, Phys. Stat. Sol. 54, K83 (1972).

12. D. G. Seiler, Proc. Int. Conf. Appl. High Magn. Fields Semicond. Phys. Univ. of Wuerzburg, Germany (1974).

13. D. G. Seiler, T. J. Joseph, and R. D. Bright, Phys. Rev. B9, 716 (1974).

14. R. C. Curby and D. K. Ferry, Proc. 11th Int. Conf. Phys. Semicond., Warsaw 1972, p. 312, E. Miasek ed., Polish Sci. Publishers 1972.

15. H. Kahlert and D. G. Seiler, Rev. Sci. Instrum. (in print)

16. H. Kahlert, D. G. Seiler, and J. R. Barker, Solid State Electr. (in print).

17. D. G. Seiler and W. M. Becker, Phys. Rev. 183, 784 (1969).

18. J. R. Barker, J. Phys. C: Solid State Phys. 5, 1657 (1972).

19. J. S. Blakemore and J. A. Kennewell: J. Phys. C: Solid State Phys. 8, 647 (1975).

20. E. J. Johnson and D. H. Dickey, Phys. Rev. B1, 2676 (1970).

21. See, for example Fig. 1 of the review article by R. L. Peterson, Ref. 2.

22. H. Kahlert and G. Bauer, Phys. Rev. B7, 2670 (1973).

23. B. T. Moore, D. G. Seiler, and H. Kahlert, Solid State Electr. (in print).

24. H. Kahlert and G. Bauer, Phys. Rev. Lett. 30, 1211 (1973).

25. H. Kahlert and G. Bauer, Proc. Coll. Int. Transition Semicond. Semimetal (Nice-Cardiff) 1973, Bureau des Publication C.N.R.S. (in print).

26. R. Dornhaus and G. Nimtz, in Springer Tracts in Modern Physics Vol. 78, p. 1, G. Hoehler ed. Springer Verlag Berlin-Heidelberg, New York, 1976.

TABLE I. Sample Properties

No.	n (cm^{-3})	μ_H(10^5 cm^2/(Vsec))	
S1	5.0×10^{13}	6.29	
S2	9.0×10^{13}	6.11	0.72
S3	6.7×10^{14}	4.22	0.88
S4	1.5×10^{15}	2.92	1.33
S5	2.0×10^{15}	2.13	
S6	7.5×10^{15}	1.64	
S7	3.0×10^{16}	1.03	
S8	7.3×10^{16}	0.87	

FIGURE CAPTIONS

Fig. 1: Second derivative of the resistance with respect to the magnetic field B versus B for the samples listed in Table I.

Fig. 2: Damping parameter γ versus Hall mobility at B = 0. The curve is a least squares fit through the data.

Fig. 3: Experimental NB values for sample S2 versus harmonic number N. The curves connect points calculated from Eq. (1) and (2) for L = 0,...3. The full lines are obtained for s = ½, the dashed lines for s = -½.

Fig. 4. Experimental NB values for sample S2 versus N. The curves are calculated from Eq. (3) with different values of m_o^*/m_o. Double-dash dotted: $m_o^*/m_o = 0.0139$; full: $m_o^*/m_o = 0.0138$; dash-dotted: $m_o^*/m_o = 0.0137$; dashed: $m_o^*/m_o = 0.0136$.

Fig. 5: Halfwidth of the resonance lines for sample S2 as a function of the harmonic number N. The straight line is a least squares fit through the data.

Fig. 6: Experimental NB values for sample S2 (dots) as a function of the harmonic number N. The curves are calculated from Eq. (4) with different values of m_o^*/m_o; dash-dotted: $m_o^*/m_o = 0.139$; full: $m_o^*/m_o = 0.0138$, dashed: $m_o^*/m_o = 0.0137$. The square represents a corrected data point taken from Ref. 8.

Fig. 7: Dependence of the normalized position of the N = 3 extremum on the Fermi energy ε_F. B_p is the extremal position found for a pure sample. Full curve: Cosine functions, dash-dotted curve: Lorentzian lines.

Fig. 8: Dependence of the normalized position for the N = 6 extremum on the Fermi energy ε_F. B_p is the extremal position found for a pure sample. Full curve: Cosine functions; dash-dotted curve: Lorentzian lines.

Fig. 9: Calculated dependence of the normalized position of the N = 3 (full curve) and the N = 6 extremum (dashed curve) versus electron temperature T_e for a sample with ε_F = -30 meV according to Eq. (4).

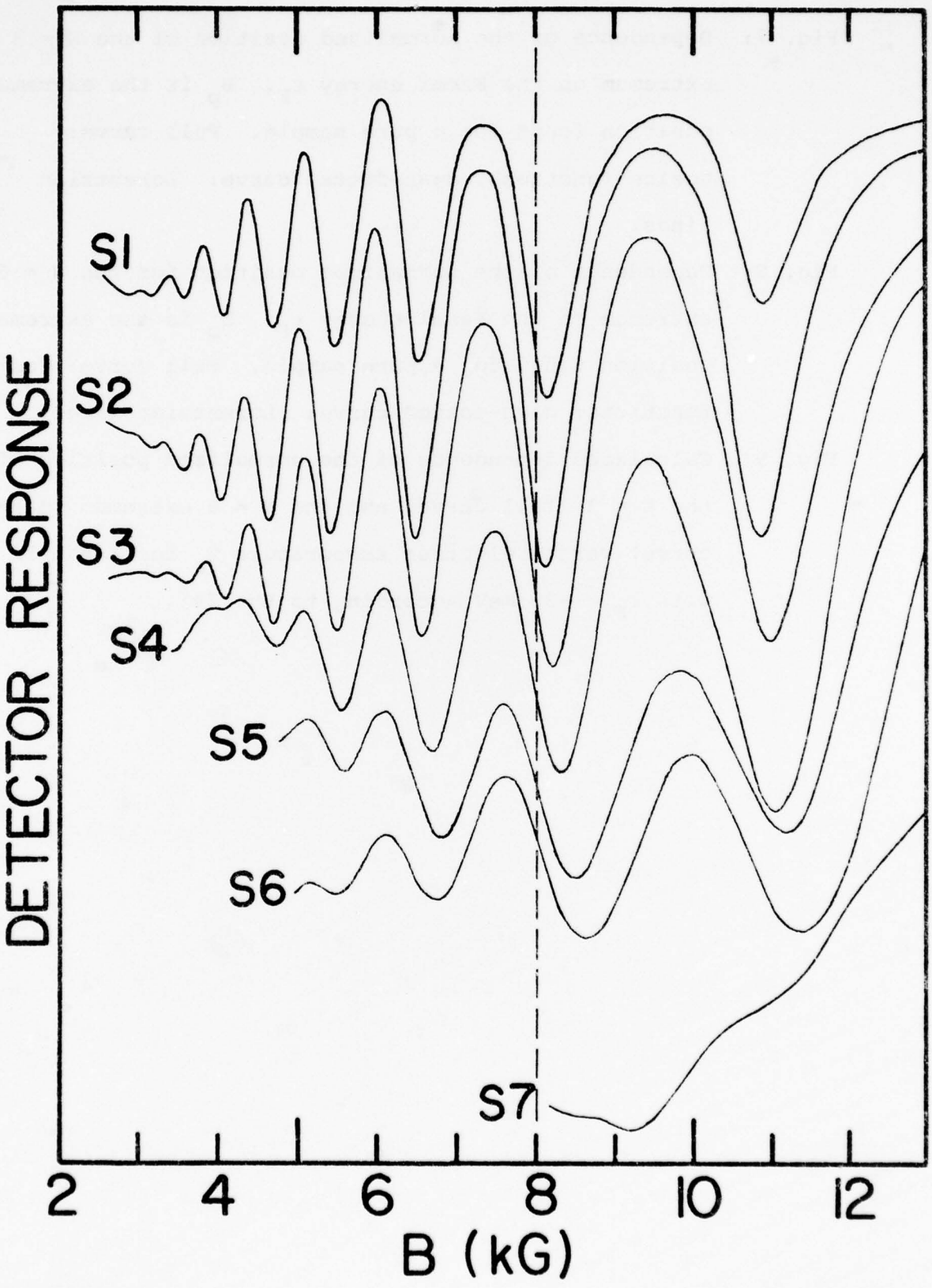
DETECTOR RESPONSE
S1
S2
S3
S4
S5
S6
S7
2
4
6
8
10
12
B (kG)

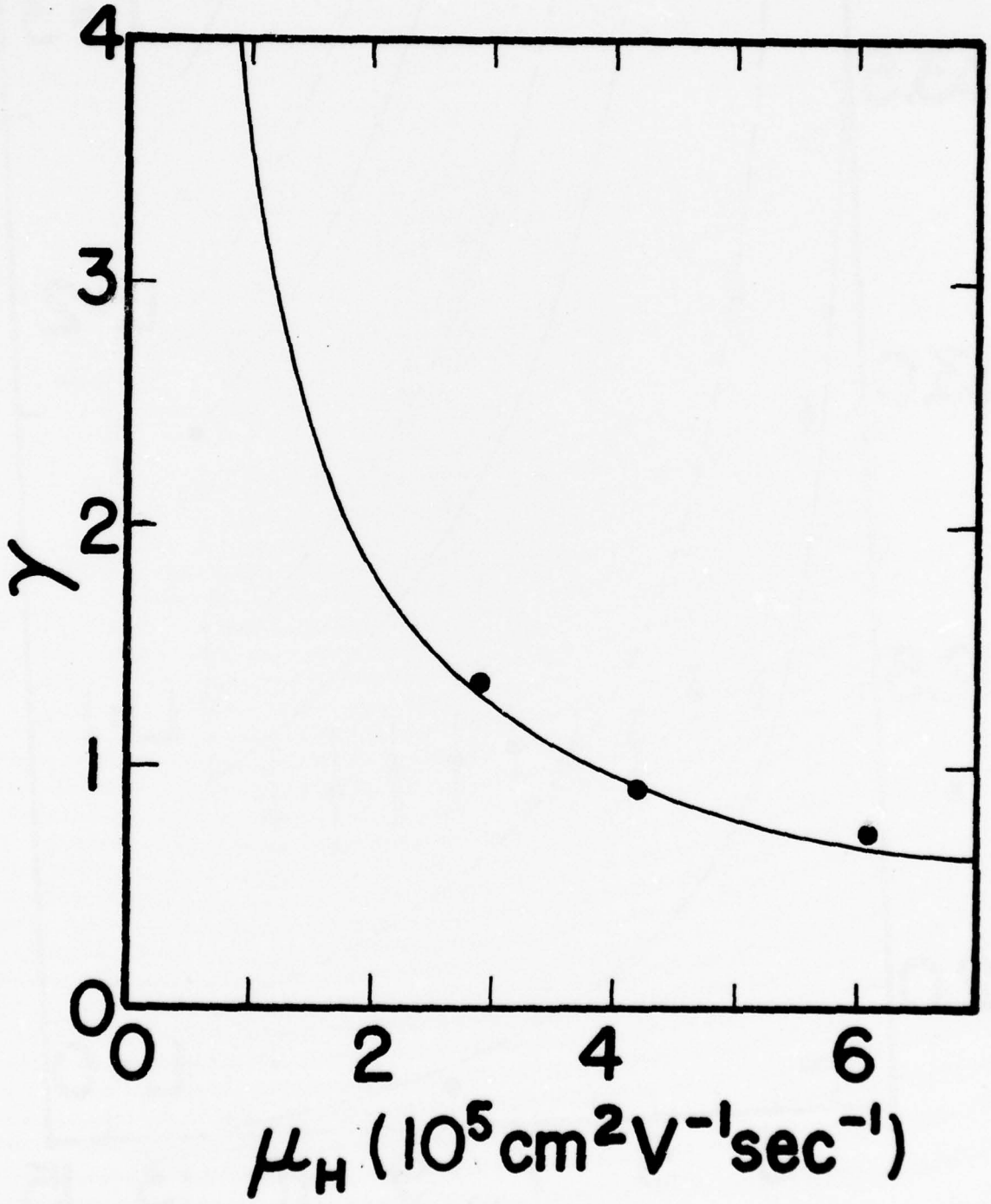
4
3
2
1
0
γ
0
2
4
6
μH (10⁵cm²V⁻¹sec⁻¹)

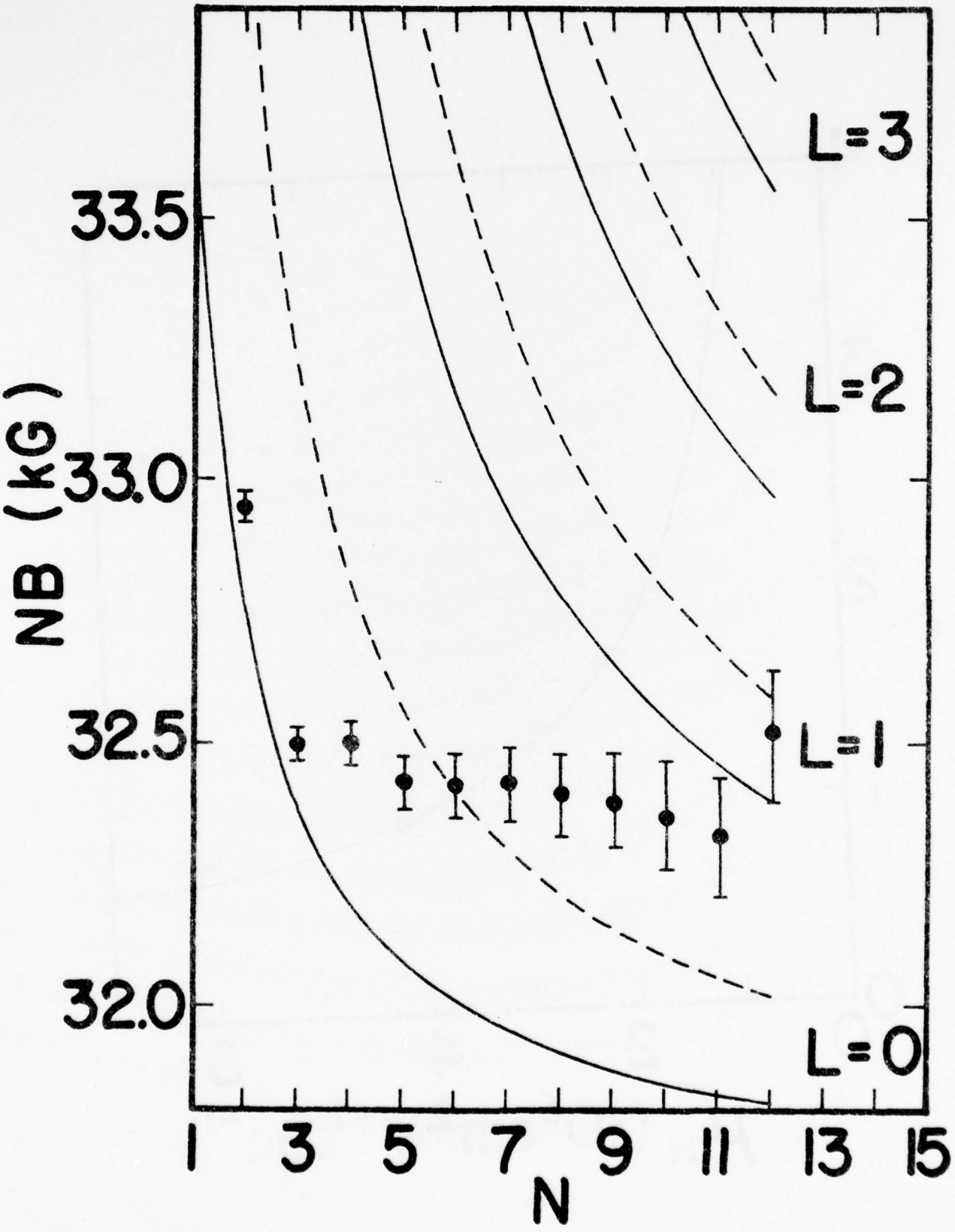
L=3
L=2
L=1
L=0
33.5
33.0
32.5
32.0
NB (kG)
1
3
5
7
9
11
13
15
N

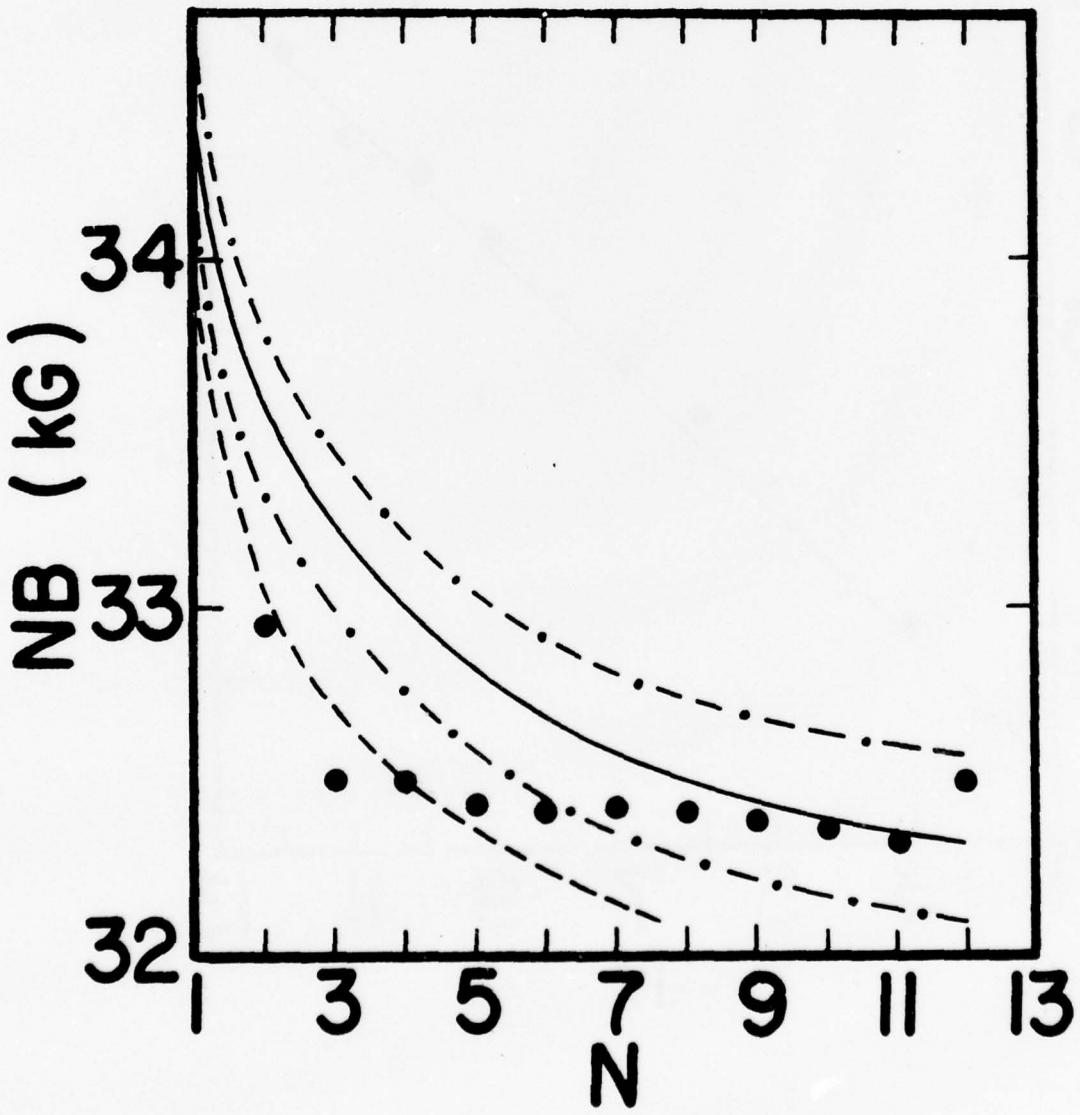
NB (kG)
34
33
32
1
3
5
7
9
11
13
N

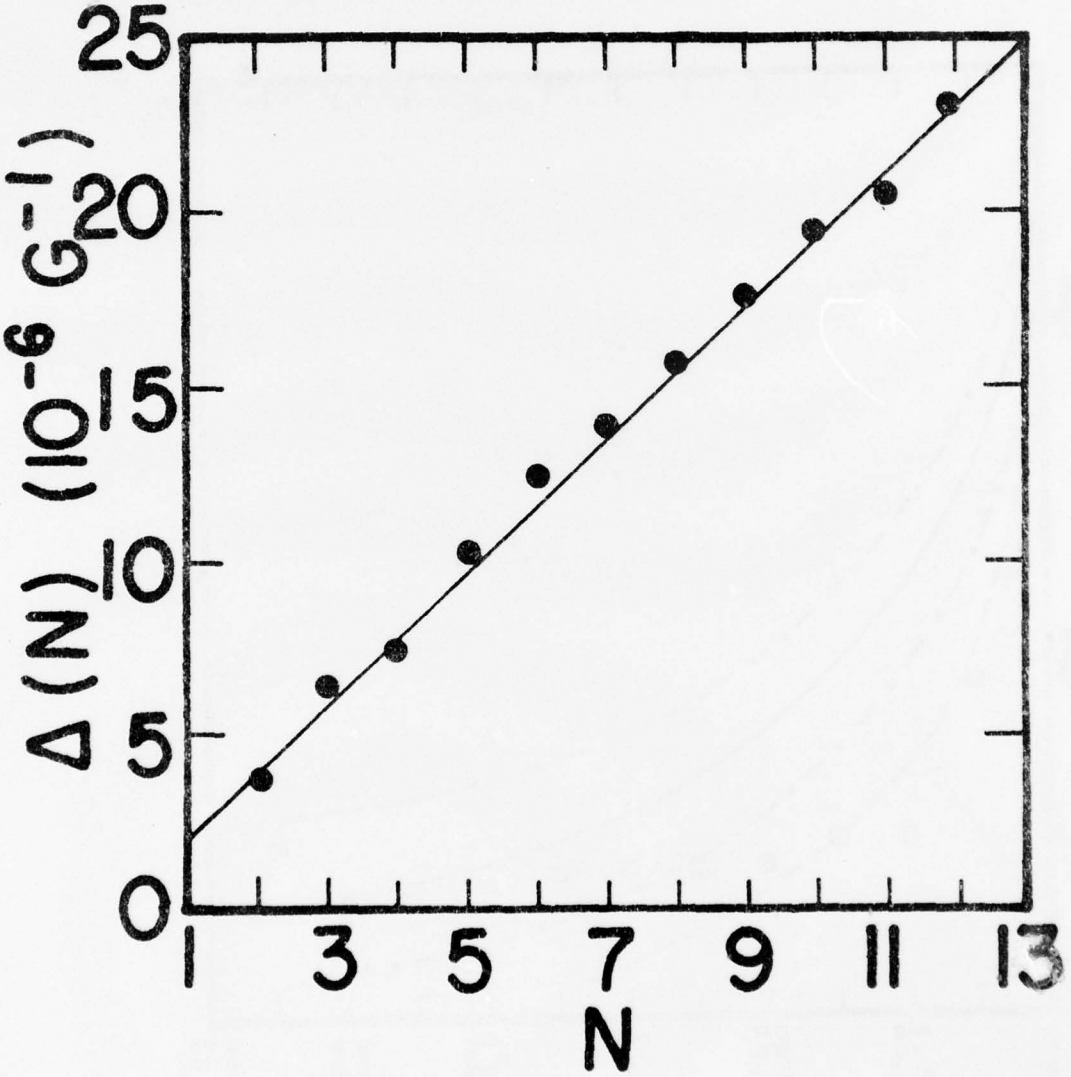
25
20
15
10
5
0
Δ(N) (10⁻⁶ G⁻¹)
1
3
5
7
9
11
13
N

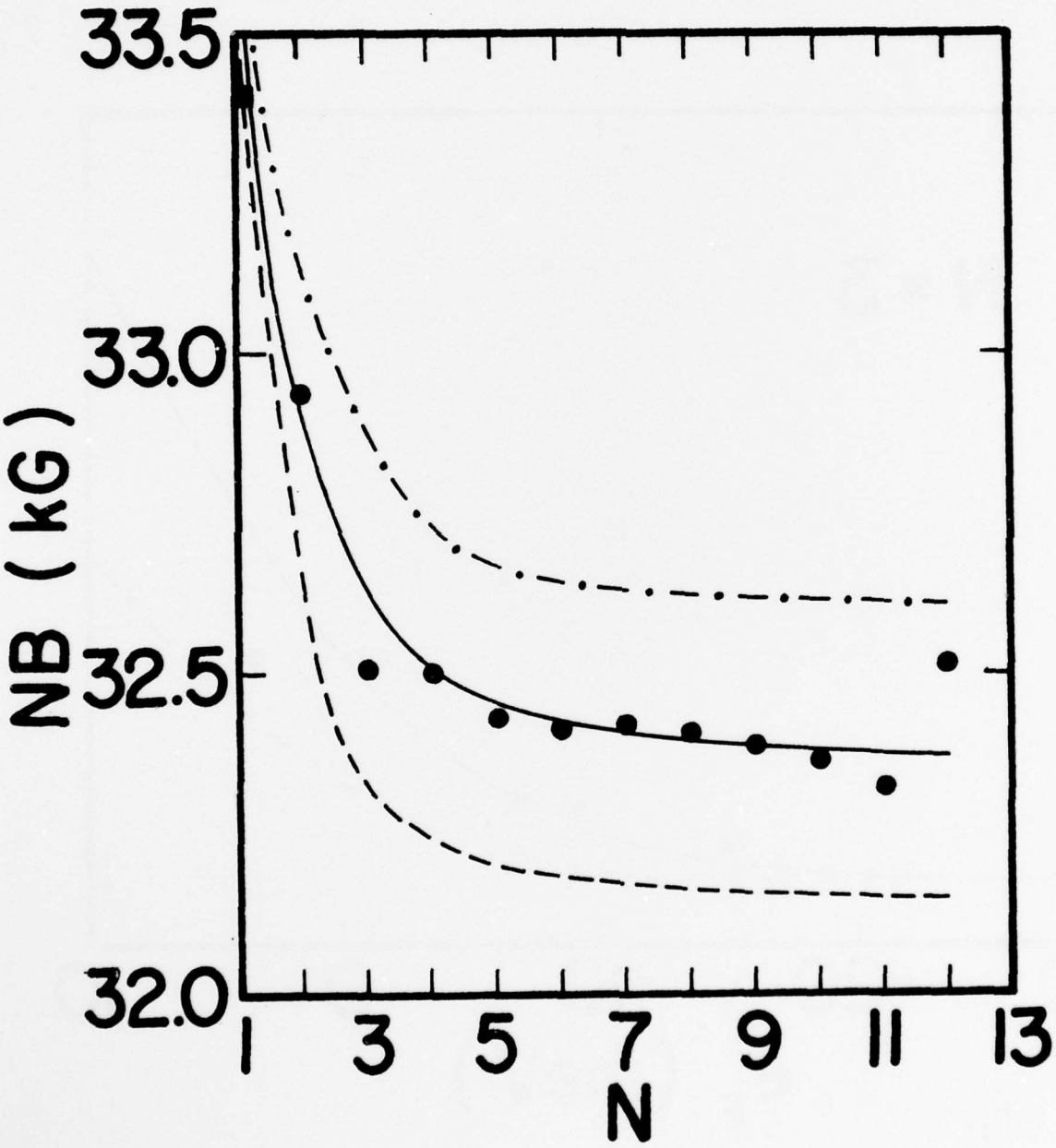
33.5
33.0
32.5
32.0
NB (kG)
1
3
5
7
9
11
13
N

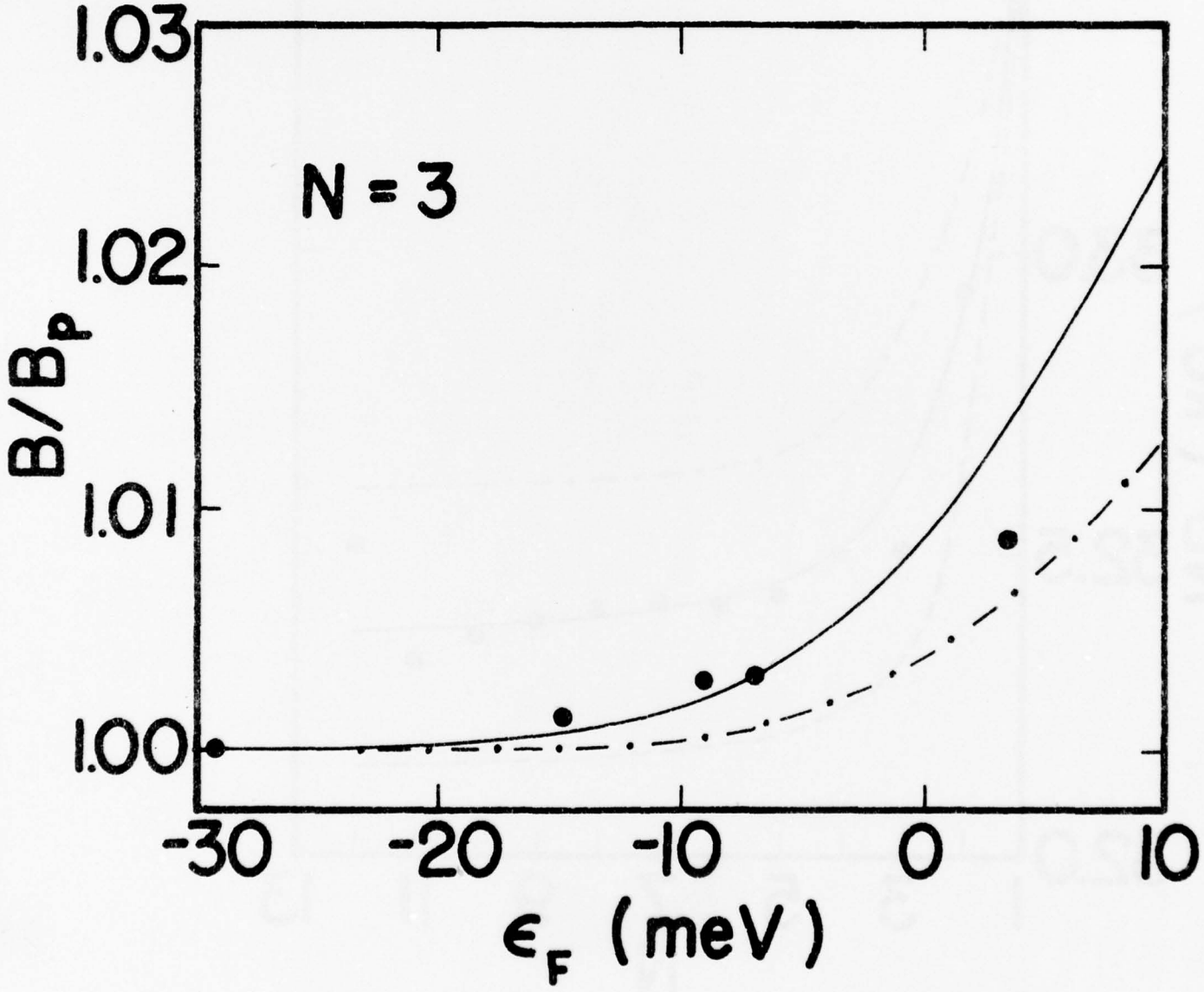
1.03
1.02
1.01
1.00
N = 3
B/B_p
-30
-20
-10
0
10
ε_F (meV)

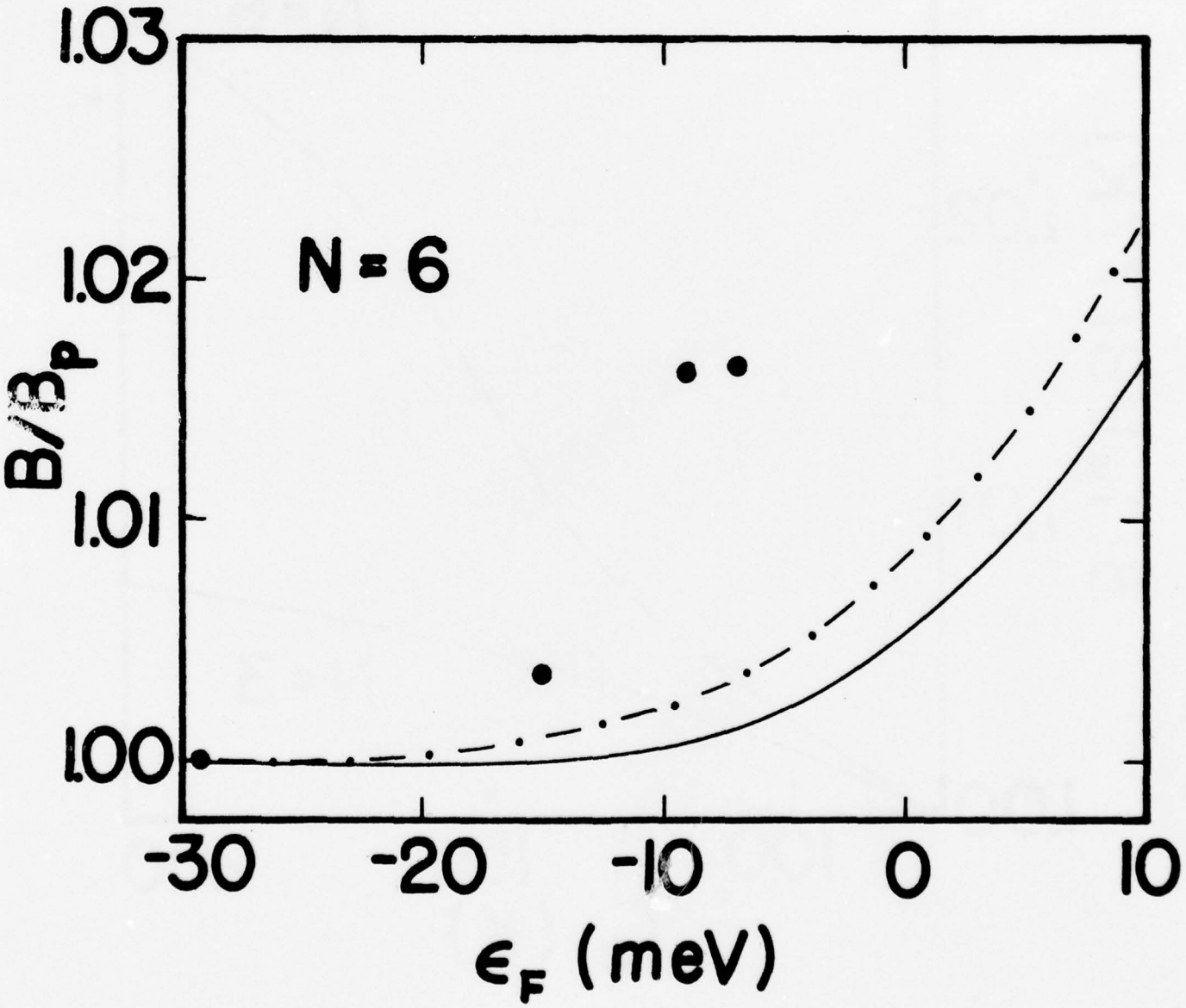
1.03
1.02
1.01
1.00
N = 6
B/B_p
-30
-20
-10
0
10
ε_F (meV)

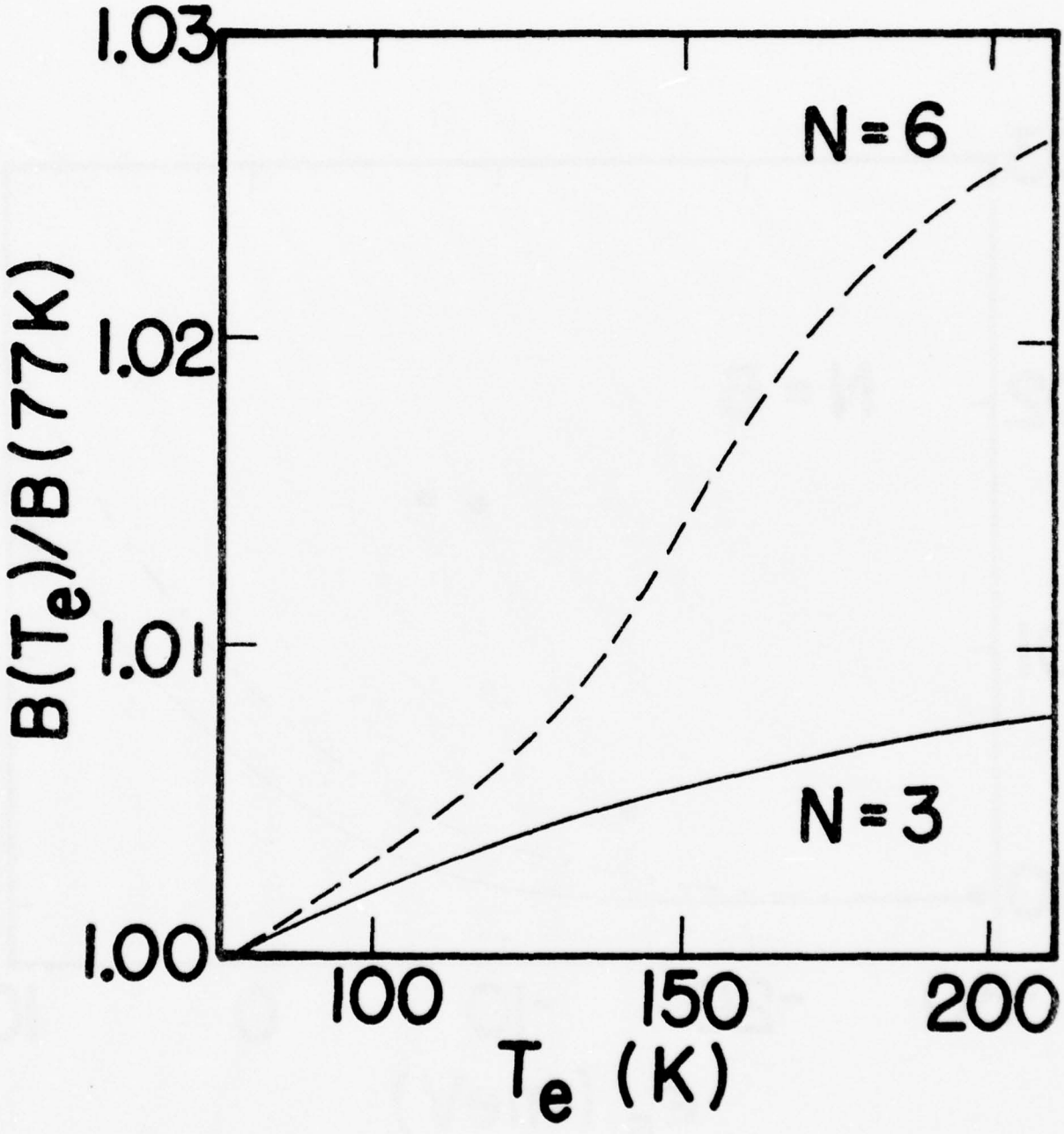
1.03
1.02
1.01
1.00
B(Te)/B(77K)
N=6
N=3
100
150
200
Te (K)

Solid-State Electronics, 1978, Vol. 21, pp. 247–250. Pergamon Press. Printed in Great Britain

CO_2 LASER-INDUCED HOT ELECTRON EFFECTS IN n-InSb†

B. T. MOORE, D. G. SEILER and H. KAHLERT‡
Department of Physics, North Texas State University, Denton, TX 76203, U.S.A.

Abstract—The influence of a 3-μsec wide CO_2 laser pulse on the Shubnikov–de Haas (SdH) effect in a $1.4 \times 10^{15}\,cm^{-3}$ sample of n-InSb has been investigated at a lattice temperature of 1.8 K. During the time the sample is illuminated the SdH amplitudes are found to decrease with increasing laser power. For a peak incident power of about 1 watt, the SdH oscillatory behavior corresponds to that measured at a lattice temperature of 4.6 K for the non-illuminated sample. These results form the first direct and quantitative evidence for electron heating induced by CO_2 laser radiation and permit the evaluation of a phenomenological energy relaxation time.

1. INTRODUCTION

Hot electrons in InSb created by d.c. electric fields have been extensively studied by a variety of experiments, both for nondegenerate and degenerate statistics. However, for the case of optical heating, much less information is available. In pure ($<10^{14}\,cm^{-3}$) samples of InSb illuminated by long wavelength radiation, free carrier absorption is known to cause an increase in the mean energy of the electron gas as observed by changes in conductivity resulting from a mobility variation[1, 2]. Determination of electron temperatures from photoconductivity data depends upon the assumptions made concerning the dominant scattering mechanisms. In addition, this technique is not as sensitive in degenerate samples of InSb since the mobility is not strongly dependent upon temperature.

In this paper, we present the first direct measurements of CO_2-laser induced hot electron temperatures in degenerate n-type InSb. These measurements involve determining the amplitude of the Shubnikov–de Haas (SdH) oscillations which are strongly dependent upon the temperature of the conduction electrons. In addition, a phenomenological value for the energy relaxation time is estimated from simple considerations of energy balance.

2. THEORY

(a) *Free carrier absorption and electron heating*

For sufficiently low intesities where two photon processes can be neglected, the absorption of CO_2 laser radiation at wavelengths between 9 and 11μm ($h\nu \simeq 0.117$ eV) in n-InSb will take place through interaction with free electrons in the conduction band. Electrons excited to high energies by absorption of a photon may undergo energy relaxation through two competing processes: electron-electron scattering and polar-optical phonon emission. This phonon emission transfers the absorbed energy of the photoexcited electrons to the lattice. Electron-electron scattering, on the other hand, distributes the absorbed photon energy within the electron gas. If this process is sufficiently fast, i.e. if the concentration is high enough, a non-equilibrium carrier distribution will be established, which is characterized by an electron temperature, T_e. It should be noted that the polar-optical phonons emitted by the photoexcited electrons decay to acoustic phonons through a three phonon interaction and thus have a long lifetime[3]. Some of these optical phonons may therefore be reabsorbed by the electron gas providing an additional source of heating besides the electron-electron thermalization process.

The ultimate transfer of the absorbed photon energy to the environment surrounding the sample takes place through acoustic phonons, either emitted directly by the gas or created (in pairs) by the decay of optical phonons. But since the rate of emission of acoustic phonons is slow compared to that for emission of optical phonons, this will not become a significant energy loss mechanism until the electron gas has cooled below the point where optical phonon emission can take place.

Hearn[4, 5] has made calculations for InSb at liquid helium temperatures which indicate that, for concentrations above a critical value of $n_c = 10^8$ to $10^{11}\,cm^{-3}$, electron-electron scattering should dominate. High magnetic field calculations[6, 7] raise the estimated concentration at which T_e is valid to $n_c \sim 10^{14}\,cm^{-3}$. However, the assumption used in these papers that the Landau levels above the bottom $N = 0$ level will not be populated is not valid under the conditions of this experiment. We assume for the electron concentrations of interest here ($n = 1.4 \times 10^{15}\,cm^{-3}$), that the energy distribution of the electron gas with laser heating will be characterized by a temperature, T_e, which is greater than the lattice temperature, T_L. This distribution will then be cooled by a combination of optical and acoustic phonons. The effects caused by emission of optical phonons prior to thermalization of the photoexcited electrons present additional complications.

(b) *Shubnikov–de Haas effect under carrier heating conditions*

Isaacson and Bridges[8] first used the SdH effect in InSb to obtain hot electron temperatures with applied

†Work supported in part by the Office of Naval Research.

‡On leave from Ludwig Boltzmann Institut fuer Festkoerperphysik and Institut fuer Angewandte Physik, Universitaet Wien, Austria.

electric fields. Further electric field induced hot carrier studies were made using the SdH effect by Bauer and Kahlert[9–11]. In this paper, we show that the SdH effect can also be used to study laser-induced hot electrons. The SdH oscillations in the longitudinal magnetoresistance of a degenerate semi-conductor can be observed under the following conditions[12]:

$$\omega_c \mathrm{T} > 1,\ \hbar\omega_c > k_B T_e,\ \epsilon_F > \hbar\omega_c, \tag{1}$$

where $\omega_c = eB/m^*c$, is the cyclotron resonance frequency and T is the collision time. Assuming that the Dingle temperature and the spin-splitting factor remain constant as the electron temperature changes, the ratio of SdH amplitudes at two temperatures is given by

$$\frac{A_1}{A_2} = \frac{X_1/\sinh(X_1)}{X_2/\sinh(X_2)} \tag{2}$$

where

$$X_i = 2\pi^2 k_B T_i/\hbar\omega_c \tag{3}$$

The use of eqn (2) to extract the temperature of the hot electron gas is presented in Section 4 of this paper.

(c) *Relaxation time*

The calculation of a phenomenological relaxation time is based upon the balance of energy gain and loss processes for the electron gas in the illuminated sample volume. The energy gain is due to the absorption of laser photons and subsequent thermalization of photoexcited electrons while the loss is due to energy transfer from the electron gas to the lattice. The energy balance equation for a single electron has the form

$$\frac{\mathrm{d}\epsilon}{\mathrm{d}t} = -\frac{\epsilon(T_e) - \epsilon(T_L)}{\tau} + P_{\mathrm{abs}} \tag{4}$$

where P_{abs} is the absorbed power per electron in the illuminated sample volume and τ is the energy relaxation time. The temperature dependence of the mean energy of an electron in a degenerate semiconductor is taken to be [13]

$$\epsilon(T) = \frac{k_B T F_{3/2}(\eta)}{F_{1/2}(\eta)}, \tag{5}$$

and where

$$\eta = \frac{\epsilon_F}{k_B T}$$

is the reduced Fermi energy.

If a steady-state condition can be established under laser illumination so that

$$\frac{\mathrm{d}\epsilon}{\mathrm{d}t} = 0, \tag{6}$$

then τ may be calculated from the equation

$$\tau = \frac{\epsilon(T_e) - \epsilon(T_L)}{P_{\mathrm{abs}}} \tag{7}$$

The assumption was made earlier that thermalization of the photoexcited electron occurs through electron-electron scattering before significant optical phonon emission from the photoexcited carriers takes place. However, when phonon emission takes place prior to thermalization, e.g. to satisfy momentum conservation during photon absorption, a more detailed theoretical treatment would be required.

3. EXPERIMENTAL WORK

The samples used were cut from a bulk sample of n-type InSb having a concentration of $1.4 \times 10^{15}\,\mathrm{cm}^{-3}$ and a Hall mobility of $12 \times 10^5\,\mathrm{cm}^2/\mathrm{V\,sec}$ at 1.5 K. The optical surfaces were ground with Al_2O_3 polish with a grit size of 0.3 μm ($\sim\lambda/30$). The absorption coefficient at 10.6 μm is taken to be $0.032\,\mathrm{cm}^{-1}$ which is an extrapolated value taken from Patel[14], who measured $0.3\,\mathrm{cm}^{-1}$ for a sample $1.3 \times 10^{16}\,\mathrm{cm}^{-3}$. The final sample dimensions were 6.5 mm × 1.8 mm × 0.07 mm thick. Two current contacts and two potential contacts were made with 25 μm diameter gold wire using indium solder.

Figure 1 shows a schematic diagram of the equipment as used in this experiment. The sample was illuminated with a pulse produced by mechanically chopping a beam (TEM_{00} mode) from a cw CO_2 laser. The pulse width used in this experiment was ~3 μsec (F.W.H.M.) with a rise time of ~2 μsec. The repetition rate was 2000 Hz. The pulse was focussed to a diameter of 1.8 mm at the sample and positioned to illuminate the region of the sample between the potential contacts. The CO_2 laser is grating tuned and produces single line outputs of several watts over most of the 9 μm to 11 μm wavelength range. The experiment reported here was carried out at λ = 10.3 μm with powers up to 10 watts available. A He–Ne laser used in conjunction with a silicon PIN photodiode produced a trigger pulse for the pulse generating and delaying electronics.

The magnetoresistance of the sample was then measured using a short (5 $n$sec) electrical probe pulse generated by a fast rise time (<1 $n$sec) Tektronix pulse generator. The electrical pulse, kept small to avoid heating by the electric field, was syncronized to coincide with the peak of the laser pulse. The difference voltage between the two potential probes was measured with a Tektronix 7904/7S14 sampling oscilloscope.

Previous pulsed d.c. SdH measurements[15] reported by the authors were made by directly recording the output of the sampling oscilloscope vs. magnetic field. However, significant improvements in signal-to-noise ratio have been obtained through the use of magnetic field modulation in combination with the fast sampling methods. This combined technique was first developed by Kahlert and Seiler[16, 17] for observing hot electron magnetophonon structure in n-InSb at 77 K. When used to observe the SdH effect, this technique produces a detector response which is proportional to the first derivative of the magnetoresistance oscillations, but it does not affect the ratio of amplitudes as given in equation (2). In this method, the output of the sampling oscilloscope is fed into a lock-in amplifier, the output of which is then recorded.

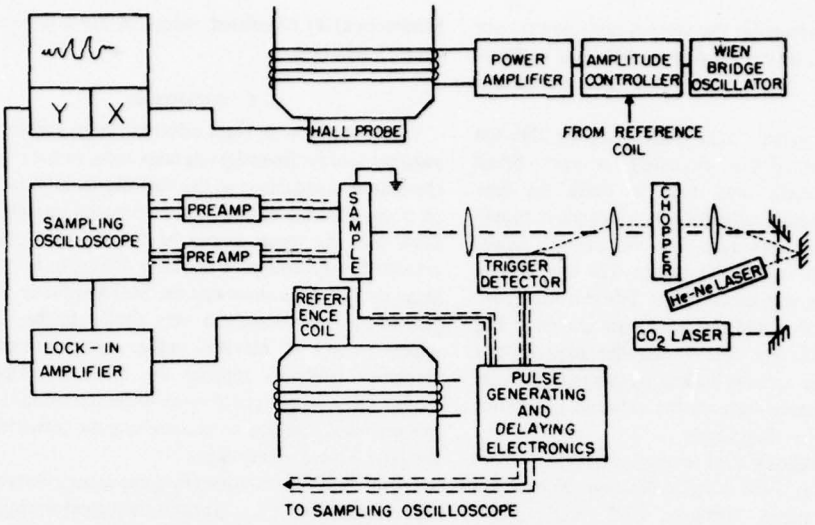

Fig. 1. Block diagram of experimental apparatus.

4. RESULTS AND ANALYSIS

Figure 2 shows SdH oscillations for lattice temperatures, T_L, between 1.8 and 9.6 K. The oscillations recorded for various incident laser powers are shown in Fig. 3 for $T_L = 1.8$ K. Qualitatively, it can be seen that the oscillations are damped by increasing laser power in a manner analogous to the damping caused by elevated lattice temperatures. These data show directly that the mean energy of the electron gas increases with laser illumination.

The SdH amplitude ratios as a function of lattice temperature (without laser illumination) are plotted on the left-hand side of Fig. 4 and exhibit the characteristic dependence given by eqn (2). The variation of the amplitude ratio with incident laser power is plotted on the right-hand side of Fig. 4. The reference amplitude A_0 for both graphs was taken at 1.8 K with no laser illumination.

The electron temperature corresponding to each laser power is determined by comparison of the amplitude ratio shown in both halves of Fig. 4. For example, the dotted lines show that, for a 0.98 W peak incident laser power, an amplitude ratio of 0.22 was obtained. From the temperature dependence it is seen that an amplitude of 0.22 corresponds to a temperature of 4.6 K. Thus, a phenomenological electron gas temperature of 4.6 K is obtained for an incident laser power of 0.98 watts at a lattice temperature of 1.8 K. The electron temperatures

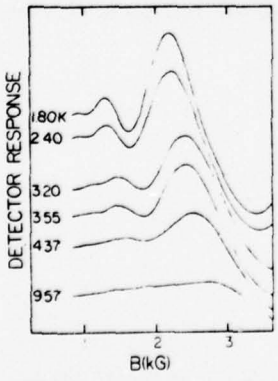

Fig. 2. SdH oscillatory magnetoresistance for several lattice temperatures taken while detecting at the first harmonic of the modulation frequency (no laser illumination).

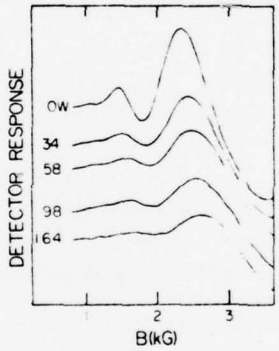

Fig. 3. SdH oscillations for various incident laser powers at a constant lattice temperature of 1.8 K. Power levels listed are peak incident power at the sample.

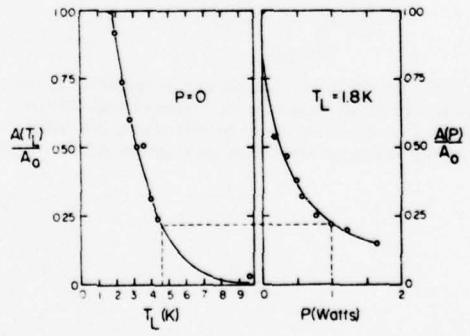

Fig. 4. SdH amplitude ratios versus lattice temp (left) and versus incident laser power (right).

obtained in this manner for the various laser powers are plotted in Fig. 5. A distinct non-linear behavior is observed which cannot be accounted for by experimental uncertainties.

In order to determine that lattice heating did not contribute to the effects discussed, a very broad (~30 μsec) laser pulse was used to study the time dependence of the SdH amplitude. A lower pulse repetition rate of 166 Hz was used, but the average power input to the sample was ~50% higher. The temperature of the electron gas was measured at different time positions during the pulse, and the results are shown in Fig. 6. This figure indicates that within the experimental uncertainties lattice heating makes an insignificant contribution to the temperature of the electron gas during laser illumination for these times.

Results of calculations of energy relaxation times based upon eqn (7) yield a value of about 25 nsec for electron temperatures between 3.2 and 5.2 K.

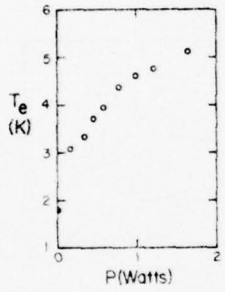

Fig. 5. Electron temperature T_e versus laser power.

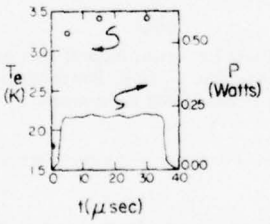

Fig. 6. Time dependence of the electron temperature T_e in conjunction with the corresponding laser pulse of long duration that was used to check for lattice heating effects. No lattice heating effects are observed on these time scales.

Sandercock[18] calculated values of $1/\tau \leq 10^7\ \text{sec}^{-1}$ between 2 and 12 K.

5. CONCLUSIONS

The Shubnikov–de Haas effect has been shown to be a valuable tool for investigating laser induced hot electrons. Qualitative comparison of the SdH oscillations as recorded under illuminated and non-illuminated circumstances show that the mean energy of the electron gas is increased by absorption of the laser radiation. In addition, these comparisons show that the SdH amplitude damping caused by laser heating is very similar to the damping which occurs at elevated lattice temperatures. This similarity tends to support the electron temperature model. Quantitative comparison of these amplitude ratios has provided a means of determining the temperature of the laser heated electron gas.

On the basis of the electron temperatures derived from these measurements, a phenomenological energy relaxation time has been determined. Further experiments are planned which should provide additional insight into the physical nature of this relaxation process.

REFERENCES

1. B. V. Rollin, *Phys. Soc. Proc.* **77**, 1102 (1961).
2. Sh. M. Kogan, *Sov. Phys.-Solid State* **4**, 1386 (1963).
3. D. K. Ferry, *Phys. Rev.* **B8**, 1544 (1973).
4. C. J. Hearn, *Proc. Phys. Soc.* **86**, 881 (1965).
5. C. J. Hearn, *Phys. Lett.* **20**, 113 (1966).
6. A. M. Zlobin and P. S. Zyryanov, *Sov. Phys.-Uspekhi* **14**, 379 (1972).
7. Sh. M. Kogan, V. D. Shadrin and A. Ya. Shulman, *Sov. Phys.-Jept.* **41**, 686 (1975).
8. R. A. Isaacson and F. Bridges, *Solid State Comm.* **4**, 635 (1966).
9. G. Bauer and H. Kahlert, *J. Phys.* **C6**, 1253 (1973).
10. H. Kahlert and G. Bauer, *Phys. Rev.* **B7**, 2670 (1973).
11. G. Bauer and H. Kahlert, *Phys. Rev.* **B5**, 566 (1972).
12. P. N. Argyes, *J. Phys. Chem. Solids* **4**, 19 (1959).
13. G. Bauer in *Springer Tracts in Modern Physics*, Vol. 74, p. 1. Springer-Verlag, New York (1974).
14. C. K. N. Patel and E. D. Shaw, *Phys. Rev.* **B3**, 1279 (1971).
15. B. Moore, D. G. Seiler, and H. Kahlert, *Bull. Amer. Phys. Soc* **22**, 460 (1977).
16. H. Kahlert and D. G. Seiler, *Rev. Sci. Inst.* **48**, 1017 (1977).
17. H. Kahlert, D. G. Seiler and J. R. Barker, *Solid-St. Electron.* **21**, 229 (1978).
18. J. R. Sandercock, *Proc. Phys. Soc.* **86**, 1221 (1965).

VOLUME 41, NUMBER 5 PHYSICAL REVIEW LETTERS 31 JULY 1978

New Hybrid Photoconductivity Technique for the Investigation of CO_2-Laser-Induced Hot-Carrier and Free-Carrier Absorption Effects in Degenerate *n*-InSb at 1.8 K

D. G. Seiler, J. R. Barker,[a] and B. T. Moore
Department of Physics, North Texas State University, Denton, Texas 76203
(Received 12 April 1978)

Free-carrier absorption of tuned CO_2-laser radiation is shown to be a valuable new tool for the extraction of information on photoheated hot carriers and the free-carrier absorption coefficients in low-concentration, degenerate *n*-InSb at liquid helium temperatures. The technique exploits parallel photoheating and dc-heating experiments conducted in a regime where conductivity changes are unambiguously determined by mobility changes.

Illumination of semiconductors with intense laser radiation leads to carrier heating.[1,2] Studies of hot-carrier distributions are important because they yield information concerning the electron-electron and electron-phonon interactions in semiconductors. Here, we report for the first time free-carrier absorption-induced photoconductivity measurements on degenerate *n*-InSb under optical excitation at CO_2-laser wavelengths that allow extraction of electron temperatures. Furthermore, we present the results of a unique combination of independent electrical and laser experiments carried out at liquid helium temperatures on the same low-concentration sample of *n*-InSb, that allows, in principle, the precision extraction of the free-carrier absorption coefficient as a function of CO_2 laser frequency and laser power. These absorption coefficients are so small at 10 μm that their determination from classical optical absorption measurements alone would prove impractical. Consequently, these novel hybrid experiments and their interpretation result in the *first* reported estimates for the free-carrier absorption coefficient of low-concentration (1.4×10^{15} cm^{-3}) *n*-InSb.

Figure 1 shows a block diagram of the equipment used in this experiment. The sample, immersed in liquid helium in a variable-temperature optical Dewar, was illuminated with a laser pulse produced by mechanically chopping a beam (TEM_{00} mode) from a grating-tuned cw CO_2 laser which provided single-line outputs of several watts from ~9.2 to ~10.9 μm. In the present experiments, a laser pulse with a width of ~20 μsec [FWHM (full width at half-maximum)], a rise and fall time of ~2 μsec, and a repetition rate of ~1700 Hz were employed. The laser pulse was positioned to illuminate the region of the sample between the potential contacts. Calibrated filters of either CaF_2 sheets or sheets of Teflon or some combination of both were used for attenuation.

Figure 2 shows comprehensive results obtained from three separate experiments on how the mobility changes with (1) applied electrical power P_E per electron (obtained from electrical heating

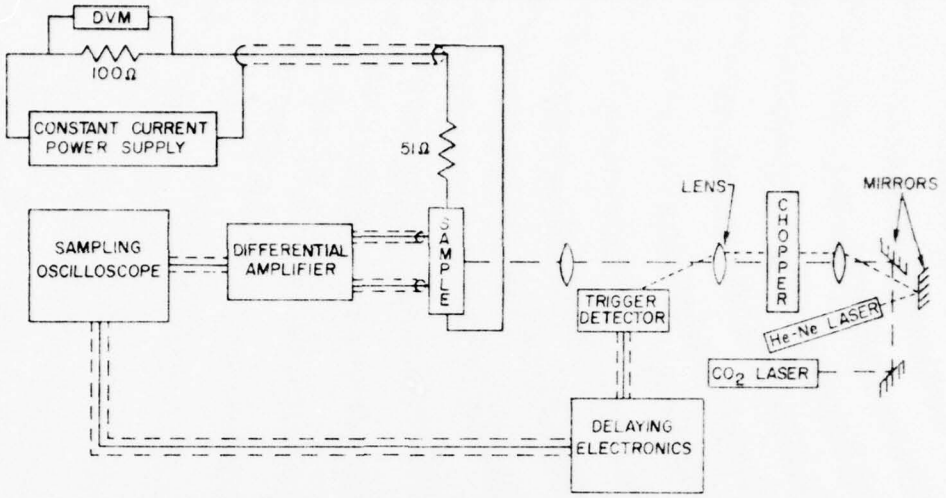

FIG. 1. Block diagram of experimental apparatus.

experiments as $e\mu E^2$) as shown in Fig. 2(a); (2) lattice temperature T_L as shown in Fig. 2(b); and (3) peak incident laser power P_I as shown in Fig. 2(c). The electron concentration was determined to be 1.4×10^{15} cm^{-3} from the period of Shubnikov–de Haas (SdH) oscillations and is *constant* at these lattice temperatures and low laser powers where two-photon absorption processes are completely negligible. Consequently,

$$\Delta\sigma/\sigma = \Delta\mu/\mu = \Delta V/V_0, \tag{1}$$

where $\Delta\sigma = \sigma - \sigma_0$, $\Delta\mu = \mu - \mu_0$, and $\Delta V = V - V_0$ are the changes in the conductivity, mobility, and voltage drop across the sample leads, as either T_L, P_I, or P_E is varied while the other two variables are held constant. The values of

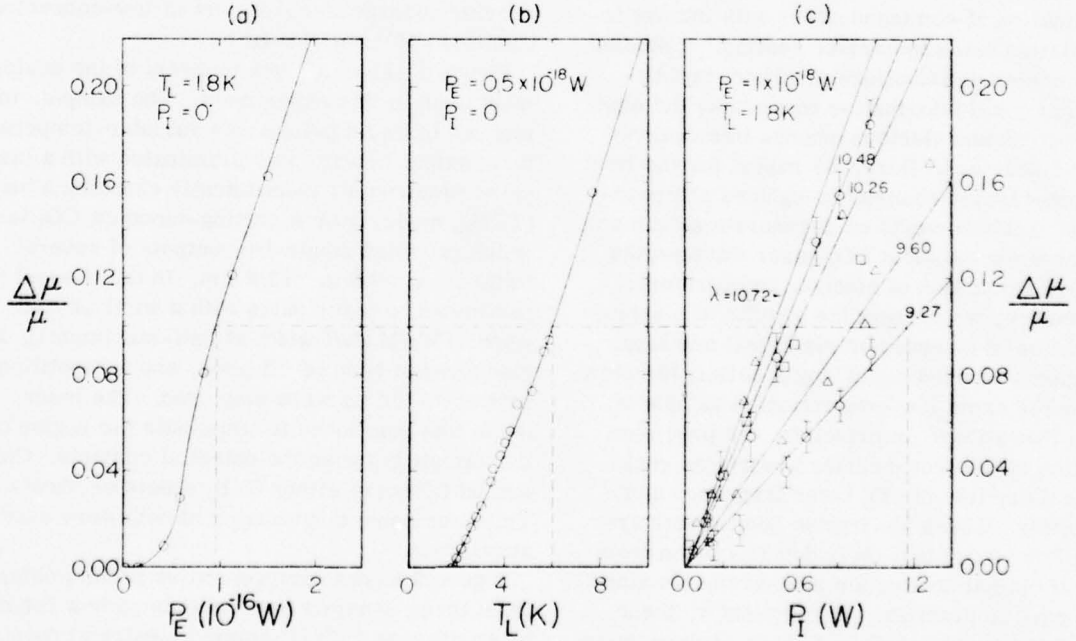

FIG. 2. Mobility changes with (a) applied electrical power per electron P_E (which for a given electric field E is calculated from $e\mu E^2$), (b) lattice temperature T_L, and (c) peak incident laser power P_I. Note that in all cases the mobility increases with either P_E, T_L, or P_I.

σ_0, μ_0, and V_0 are determined at zero laser power ($P_I = 0$) under Ohmic conditions at a lattice temperature of 1.8 K.

As shown in Fig. 2(b), the mobility at $P_I = 0$ obtained using Ohmic electric fields increases with lattice temperature which is consistent with completely dominant ionized-impurity momentum relaxation.[3] We find $\sigma_0 \sim 19.3\ (\Omega\ \mathrm{cm})^{-1}$, $\mu_0 \sim 8.6 \times 10^4\ \mathrm{cm^2/V \cdot sec}$, in agreement with other experimentally determined mobilities with similar electron concentrations and lattice temperatures.[4,5] At 77 K, σ_0 and μ_0 rise to 75 $(\Omega\ \mathrm{cm})^{-1}$ and $3.2 \times 10^5\ \mathrm{cm^2/V \cdot sec}$, respectivley.

The CO_2-laser radiation is partially absorbed via free-carrier absorption processes and subsequently leads to a mobility increase as observed in Fig. 2(c) where $\Delta\mu/\mu$ is plotted versus P_I, the peak incident laser power at a constant lattice temperature of 1.8 K. An electron temperature $T_e{}^0$ can be determined for each wavelength and value of P_I by making a one-to-one correspondence between the mobility changes in the two cases shown in Figs. 2(b) and 2(c). For example, Fig. 2(c) shows that for a peak incident power of about 1.16 W, $\Delta\mu/\mu \approx 0.10$, which corresponds to a temperature $T_e{}^0 \sim 6$ K.

The lines shown in Fig. 2 are the "best fit" lines through the data points. Consequently, a plot of $T_e{}^0$ versus P_I can be made as shown in Fig. 3. Provided the steady state is controlled by intercarrier collisions, the carrier distribution will be a heated Fermi-Dirac distribution with a true electron temperature T_e which may be identified with $T_e{}^0$ if the carrier heating maintains the system within the regime dominated by ionized-impurity–limited mobilities. The steady-state remnant excitation pulse at $\epsilon \sim \hbar\omega + \epsilon_F$ will have negligible effect on the mobility at our low excitation rates: The low-energy carrier assembly is only minutely depleted by photoexcitation.

The procedure may be repeated at zero laser power ($P_I = 0$) with $T_L = 1.8$ K but instead using a pulsed dc electric field of 20-μsec duration to heat the carriers into the warm-electron regime. These pulsed-current techniques were used to avoid sample lattice heating at high electric fields. Figure 2(a) shows the resultant mobility change versus applied electrical power P_E for the same sample. The extracted effective electron temperatures $T_e{}^E(P_E)$ may be again identified with the true electron temperature T_e under appropriate conditions. In such a case, we may invert the functional relations $T_e{}^0 = T_e{}^0(P_I)$ and $T_e{}^E = T_e{}^E(P_E)$ to deduce the thermodynamic relationship $P_E = P_a(P_I)$ under the constraint $T_e{}^0 = T_e{}^E = T_e$, where P_a is the portion of absorbed optical power per electron transferred to the carrier assembly via intercarrier collisions prior to dissipation to the lattice. The *extreme* case (*Model I*) occurs when the intercarrier energy-loss rate Γ_{ee} (scattering-out term) exceeds all other energy-loss rates $\Gamma_{e\,\mathrm{ph}}$ due to photon scattering at all energies up to and exceeding the photoexcitation energies ($\sim \epsilon_F + 4k_B T_e + \hbar\omega$). In this instance $P_a = \alpha(\lambda) d P_i$, where $\alpha(\lambda)$ is the steady-state free-carrier absorption coefficient, d is the sample thickness, and P_i is the incident laser power per illuminated electron. It follows that $\alpha(\lambda, T_e)$ may be extracted exactly as the ratio

$$\alpha(\lambda, T_e) = \frac{P_E(T_e)}{P_i(T_e, \lambda)} \frac{1}{d}, \tag{2}$$

where we make explicit the wavelength (λ) and electron temperature (T_e) dependences.

Our estimates of the critical carrier concentration n_c for which the condition that $\Gamma_{ee} \gg \Gamma_{e\,\mathrm{ph}}$ ensures a valid electron temperature model are based on similar calculations due to Stratton[6] but for relaxation against a *degenerate* distribution in the presence of Thomas-Fermi screening. While the present sample concentration satisfies $n \gg n_c$ for energies $\epsilon \lesssim \epsilon_F + \hbar\omega_L$, where ϵ_F is the Fermi energy and $\hbar\omega_L$ the LO phonon energy, we

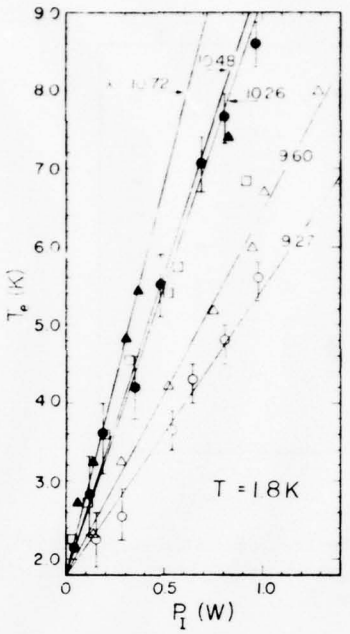

FIG. 3. Electron temperature T_e vs peak incident laser power P_I for various CO_2-laser wavelengths.

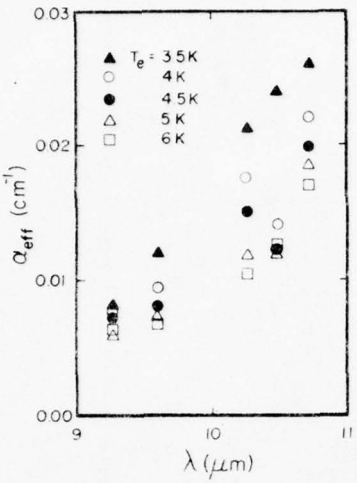

FIG. 4. Effective free-carrier absorption coefficient, α_{eff}, vs wavelength of the CO_2 laser at various electron temperatures T_e.

find $n < n_c$ for higher energies where energy loss to the lattice is controlled by fast polar-mode optical-phonon emission processes. In these circumstances (*Model II*) we might anticipate that a substantial fraction β of the optically absorbed power per electron, $P_a^0 = \alpha d P_i$, is transferred to the lattice by optical-phonon cascading as the photoexcited electrons scatter to energies below the threshold for which $\Gamma_{e\,ph} > \Gamma_{ee}$. The residual power, $P_a = [1 - \beta(\lambda)]P_a^0$, will then be effective in heating the carriers into a Fermi-Dirac distribution with electron temperature T_e via intercarrier collisions. The subsequent quasithermalized distribution will then lose energy to the lattice via predominantly acoustic phonon processes at the rate $[1 - \beta(\lambda)]P_a^0$. In this case we find

$$[1 - \beta(\lambda)]\alpha(\lambda, T_e) = \frac{P_E(T_e)}{P_i(T_e, \lambda)} \frac{1}{d}. \tag{3}$$

The analysis of Models I and II may be summarized by the general expression

$$\alpha_{eff}(\lambda, T_e) = P_E(T_e)/P_i(T_e, \lambda)d, \tag{4}$$

which relates an *effective* free-carrier absorption coefficient $\alpha_{eff} = \alpha(1 - \beta)$ to experimentally accessible quantities. Model I involves $\beta = 0$. Experimentally, as shown in Fig. 4, we find values for α_{eff} in the range 0.005–0.03 cm^{-1} for the electron temperature and wavelength ranges 3.5–6 K and 9.27–10.72 μm, respectively. We note that at 10.6 μm typical values for α have been reported in the range 0.3 to 0.6 cm^{-1} for a higher concentration of $\sim 10^{15}$ cm^{-3} at low temperature.[7]

Plots of α_{eff} versus λ^2 for the range of available wavelengths indicate an approximately linear variation with values extrapolated to zero wavelength of order -0.03 cm^{-1}. These nonzero *negative* extrapolated values are consistent with a *nonzero* loss factor $\beta(\alpha)$. The finite width of the excitation pulse $\Delta\epsilon \sim \epsilon_F + 4k_B T_e$ precludes a strong oscillatory photoconductivity effect [$\beta(\lambda) \sim 1$]. Indeed, the presently available spread of photoexcitation energies $\Delta\epsilon < \hbar\omega_L$ is not sufficient to expose any definite oscillatory structure although a minimum in α_{eff} may be indicated at $\lambda = 10.49$ μm. Further experiments are in progress on other concentration samples to investigate the physical origin of the nonzero loss factor β.

The authors gratefully acknowledge the partial support of this research by the U. S. Office of Naval Research and helpful discussions with A. L. Smirl.

---

[a]On leave from Department of Physics, University of Warwick, Coventry, United Kingdom.

[1]J. Shah, Solid State Electron. 21, 43 (1978).

[2]B. T. Moore, D. G. Seiler, and H. Kahlert, Solid State Electron. 21, 247 (1978).

[3]G. Bauer, in *Springer Tracts in Modern Physics* (Springer, Berlin, 1975), Vol. 74, p. 1.

[4]H. P. R. Frederikse and W. R. Hosler, Phys. Rev. 108, 1136 (1957).

[5]E. H. Putley, Proc. Phys. Soc., London 73, 280 (1958).

[6]R. Stratton, Proc. Roy. Soc. London, Ser. A 246, 406 (1958).

[7]R. B. Dennis, C. R. Pidgeon, S. D. Smith, B. S. Wherret, and R. A. Wood, Proc. Roy. Soc. London, Ser. A 331, 203 (1972).

PHOTOCONDUCTIVITY OF LASER EXCITED HOT ELECTRONS IN DEGENERATE n-InSb*

D G Seiler, J R Barker, B T Moore, and K E Hansen
Department of Physics, North Texas State University
Denton, Texas 76203

CO_2 laser-induced hot carrier and free carrier absorption effects are investigated at 1.8 K. Electron temperatures are extracted for various laser frequencies and powers. Parallel photo- and electrical heating experiments provide information about the photoexcitation and hot carrier generation process.

Optical heating of carriers in semiconductors illuminated by intense laser radiation has been extensively studied with transmission or photoluminescence measurements. Here we examine CO_2 laser-induced heating of electrons in degenerate *n*-InSb at liquid helium temperatures by investigating the corresponding conductivity changes. The free carrier absorption of this CO_2 laser radiation is thus shown to be a valuable new tool for the extraction of information on photoheated hot carriers.

The sample of n-InSb, immersed in liquid helium at 1.8 K, was illuminated with a laser pulse produced by mechanically chopping a beam (TEM_{00} mode) from a grating-tuned cw CO_2 laser. The laser pulse had a width of ~20 μsec (F.W.H.M.), a rise and fall time of ~2 μsec, repetition rate of 1700 Hz, and a peak power of several watts over a number of lines between 9.2 and 10.8 μm. Calibrated filters of either CaF_2 or BaF_2 were used after the chopper for beam attenuation.

Figures 1(a), (b) and (c) show results of three separate experiments on how the mobility ratio μ/μ_0 changes with (a) applied electrical power per electron $P_E(=e\mu E^2)$; (b) lattice temperature T_L; (c) peak incident laser power P_I. The electron concentration (1.4×10^{15} cm^{-3}) is constant at these lattice temperatures and low laser powers where two-photon absorption processes are completely negligible. Consequently, the measured changes in conductivity are simply related to the changes in mobility. As seen in Fig. 1(b), the mobility increases with lattice temperature, T_L, which is consistent with dominant ionized impurity momentum relaxation. Pulsed dc electric fields of 20 μsec duration were used to electrically heat the carriers into the warm electron region as shown in Fig. 1(a) for zero laser power. Additional mobility ratio data were taken at higher values of T_L and P_E

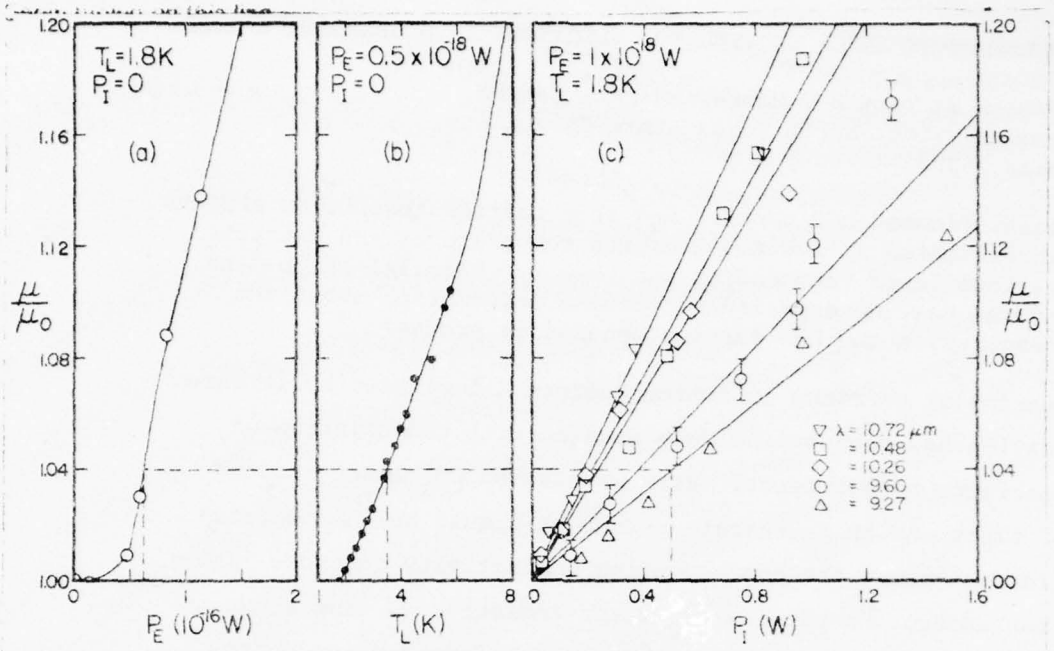

Fig. 1. Mobility changes with (a) P_E, (b) T_L, and (c) P_I.

than are shown on these two plots. The CO_2 laser radiation is partially absorbed via free carrier absorption processes which subsequently leads to a mobility increase as seen in Fig. 1(c) where μ/μ_0 is plotted versus P_I. The laser beam was positioned to illuminate the region of the sample between the potential contacts. In all cases the beam diameter was larger than the width of the sample, but smaller than the distance between the potential leads. From the measured voltage drop across the leads, which contain resistances from both illuminated and unilluminated regions and geometrical considerations of the laser spot size, one can calculate the mobility of only the illuminated region. It is this mobility μ which is plotted in Fig. 1(c).

Electron temperatures can be determined for each wavelength and value of P_I by making a one-to-one correspondence between the mobility changes in the two cases shown in Fig. 1(b) and (c). For example, for λ=9.27 μm and P_I=0.5 W, $\mu/\mu_0 \simeq 1.04$ which corresponds to the same mobility ratio for a temperature $T_L \simeq 3.5$ K. Provided the steady state is controlled by intercarrier collisions, the carrier distribution will be a heated Fermi-Dirac distribution with a true electron temperature T_e if the carrier heating maintains the system within the regime dominated by ionized impurity limited mobilities. A plot of T_e versus P_I

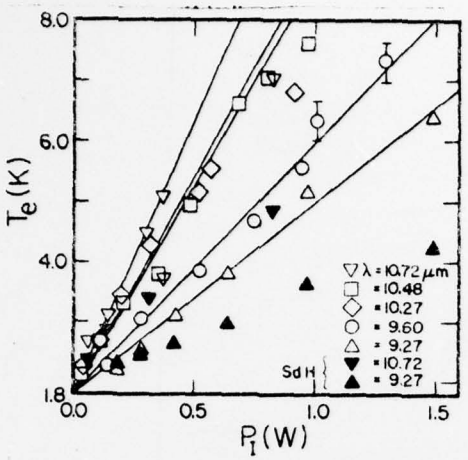

Fig. 2. T_e versus P_I for several CO_2 laser wavelengths.

is shown in Fig. 2.

We have estimated the initial carrier concentration n_c^* for which the energy loss rate $\Gamma_{ee}(\varepsilon)$ (scattering out) due to an excited electron of high energy ε scattering against the background carriers equals the energy loss rate $\Gamma_{eph}(\varepsilon)$ due to phonon scattering using a similar calculation to Stratton but allowing for the degeneracy of the low energy carrier distribution and Thomas-Fermi screening. For the present sample, $n<<n_c^* \sim 10^{18}$ cm^{-3}, for energies $\varepsilon>>\varepsilon_F+\hbar\omega_L$, where energy loss is controlled by polar mode optic phonon emission (phonon energy, $\hbar\omega_L$). However, for $\varepsilon<\varepsilon_F+\hbar\omega_L$, $n>>n_c \sim 10^{14}$ cm^{-3}, where n_c is the electron concentration for a valid electron temperature model computed using a modified Hearn criterion.

We assume therefore that a fraction β of the optically absorbed power $P_a^o=\alpha d P_I$ (Multiple reflections, but not interference effects, are taken into account here. The sample thickness is d, α is the free carrier absorption coefficient and $\alpha d<<1$.) is transferred to the lattice by optic phonon cascading as the photoexcited electrons scatter to energies below the threshold, $\varepsilon \sim \varepsilon_F+\hbar\omega_L$ for which $\Gamma_{eph}>\Gamma_{ee}$. The residual power $P_a=[1-\beta(\lambda)]P_a^o$ is then effective in heating the carriers into a Fermi-Dirac distribution with electron temperature T_e via intercarrier collisions. The subsequent quasi-thermalized distribution will then lose energy to the lattice via predominantly acoustic phonon processes at the rate $[1-\beta(\lambda)]P_a^o$.

By comparing the power balance in the electric field and separate laser heating experiments, we are able to extract an effective free carrier absorption coefficient α_{eff}, related to the true value $\alpha(\lambda,T_e)$ by $\alpha_{eff}=[(1-\beta(\lambda)]\alpha(\lambda,T_e)$ and determined experimentally by the ratio $\alpha_{eff}=P_e(T_e)/dP_i(T_e,\lambda)$. $P_e(T_e)$, as defined previously, is the electrical power per electron producing an electron temperature T_e at zero laser power and $P_i(T_e,\lambda)$ is the incident laser power per

illuminated electron. For samples with $n>n_c^*$, we have $\beta=0$ where $\alpha_{eff}=\alpha$ and a precision extraction of the true absorption coefficient becomes possible.

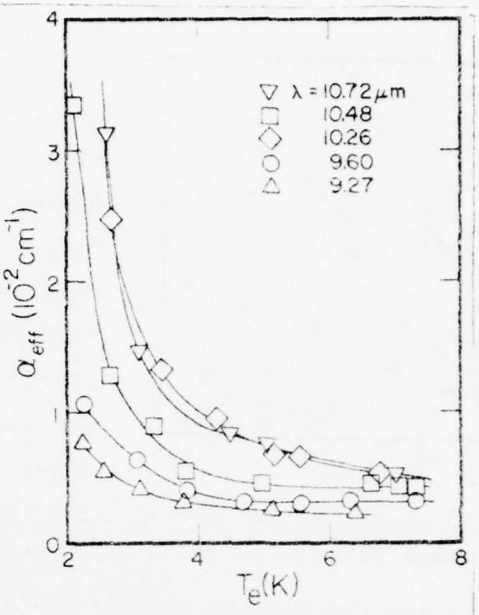

Fig. 3. α_{eff} versus T_e for several values of λ.

Figure 3 shows the variation of α_{eff} with T_e for different constant values of λ for which we expect β=constant. The behavior of α_{eff} can be understood from energy balance considerations for a degenerate electron gas where $\alpha_{eff}=\Delta\varepsilon(T_e)/dP_i\tau_\varepsilon$ and τ_ε is the phenomenological energy relaxation time and $\Delta\varepsilon(T_e)=\varepsilon(T_e)-\varepsilon(T_L)$ where $\varepsilon(T)$ is the average energy of an electron. [At low values of T_e, α_{eff} decreases because $\Delta\varepsilon$ is almost independent of T_e and both P_i and τ_ε increase with increasing T_e. At the higher T_e values shown, $\Delta\varepsilon\sim T_e^2$ and α_{eff} becomes independent of T_e.] A plot of α_{eff} versus λ at a constant value of T_e shows that extrapolated values of α_{eff} at $\lambda=0$ gives nonzero negative values which are consistent with a non-zero loss factor $\beta(\lambda)$. In addition a minimum in α_{eff} at 10.49 μm is observed and is consistent with a maximum occuring in $\beta(\lambda)$ close to the oscillatory photoconductivity (OPC) condition $\hbar\omega=5\hbar\omega_L$. A strong ($\beta$=1) OPC effect is excluded because of the finite width of the excitation pulse $\sim\varepsilon_F+4k_BT_e$. The presently available range of photoexcitation energies from the CO_2 laser is not sufficient to expose other minima expected near $\hbar\omega=N\hbar\omega_L$ (N integer). Experiments are in progress on other concentration samples to investigate the physical origin of the non-zero loss factor β.

*Work supported in part by the Office of Naval Research.

You have 4 ones left including this one

Shubnikov-de Haas Effect Studies on Optically Heated Electrons in n-InSb*

by

D.G. Seiler, L.K. Hanes, M.W. Goodwin, and A.E. Stephens†
Department of Physics
North Texas State University
Denton, Texas 76203

ABSTRACT

CO laser-induced hot electrons in n-InSb at 1.8 K have been studied with the Shubnikov-de Haas effect which permits extraction of the electron temperature as a function of peak incident laser power.

KEY WORDS: Shubnikov-de Haas
InSb
Hot Electrons

RUNNING TITLE: Optically Heated Electrons in n-InSb

I. INTRODUCTION

Hot electrons generated by dc electric fields in InSb have been widely studied using a number of experimental methods. However, optically induced hot electrons generated by intense laser radiation have been much less extensively investigated. Recently, the Shubnikov-de Haas (SdH) magnetoresistance oscillations have been used as a tool to determine the temperature of hot electrons produced by a CO_2 laser in degenerate n-InSb [1,2]. Only free carrier absorption processes needed to be considered because of the low intensity of the cw CO_2 laser and because the photon energy of the 10 μm CO_2 laser radiation is about half of the direct band gap energy E_g of InSb. In contrast, both intra- and inter-band effects are expected to be important in CO laser-induced hot electron effects in InSb where the photon energies can be tuned from below E_g to above E_g.

In this paper, we present the results of an investigation of the SdH effect in a sample of n-InSb irradiated with a CO laser. In Section II, we describe features of the SdH effect pertinent to its use in studying hot electrons. The experimental work, including sample properties and the apparatus, is given in Section III. The results and conclusions are then presented in Section IV.

II. THE SHUBNIKOV-DE HAAS EFFECT

The Shubnikov-de Haas (SdH) effect is an oscillatory variation of magnetoresistance with magnetic field which can occur in a degenerate material at low temperatures. The conditions necessary for the SdH oscillations to be observed are $\omega_c \tau >> 1$ and $k_B T_e < \hbar\omega_c < E_F$, where $\omega_c = eB/m^*c$ is the cyclotron frequency, τ is the lifetime of a state at the Fermi energy E_F, and T_e is the temperature of the electron gas, which may or may not be equal to the temperature of the lattice T_L. As the magnetic field B is increased, successive Landau levels rise past E_F and depopulate. As long as E_F remains constant, the magnetoresistance oscillations are periodic in B^{-1} with the period given by

$$P = \hbar e/E_F m^* c \quad . \tag{1}$$

Provided the magnetic field does not become too large, the amplitude of the SdH oscillations in the longitudinal magnetoresistance of a material such as n-InSb can be expressed as [3,4]

$$A = \left(\frac{P}{2B}\right)^{1/2} \frac{\beta T_e m' \cos(\pi\nu)}{\sinh(\beta T_e m'/B)} e^{-\beta T_D m'/B} \quad , \tag{2}$$

where $\beta = 2\pi^2 k_B cm/\hbar e$, $m' = m^*/m$ is the ratio of effective mass to free electron mass, T_D is the Dingle or nonthermal broadening temperature, and ν is the spin splitting factor related to the effective g factor g^* by $\nu = m^* g^*/2m$.

Although the SdH oscillations can be observed with straightforward dc techniques, magnetic field modulation and a lock-in amplifier are often used to improve the signal to noise ratio and to observe a larger number of oscillations. When the lock-in amplifier is tuned to the modulation frequency, it measures an oscillatory signal with an envelope-to-envelope amplitude of [5,6]

$$V = 4 A J_1(\alpha) \qquad (3)$$

at a particular value of B. The argument of Bessel function J_1 is given by $\alpha = 2\pi B_M/PB^2$, where B_M is the amplitude of the modulation field.

The first hot electron SdH experiment in n-InSb was performed by Komatsubara [7], who applied large electric fields (>0.1 V/cm) to a 1.5×10^{15} cm^{-3} sample and observed a decrease in the SdH amplitude for the transverse configuration and a shift of the SdH extrema to higher B values as the electric field was increased. Later Isaacson and Bridges [8] studied a 1.7×10^{15} cm^{-3} sample of n-InSb and found that either an increase in the lattice temperature or an increase in the large electric field would decrease the transverse SdH amplitude and shift the extrema to higher B values. By matching the SdH curves for various lattice temperatures at a fixed low electric field with the curves for various high electric fields at a fixed low lattice temperature, Isaacson and Bridges determined the electron temperatures corresponding to given values of the electric field.

Bauer and Kahlert have investigated the hot electron SdH effect in n-InSb [9,10] (as well as in n-InAs [11] and n-GaSb [12]) using a pulsed electric field technique to avoid lattice heating [13]. For 5.9×10^{15} and 1×10^{16} cm^{-3} samples, T_D varied with T_L, so the T_e values for various electric fields were determined from the longitudinal oscillations by the direct comparison method used by Isaacson and Bridges [8]. For a 6.9×10^{16} cm^{-3} (more highly degenerate) sample, T_D was independent of T_L, so T_e values were obtained using

$$\frac{A(T_{e,1})}{A(T_{e,0})} = \frac{T_{e,1}\sinh(\beta T_{e,0} m'/B)}{T_{e,0}\sinh(\beta T_{e,1} m'/B)} \qquad (4)$$

from the amplitudes of longitudinal SdH oscillations. Little or no shift in the longitudinal SdH extremal positions was observed for these high concentration samples.

In the present study the conduction electrons were heated, not by a large electric field, but by optical excitation. For photon energies much less than the band gap energy E_g, carrier heating should take place due to free carrier absorption and thermalization by electron-electron collisions. For larger photon energies, carriers should also be excited from impurity levels and from the valence band into the conduction band. A radiation induced increase in the steady state concentration should raise E_F and decrease the SdH period. This would shift the SdH extrema to higher B values. Also, according to the work of Kalushkin et al. [14],

even if the concentration remains constant, the B and T_e dependence of E_F caused by incomplete degeneracy should cause P to decrease and the extrema to move to higher B values as T_e is increased. To take period changes into account, we define the function

$$F \equiv \frac{V(T_{e,1},P_1)P_0^{1/2}J_1(\alpha_0)}{V(T_{e,0},P_0)P_1^{1/2}J_1(\alpha_1)} \quad , \tag{5}$$

where V is given by Eq. (3). If P, T_D, m', and ν are all constant, F is equal to Eq. (4). The use of F in determining T_e values is given in Section IV.

III. EXPERIMENTAL WORK

A block diagram of the experimental apparatus is shown in Fig. 1. The laser is a sealed off, electric discharge cw CO laser capable of up to 2 W on many lines between 5.15 and 5.6 μm. The laser is grating tunable and has a short term (~1 sec) amplitude stability of ±1% [15]. The TEM_{00} laser beam is passed through a Galilean type collimator to reduce the spot size and is then mechanically chopped to produce 20 μsec wide pulses (F.W.H.M.) at a repetition rate of 1700 Hz. The 3.3% duty cycle of the chopper prevents lattice heating by the laser. The beam is focused onto the sample so that the region between the potential probes is as uniformly illuminated as possible. A He-Ne laser is used with a silicon PIN photodiode to produce a trigger pulse for the sampling oscilloscope. Calibrated filters are used after the chopper for beam attenuation.

The SdH oscillations are recorded using magnetic field modulation and sampling techniques developed by Kahlert and Seiler for pulsed experiments [16]. In the present work a constant dc current of 0.5 mA is applied to the sample. An ac magnetic field with an amplitude of 75 G modulates the sample conductivity at a frequency of 43 Hz. The signal at the sample potential contacts, produced by the laser pulse and the field modulation, is fed through a high impedance differential amplifier into a Tektronix 7904/7S14 sampling oscilloscope. The output of the sampling oscilloscope is fed into a lock-in amplifier tuned to 43 Hz. The lock-in output is then plotted on an X-Y recorder against 1/B.

The sample was cut from a bulk specimen of n-InSb with an electron concentration of 1×10^{15} cm^{-3} and a Hall mobility of about $10^5 cm^2/Vsec$ at 1.8 K. The front surface was optically polished with 0.3 μm Al_2O_3 polishing grit. The rear surface was left rough to eliminate multiple reflections and etalon effects. The sample dimensions were 5.63 mm × 1.65 mm × 0.1 mm thick. Two current contacts and two potential contacts were made using indium solder.

IV. RESULTS AND CONCLUSIONS

Figure 2 shows SdH oscillations for lattice temperatures T_L of 1.8 to 11 K. It is quite apparent that the SdH amplitudes decrease with increasing values of T_L. One also observes a slight shift of the extrema to higher magnetic field positions as observed in previous SdH work by other authors [7,8,14]. This reflects an increase in electron temperature since the electrons are in equilibrium with the lattice during these measurements. The fact that ionized impurity

scattering, which depends only on carrier energy, dominates the momentum relaxation in InSb below 40 K insures that the SdH amplitudes will be functions of electron temperature and not lattice temperature.

Figure 3 shows several SdH traces taken with a constant T_L = 1.8 K. The bottom trace was taken with the laser blocked (i.e., P_I = 0). For all wavelengths used, increasing the laser power decreases the SdH amplitudes and again a slight shift of the extrema to higher magnetic fields is generally observed. Lattice heating effects are not present during the time scales of the 20 μsec laser pulses. This has been verified by measuring the electron temperature at different time positions during the 20 μsec wide laser pulse. No changes in electron temperature were observed during the 20 μseconds where the laser power was constant. These measurements show that any lattice heating makes an insignificant contribution to the electron temperature for illumination on these time scales. The lattice time constants have been estimated elsewhere and are found to be on the order of milliseconds.[17] Thus the SdH oscillations are damped by increasing laser power in a similar manner to the damping caused by higher lattice temperatures. Also shown in Fig. 3 is a SdH trace for λ = 5.39 μm for which P_I = 42.5 mW. The decrease in the SdH amplitude is less than that observed for λ = 5.155 μm with P_I = 11.8 mW even though the laser power is almost a factor of four greater. This indicates that the laser heating is certainly much greater for the shorter wavelength where the photon energy is greater than $E_g + E_F$. The direct gap is ≈235 meV and the Fermi energy is ≈2.5 meV.

Plots of the function F, defined in Eq. (5), versus T_L and P_I can be used to determine the electron temperature for

each particular wavelength and value of P_I as shown in Fig. 4 by making a one-to-one correspondence between the two curves. An electron temperature can be extracted by the direct comparison method since the quantities compared are not explicit functions of the lattice temperature.[18] As noted earlier, this comparison method was first used by Isaacson and Bridges[8] in high electric field measurements to extract electron temperatures from SdH data and has since been used extensively.[19] For example, for λ = 5.315 μm, a value of P_I = 72 mW corresponds to a temperature of about 2.8 K. The electron temperatures determined from the SdH data in this manner are shown in Fig. 5, together with some results for the case of electron heating with a CO_2 laser. There is a quite striking non-linear behavior observed for all CO wavelengths. In addition, for λ = 5.245 μm an unusual dependence of T_e on P_I is seen, i.e., T_e rises rapidly and then remains relatively flat. At the highest powers used, a decrease of about 20% is observed in the SdH period at λ = 5.245 μm compared to the period at the other CO wavelenghts.

Comparing the CO laser heating data with the CO_2 laser data shows that for fixed laser power T_e increases with decreasing wavelength in the 5 μm CO region while T_e increases with increasing wavelength for the two different wavelengths shown

in the 10 μm CO_2 region. Clearly, different absorption processes are at work in the two spectral regions. Free carrier absorption mechanisms must be used to analyze the CO_2 laser data; this is obviously not the case with the current CO laser measurements.

Absorption in InSb in the 5 μm region is interesting, since it involves a variety of processes such as interband and impurity level transitions, and free carrier absorption. The results presented in Fig. 5 are due to hot electron effects which involve these absorption processes. The results can be partially explained from a three level model consisting of a valence band, conduction band, and an acceptor level lying 7-10 meV above the valence band. The effects of free carrier absorption are negligible compared to those of direct interband and acceptor level absorption processes. The photoexcited electrons are created with an excess energy ΔE above the Fermi level by impurity level or interband transitions. The photoexcited electrons then heat the carriers in the conduction band via carrier-carrier scattering resulting in a quasi-equilibrium state with an increased electron temperature T_e.

The 5.39 and 5.315 μm wavelengths used correspond to photon energies of 230.2 and 233.5 meV respectively. These photon energies are sufficient to stimulate transitions from the acceptor level (but not the valence band) to the conduction band with a rather small ΔE remaining. T_e is seen to rise with P_I since the number of photoexcited electrons and hence the amount of electron heating is increased as P_I is

increased. T_e finally appears to saturate due to depletion of the acceptor level; as there are only about 10^{13} cm^{-3} uncompensated acceptors, the change in concentration of a 10^{15} cm^{-3} n-type sample is limited to approximately 1%. T_e is higher for the higher photon energy line for a fixed P_I since here the excess energy ΔE is greater, so more heating occurs.

The photon energy of the 5.245 μm wavelength is 236.6 meV and is sufficient to excite acceptor level transitions but falls just short of being energetic enough to excite direct interband transitions at $T_e \approx 1.8$ K. However, the electrons excited from the impurity level have a larger excess energy than in the 5.315 μm case and therefore substantial heating of the electron gas occurs for small incident laser powers. As the electron gas is heated, the electron distribution function changes so that states are made accessible for direct interband transitions. Hence, initially at lower electron temperatures the direct transitions were forbidden, but after heating of the electron gas by the photoexcited electrons produced from the acceptor level, these transitions become possible. However, the electrons excited from the valence band have very little excess energy and thus make no significant contribution to the electron temperature. Thus, the electron temperature is seen to rise quickly and then level off as the acceptor levels are depleted and interband transitions commence.

This interpretation of the variation of the electron temperature with peak incident laser power is also confirmed

by the observed changes in SdH period at 5.245 μm. The electron concentration (as determined by the SdH period) remains constant until the electron temperature reaches about 3.3 K at a peak laser power of ≈ 40 mW. Thereafter, the electron concentration increases with laser power. There is about a 25% increase in concentration when the laser power is increased from 40 mW to 240 mW, even though the electron temperature remains fairly constant over this range.

The two shortest wavelengths studied (5.185 and 5.155 μm) have photon energies of 239.3 and 240.7 meV which are sufficient to excite direct interband transitions with a significant ΔE remaining as well as acceptor level transitions. The absorption coefficient here becomes extremely large, so that the sample is no longer uniformly illuminated through its entire thickness. Instead, the radiation is absorbed almost entirely in the first surface layers, resulting in intense carrier heating there. Consequently, T_e shows a rapid rise to high values for relatively small P_I.

The optical heating data presented here can be compared to that which is obtained using only pulsed, dc electric fields to heat the carriers. The increase of electron temperature with applied electrical power is controlled by energy loss rates of the conduction electrons to the lattice from some combination of deformation-potential, piezoelectric, or polar-optical phonon scattering. We find that it takes an applied electric field of ≈70 mV/cm to heat the conduction electrons up to an electron temperature of 5 K with the lattice at a temperature of

1.8 K. In contrast, the increase of electron temperature in the optical case is controlled by absorption and recombination processes, as well as the above energy loss rates.

In summary, Shubnikov-de Haas experiments have been used to determine the increase in temperature of the electron gas in InSb irradiated by a CO laser. The dependence of the electron temperature upon incident laser power and photon energy is shown to provide information on the absorption processes in InSb in the vicinity of the band gap. Further experiments using different concentration samples, higher powers, and more wavelengths will be performed to provide additional information on these absorption and hot carrier generation processes.

REFERENCES

[1] B.Moore, D.G.Seiler, and H.Kahlert, Bull. Amer. Phys. Soc. 22(1977)460.

[2] B.T.Moore, D.G.Seiler, and H.Kahlert, Solid-State Electron. 21(1978)247.

[3] A.E.Stephens, D.G.Seiler, J.R.Sybert, and H.J.Mackey, Phys. Rev. B 11(1975)4999.

[4] L.M.Roth and P.N.Argyres, in: Semiconductors and Semimetals, ed. by R.K.Willardson and A.C.Beer (Academic Press,New York,1966), Vol.I, Chap.6, p.159.

[5] A.Goldstein, S.J.Williamson, and S.Foner, Rev. Sci. Instr. 36 (1965)1356.

[6] D.G.Seiler, B.D.Bajaj, and A.E.Stephens, Phys. Rev. B 16(1977)2822.

[7] K.F.Komatsubara, Phys. Rev. Lett. 16(1966)1044.

[8] R.A.Isaacson and F.Bridges, Solid State Commun. 4(1966) 635.

[9] G.Bauer and H.Kahlert, J. Phys. C 6(1973)1253.

[10] H.Kahlert and G.Bauer, Phys. Rev. B 7(1973)2670.

[11] G.Bauer and H.Kahlert, Phys. Rev. B 5(1972)566.

[12] H.Kahlert and G.Bauer, Phys. Status Solidi 46(b)(1971) 535.

[13] A review of these and other electric field induced hot electron experiments is given by G.Bauer in: Springer Tracts in Modern Physics, ed. by G. Höhler (Springer-Verlag,New York,1974), Vol.74, p.1.

[14] V.I.Kalushkin, E.A.Protasov, A.G.Rodionov, and N.A. Toloknov, Fiz. Tekh. Poluprovodn. 8(1974)1786 [Sov. Phys. Semicond. 8(1975)1154].

[15] L.K.Hanes, M.S. Thesis, North Texas State University, Denton, Texas (1977).

[16] H.Kahlert and D.G.Seiler, Rev. Sci. Instrum. 48(1977) 1017.

[17] C.D.Cantrell, J.F.Figueira, J.F.Scott, and M. O.Scully, Appl. Phys. Lett. 28, 442(1976).

[18] G.Bauer, in Springer Tracts in Modern Physics, (Springer, Berlin, 1975) Vol.74, p.15.

[19] For example, see Ref. 9-12.

*Work supported in part by the Office of Naval Research
†Permanent address: Department of Physics, Austin College. Sherman, Texas 75090

FIGURE CAPTIONS

1. Block diagram of experimental apparatus.

2. SdH oscillations for various lattice temperatures without laser irradiation.

3. Effect of laser irradiation at different wavelengths and incident powers on the SdH oscillations at constant lattice temperature.

4. Plots of the function F of Eq. (5) vs. lattice temperature and peak incident laser power. The electron temperature is extracted by comparing the two graphs for a fixed value of F. The wavelengths are in micrometers.

5. Electron temperatures (from Fig. 4) vs. peak incident CO laser power for different wavelengths at $T_L = 1.8$ K, together with CO_2 laser heating data.

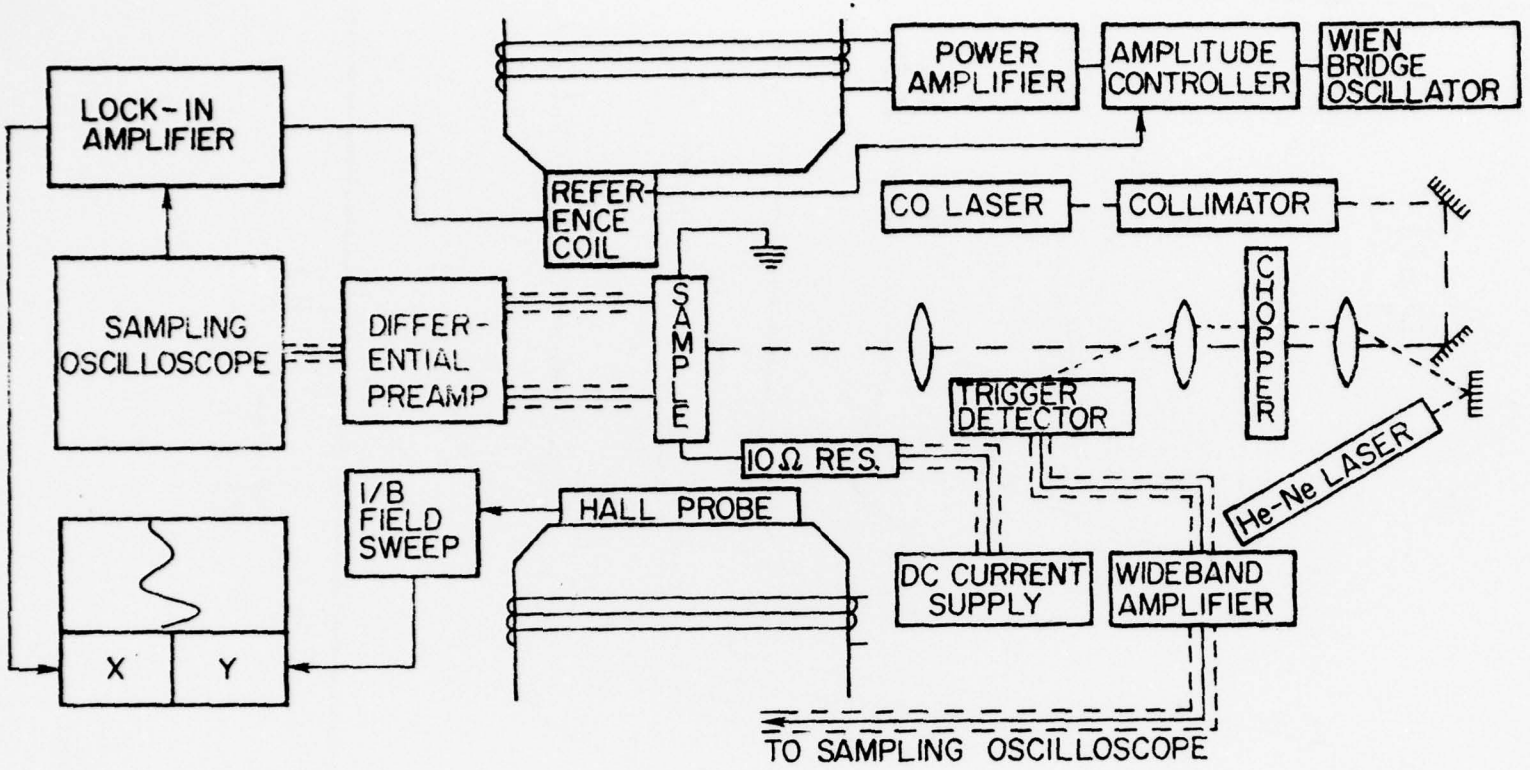
LOCK-IN AMPLIFIER
POWER AMPLIFIER
AMPLITUDE CONTROLLER
WIEN BRIDGE OSCILLATOR
REFERENCE COIL
CO LASER
COLLIMATOR
SAMPLING OSCILLOSCOPE
DIFFERENTIAL PREAMP
SAMPLE
CHOPPER
TRIGGER DETECTOR
10Ω RES.
He-Ne LASER
I/B FIELD SWEEP
HALL PROBE
DC CURRENT SUPPLY
WIDEBAND AMPLIFIER
X
Y
TO SAMPLING OSCILLOSCOPE

Fig. 1

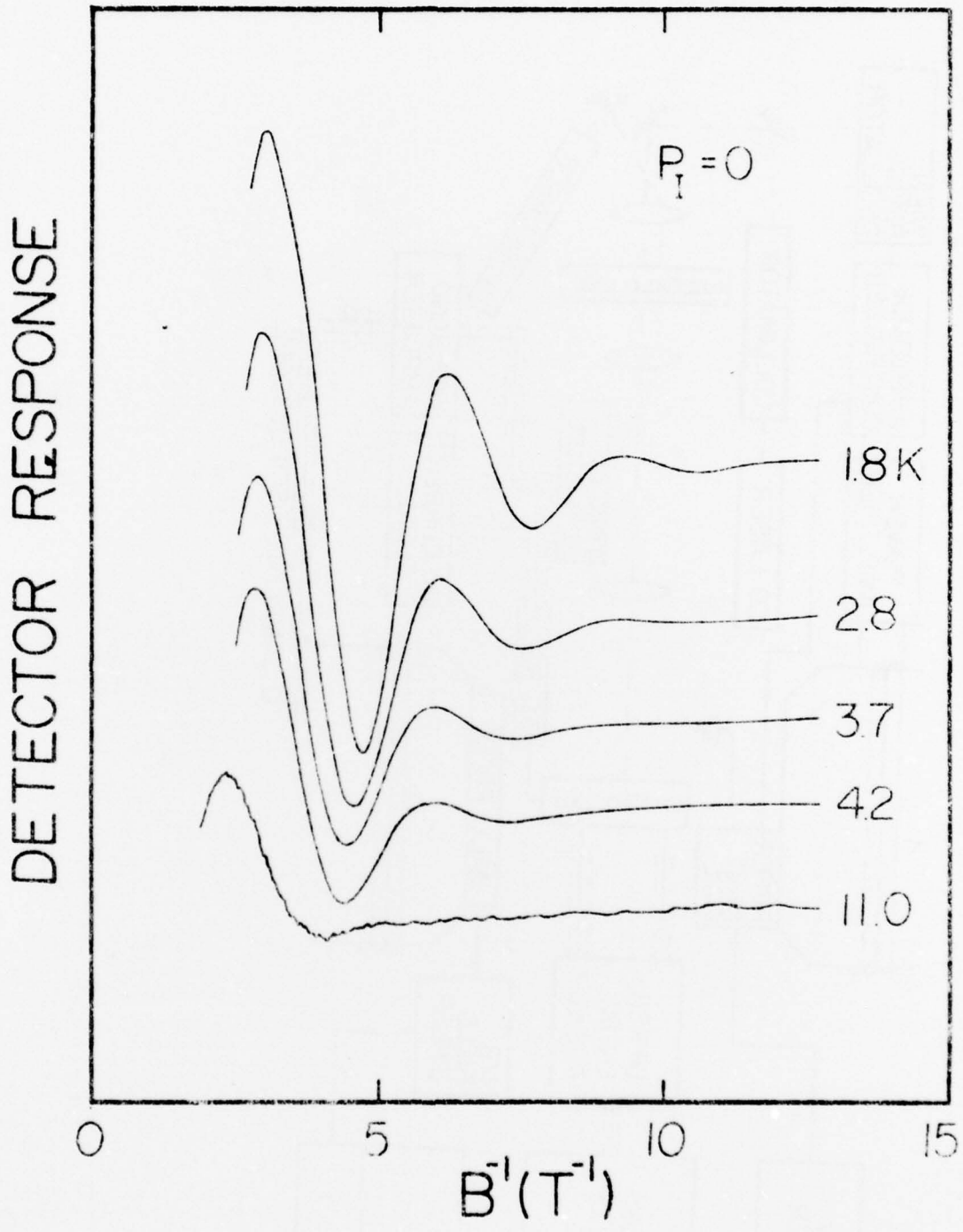

Fig. 2

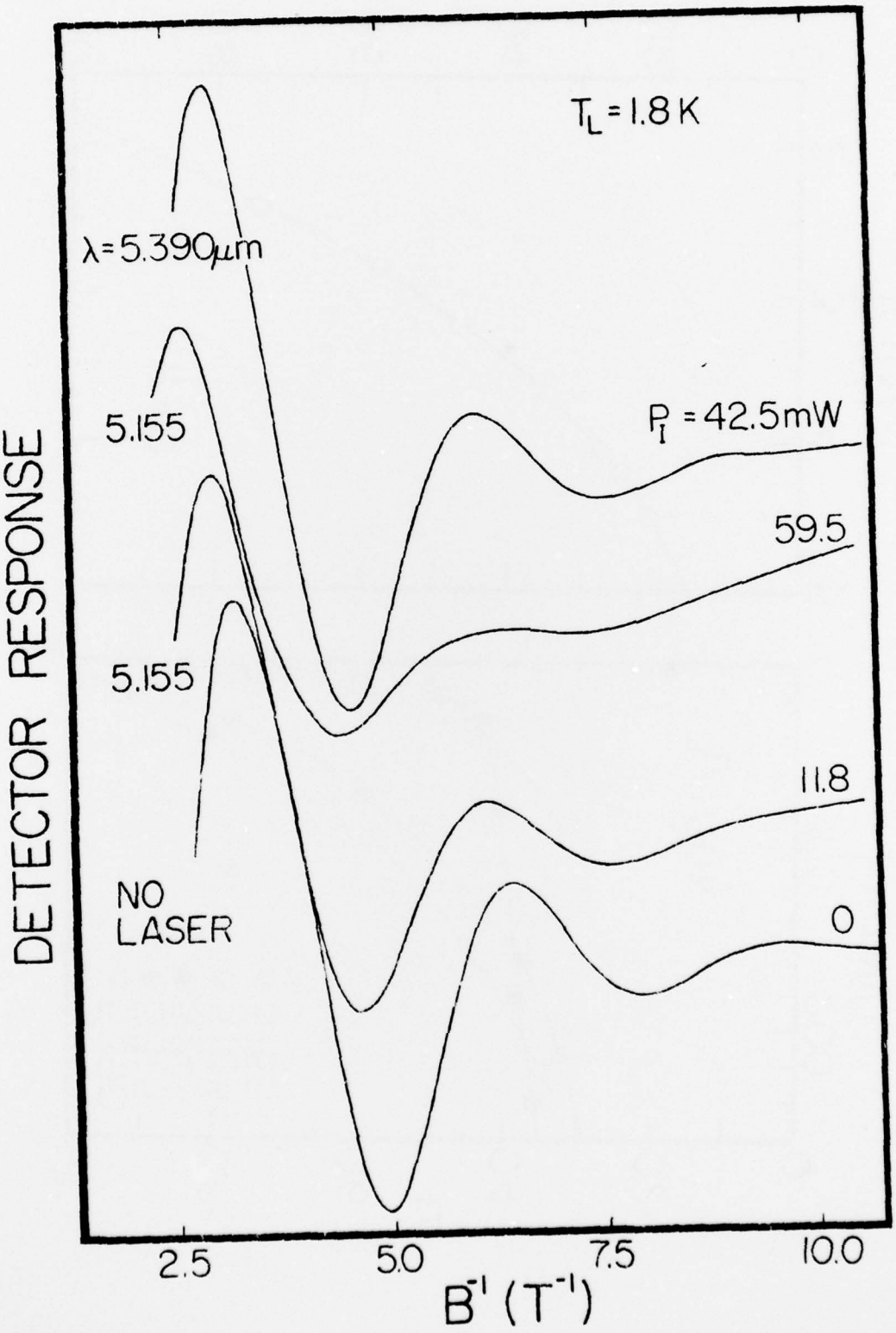
T_L = 1.8 K
λ = 5.390 μm
5.155
P_I = 42.5 mW
59.5
5.155
11.8
NO LASER
0
DETECTOR RESPONSE
2.5
5.0
7.5
10.0
B^{-1} (T^{-1})

Fig. 3

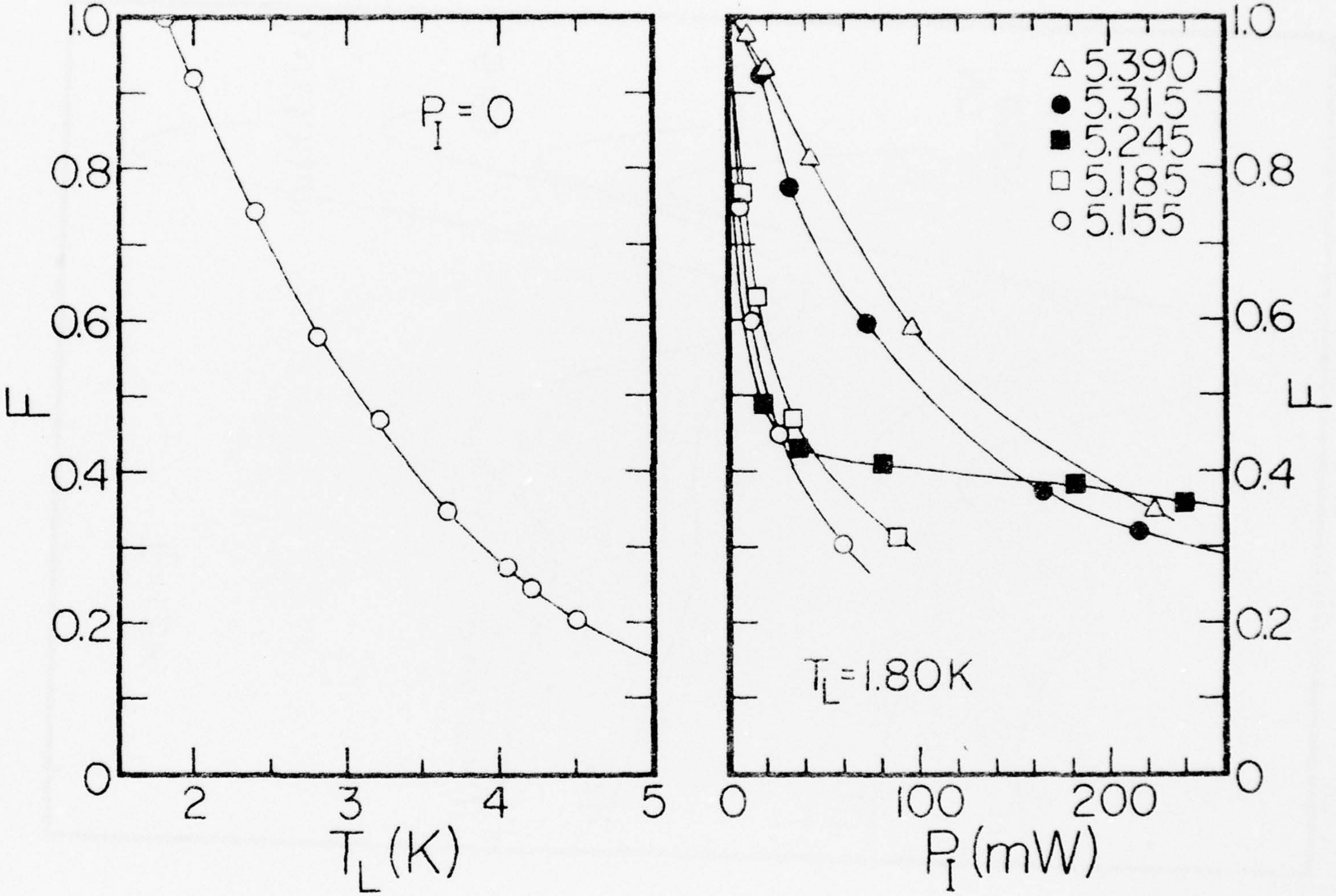

1.0
0.8
0.6
0.4
0.2
0
F
$P_I = 0$
2
3
4
5
T_L(K)
△ 5.390
● 5.315
■ 5.245
□ 5.185
○ 5.155
T_L=1.80K
0
100
200
P_I(mW)
1.0
0.8
0.6
0.4
0.2
0
F

Fig. 4

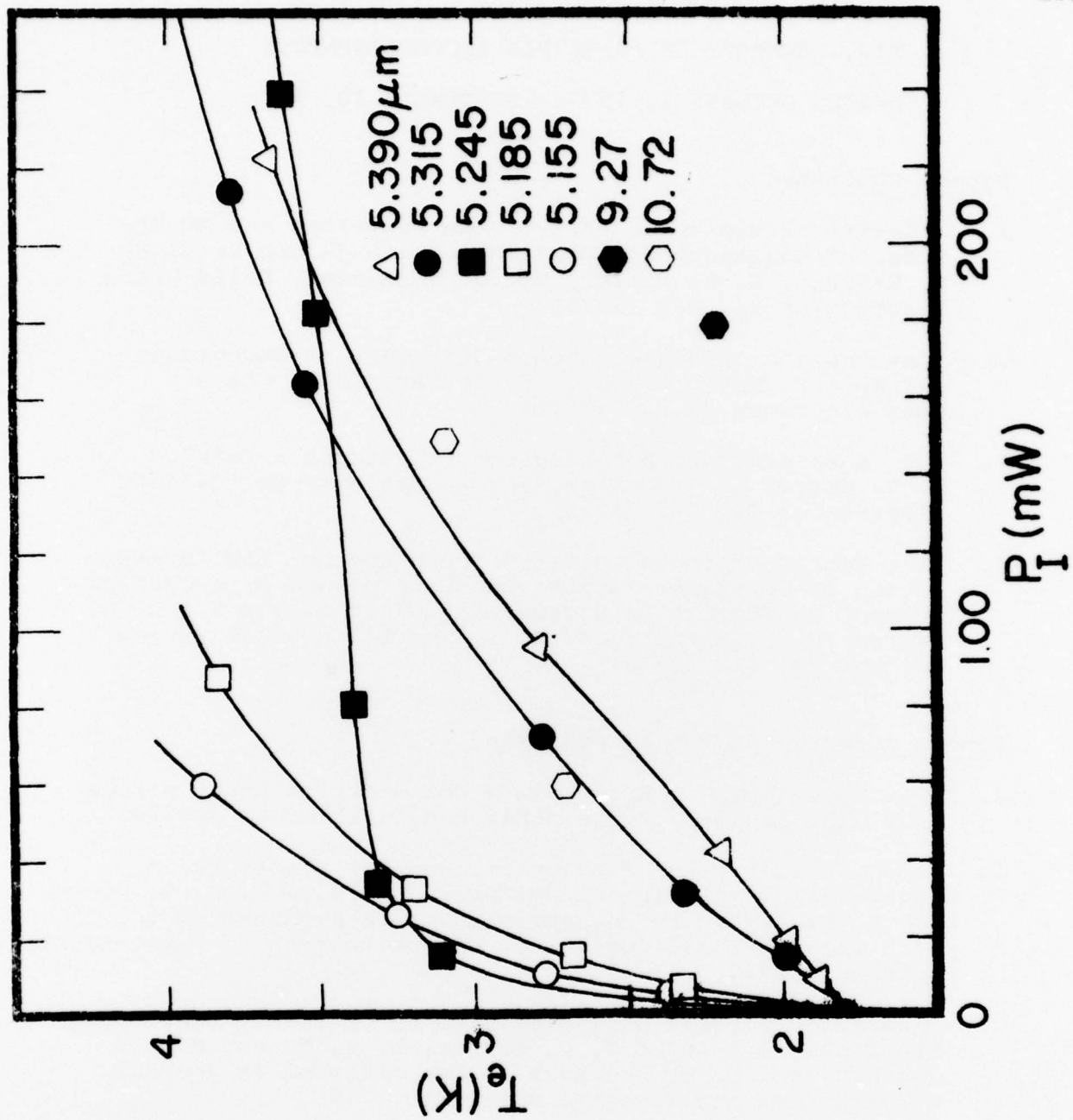

Fig. 5

XIV. SUMMARY OF PRINCIPLE ACCOMPLISHMENTS

DURING OCTOBER 1, 1977 - SEPTEMBER 30, 1978

Papers Published

1. "Electric Field Dependence of the Positions and Amplitudes of Magnetophonon Oscillations in n-InSb at 77 K, H. Kahlert, D. G. Seiler, and J. R. Barker, Solid-State Electronics 21, 229 (1978).

2. "Observation of Magnetophonon Structure in Degenerate n-InSb", H. Kahlert and D. G. Seiler, Solid State Communications 25, 61 (1978).

3. "CO_2 Laser-Induced Hot Electron Effects in n-InSb", B. T. Moore, D. G. Seiler, and H. Kahlert, Solid-State Electronics 21, 247 (1978).

4. "New Hybrid Photoconductivity Technique for the Investigation of CO_2-Laser-Induced Hot-Carrier and Free-Carrier Absorption Effects in Degenerate n-InSb at 1.8 K," D. G. Seiler, J. R. Barker, and B. T. Moore, Physical Review Letters 41, 319 (1978).

Papers Accepted and To Be Published

1. "The Magnetophonon Effect in a Nonparabolic Band: n-type InSb", H. Kahlert, to be published in Physical Review.

2. "Photoconductivity of Laser Excited Hot Electrons in Degenerate n-InSb" D. G. Seiler, J. R. Barker, B. T. Moore, and K. E. Hansen to be published in Proceedings of the 14th International Conference on the Physics of Semiconductors, Edinburg, 1978.

3. "Shubnikov-de Haas Effect Studies on Optically Heated Electrons in n-InSb" D. G. Seiler, L. K. Hanes, M. W. Goodwin, and A. E. Stephens to be published in Journal of Magnetism and Magnetic Materials.

Talks Given at International Conferences

1. 14th International Conference on the Physics of Semiconductors, Edinburg, 1978. "Photoconductivity of Laser Excited Hot Electrons in Degenerate n-InSb" by D. G. Seiler.

2. International Conference on Solids and Plasmas in High Magnetic Fields, Cambridge, 1978. "Shubnikov-de Haas Effect Studies on Optically Heated Electrons in n-InSb", by D. G. Seiler.

Talks Given at American Physical Society Meeting - March, 1978 in Washington, DC

3. "Wavelength Dependence of CO_2 Laser-Induced Hot Electron Effects in n-InSb, B. T. Moore and D. G. Seiler, Bull. Amer. Phys. Soc. 23, 329 (1978).

4. "Determination of CO_2 Laser-Induced Hot Electron Temperatures from the Photoconductivity of n-InSb", D. G. Seiler and B. T. Moore, Bull. Amer. Phys. Soc. 23, 329 (1978).

Other Accomplishments or Honors

Invited to be a chairman of a scientific session at the international conference on The Application of High Magnetic Fields in Semiconductors Physics, Oxford, 1978.